Spectroscopic Properties and Potential Energy Curves for Heavy p-Block Diatomic Hydrides, Halides, and Chalconides

K. BALASUBRAMANIAN†

Department of Chemistry, Arizona State University, Tempe, Arizona 85287-1604

Received February 8, 1989 (Revised Manuscript Received April 3, 1989)

Contents

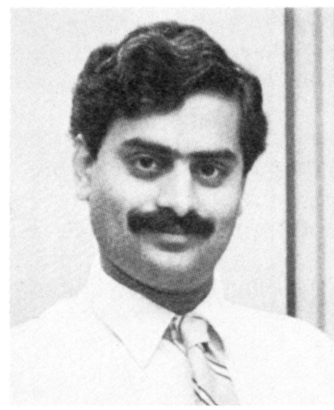

Krishnan Balasubramanian has been as Associate Professor of Chemistry since 1987 at Arizona State University, Tempe, AZ. He was born in Bangalore, India, in 1956. He received his M.Sc. (Honors) degree from the Birla Institute of Technology and Science, Pilani, India, in 1977 and his M.A. and Ph.D. degrees from The Johns Hopkins University in 1980. He was a postdoctoral associate and visiting lecturer in the Department of Chemistry and Lawrence Berkeley Laboratory, University of California, Berkeley, from 1980 to 1983. He was an Assistant Professor at Arizona State University during 1983–1986. He received the Alfred P. Sloan Fellowship in 1984 and the Camille and Henry Dreyfus Teacher–Scholar Award in 1985. Professor Balasubramanian's research interests include relativistic quantum chemistry of molecules containing very heavy atoms, chemical applications of group theory, and artificial intelligence. He is an author or coauthor of over 160 research publications.

I. Introduction

The spectroscopic properties, potential energy curves, dipole moments, and transition moments of very heavy main-group molecules containing p-block elements have been the topics of many investigations over the past six decades. While the first spectroscopic investigation of heavy hydrides, halides, and chalconides dates back to the early 1920s, a complete and definitive understanding of the electronic states and observed electronic transitions was accomplished only in this decade. Much of the problem centered around not having any theoretical calculations or insight into the electronic energy levels of very heavy molecules. However, in recent years, with the advent of ab initio relativistic quantum mechanical methods, theoretical calculations of spectroscopic properties and potential energy curves of almost any molecule in the periodic table have been made possible.[1-31] These theoretical calculations together with the experimental spectroscopic and high-temperature thermodynamic studies have provided a wealth of information which needs to be collected together and understood.

The theoretical works in the past decade culminated into many manuscripts in this area.[1-31] The increased interest in the spectroscopic properties of heavy molecules is in part attributed to large relativistic effects. It is now fairly well-known that for molecules containing very heavy atoms relativistic effects are quite significant. Relativistic effects arise from the difference in the true velocity of light as opposed to the assumed

† Camille and Henry Dreyfus Teacher–Scholar.

0009-2665/89/0789-1801$06.50/0

infinite velocity of light in the nonrelativistic classical and quantum mechanical methods. Relativistic effects such as mass-velocity correction (correction to the kinetic energy arising from the variation of mass with speed), Darwin correction, and spin-orbit correction make significant contributions to molecules containing very heavy atoms.

The theoretical progress in this area was hampered in part due to a large number of electrons present in such heavy molecules, making these calculations formidably difficult. Nevertheless, thanks to the effective core potential methods developed by Pitzer and coworkers,[15-23] Hay and Wadt,[24-27] Krauss and Stevens,[4] and others, such calculations have become possible and viable. The advantages of the effective core potential methods are elimination of chemically unimportant core electrons, facilitation of inclusion of a larger basis set for valence and Rydberg orbitals, acceleration of convergence, and reduction of configurations in the configuration interaction (CI) calculations.

The theoretical investigations of heavy hydrides are especially attractive since hydrides are the least complex from a theoretical standpoint and the understanding of the bonding of heavy metal and other elements with hydrogen is important.

The experimental investigations of heavy chalconides and halides have been motivated by the suitabilities of these species as candidates for chemical lasers. For example, the reactions of heavy group IV atoms such as Ge, Sn, and Pb with O_3, F_2, N_2O, OCS, etc. are chemiluminescent. The diatomic halides and chalconides are formed in excited states in these reactions, which in turn emit photons relaxing to the ground states. The photon yields of these reactions have been so considerable that many of these reactions and their mechanisms have been the topics of many investigations.

The objective of this review is to organize and assimilate the wealth of experimental and theoretical information accumulated to date on these species. A comparison of both experimental and theoretical spectroscopic constants is provided. The nature of the electronic states of these species is discussed. The importance of the relativistic effects for the electronic states of these molecules is outlined. A critical comparison of the periodic trends within a group is made to develop a comprehensive understanding of the nature of electronic states and spectroscopic properties of these compounds. The potential energy curves of the various diatomic compounds considered here are given. The dipole moments and transition moments of some of the heavy main-group compounds are also discussed.

Detailed descriptions of the various methods employed to investigate the spectroscopic properties of molecules containing heavy atoms can be found in the reviews of ref 8 and 13. In this article, we briefly describe the various methods explaining the ab initio acronyms used in subsequent sections so that readers are provided with a reasonable description of the level of theory employed.

A critical comparison of the various hydrides, halides, and chalconides has not been accomplished up to now. In this review we compare the spectroscopic properties, spin-orbit constants, dipole moments, and other properties of these compounds and obtain periodic trends. In every case, the sixth-row compounds exhibit anomalous trends that are explained based on relativistic effects.

II. Method of Theoretical Calculations

All the calculations of molecules reviewed here were made with relativistic effective core potentials (RECPs), which include relativistic effects in these potentials. In earlier investigations these potentials were used in conjunction with Slater-type-orbital (STO) basis sets of double ζ + polarization or higher quality. The calculations that employed STO basis sets were done mostly by using the single-configuration self-consistent field (SCF) method followed by relativistic configuration interaction (RCI) calculations. The RCI calculations included the spin-orbit term derived from RECPs as suggested by Ermler et al.[20] The CI calculations including the spin-orbit term are called relativistic CI calculations (RCI) and they included single and double excitations from a multireference list of configurations. In general, the RCI included all low-lying λ-s states of the same Ω symmetry as reference configurations. For example, the RCI calculations of a state of 0^+ symmetry could include as reference configurations that describe $^1\Sigma^+_{0^+}$, $^3\Pi_{0^+}$, $^3\Sigma^-_{0^+}$, and other states of 0^+ symmetry. The RCI thus differs from a normal CI that in the normal CI $^3\Pi$ cannot mix with $^1\Sigma^+$ or $^3\Sigma^-$ states.

Most of the theoretical calculations made after 1986 were done by using the complete active-space MCSCF followed by multireference singles + doubles (CASSCF/MRSDCI/RCI) methods employing valence Gaussian basis sets of higher than double ζ + polarization quality.

In the CASSCF method a set of the most important electrons for chemical bonding (active or valence electrons) are distributed in all possible ways among orbitals referred to as the internal or active orbitals. The active orbitals are normally chosen as the set of orbitals that correlate into valence atomic orbitals at infinite separation of the various atoms in the molecule. The CASSCF method thus provides a zeroth-order starting set of orbitals for inclusion of higher order correlation effects.

The higher order electron correlation effects not included in the CASSCF are taken into account by using the configuration interaction method. The CI calculations we have carried out are second-order CI (SOCI), MRSDCI (multireference singles + doubles CI), and first-order CI (FOCI). The first two methods are more accurate than the latter method. The SOCI calculations included (i) all configurations in the CASSCF, (ii) configurations generated by distributing $n - 1$ electrons in the internal space and 1 electron in the external space (n = number of active electrons), and (iii) configurations generated by distributing $n - 2$ electrons in the internal space and two electrons in the external space in all possible ways. The FOCI calculations included the first two sets described above for the SOCI. The MRSDCI calculations included a subset of configurations determined by the important configurations in the CASSCF (coefficient $\geq$ 0.07 or 0.05) as reference configurations.

Throughout this article we use the acronyms CASSCF, SOCI, FOCI, MRSDCI, SCF/RCI, etc. to describe the nature of the calculations done on various species. Readers are referred to this section to find the

TABLE 1. Theoretical Spectroscopic Constants for GaH[a]

state	R_e, Å	T_e, cm^{-1}	ω_e, cm^{-1}
$X^1\Sigma^+$(I)	1.662 (1.663)	0	1612 (1605)
$a^3\Pi$(I)	1.603 (1.633)	16836 (17300)	1559 (1631–1640)
$A^1\Pi$	1.780	24206	
$^3\Sigma^+$	1.935	39271	2245
$^1\Sigma^+$(II)	3.582	40933	447
$^3\Sigma^-$	1.564	45649	1772
$^1\Sigma^{+\prime}$(II)	1.747	46632	931
$^3\Pi$(II)	2.091	46737	1218
$^1\Sigma^+$(III)	4.609	50573	219
$^1\Delta$(I)	1.541	51319	1907
$^1\Delta$(II)	1.553	51982	1835
$^1\Sigma^{+\prime}$(III)	1.612	52076	2192
$^3\Pi$(III)	1.737	54243	1660
$^3\Delta$(I)	3.440	64415	
$^3\Pi$(IV)	1.813	65420	831
$^1\Delta$(III)	1.615	72554	1567
$^3\Delta$(II)	2.039	79284	917
$^3\Delta$(III)	2.033	82295	956
$^1\Sigma^-$	1.606	83271	1497
$^1\Delta$(IV)	2.321	85703	1744

[a] Numbers in parentheses are experimental values. $D_0{}^\circ$(GaH) = 2.81 (theory), 2.8 eV (experiment). From ref 42.

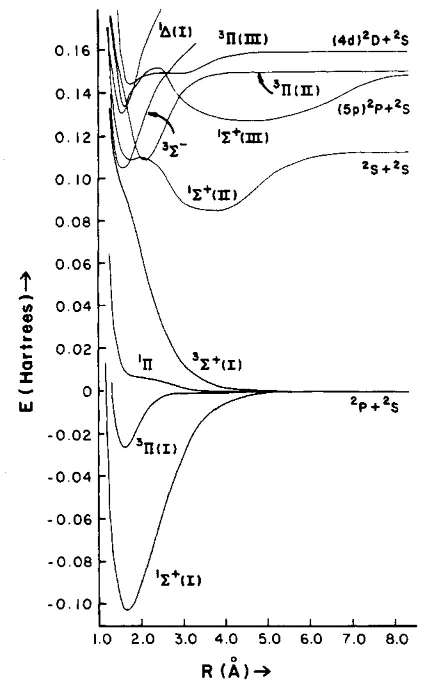

Figure 1. Potential energy curves of several electronic states of GaH (reprinted from ref 42; copyright 1989 Academic Press, Inc.). For spectroscopic labels of assigned states, see Table 1.

meanings of the acronyms and to develop an understanding of the approximations in these methods.

III. Spectroscopic Properties and Potential Energy Curves of Heavy Hydrides

A. GaH

The experimental works on GaH are contained in ref 33–41. Kim and Balasubramanian[42] made relativistic CASSCF/SOCI calculations on several valence and Rydberg electronic states of GaH. The spectroscopic properties, dipole moments, and potential energy curves of several electronic states were reported, among which 17 new electronic states were found.[42]

Early spectroscopic studies on GaH included those by Garton,[33] Neuhaus,[34,35] and Ginter and co-workers.[36] Ginter and Battino[37] calculated the potential curves for the third-group hydrides using the Rydberg–Klein–Rees (RKR) method. Poynor et al.[38] studied the $^3\Pi_{0^-} \rightarrow X^1\Sigma^+$ emission system. Kronekvist et al.[39] studied the $A^1\Pi$–$X^1\Sigma^+$ system and suggested that there should be a barrier due to some avoided crossing. The line widths in the A–X system were found to increase with increasing J, suggesting a tunneling effect and a small barrier prior to dissociation. On the basis of the predissociation of the A–X bands, the D_e of GaH was estimated as <22 900 cm^{-1}. Urban et al.[311] recently obtained the infrared spectrum of GaH in its $^1\Sigma^+$ ground state using a laser diode spectrometer. A total of 113 transitions were measured which were used to obtain accurate ground-state Dunham parameters and an improved R_e = 1.6621 Å. Lakshminarayana and Shetty[332] recently carried out the rotational analysis of the $a^3\Pi$–$X^1\Sigma^+$ bands of GaD. The only theoretical calculation on GaH before Kim and Balasubramanian[42] is that of Hurley et al.,[22] who obtained the R_e and ω_e values of the ground state of GaH in an attempt to gauge the RECPs.

Table 1 shows the calculated spectroscopic properties, and Figure 1 shows the actual potential energy curves (PEC) obtained by Kim and Balasubramanian.[42] The experimental spectroscopic constants were known for the $X^1\Sigma^+$ state and the spin–orbit components of the $^3\Pi$ state. In addition, the A–X system was studied although the constants of the A state are not yet known. As seen from Table 1 the theoretical constants for the ground state are almost in exact agreement with the experimental values. The spin–orbit interaction was not introduced in these theoretical calculations[42] since its effect was found to be rather small.

The first excited state of GaH is a $^3\Pi$ state, which was seen experimentally. The calculated R_e, T_e, and ω_e values of the $^3\Pi$ state were also found to be in very good agreement with the experimental results. Another system designated as the A–X system was found to be predissociated. The A state was tentatively assigned to a $^1\Pi$ state with an experimental T_0 value of 22 745 cm^{-1} obtained by Kronekvist et al.[39] The experimental R_e value of the A state was 1.82 Å in comparison to a theoretical value of 1.78 Å. The $^1\Pi$ curve has a very shallow minimum with a theoretical T_e value of 24 206 cm^{-1} in comparison to an experimental value of 22 745 cm^{-1}. The theoretical value was a bit high as anticipated for the level of electron correlations and basis sets included in those calculations.

The predissociation of the experimental A state was found to be consistent with the potential energy curve in Figure 1, which has a shallow short-range minimum and a long-range minimum separated by a very small barrier. The D_e calculated by using the predissociation of the $^1\Pi$ state should, however, be quite accurate since the predissociation energy and the energy of ^2P + ^2S atoms are very close. Kim and Balasubramanian[42] estimated that the D_e of 2.84 eV obtained by using extrapolation of the predissociation of the A–X bands should only be 0.04 eV lower, yielding a corrected value of 2.80 eV. A direct theoretical SOCI D_e value of the $X^1\Sigma^+$ state of 2.81 eV is almost in exact agreement with this experimental result.

Kronekvist et al.[39] noted that the observed line width in the A–X bands increased with increasing J, indicating a tunneling effect. These authors predicted that there should be an avoided crossing between a deep $^1\Pi$

TABLE 2. Dipole Moments near Equilibrium Geometries of the Various Electronic States of GaH[a]

state	μ_e, D	state	μ_e, D	state	μ_e, D
$^1\Sigma^+$(I)	−0.460	$^3\Pi$(II)	0.239	$^3\Pi$(IV)	0.684
$^3\Pi$(I)	−0.221	$^1\Sigma^+$(III)	0.010	$^1\Delta$(III)	0.117
$^1\Pi$	0.107	$^1\Delta$(I)	0.572	$^3\Delta$(II)	0.424
$^3\Sigma^+$	2.799	$^1\Delta$(II)	0.745	$^3\Delta$(III)	0.745
$^1\Sigma^+$(II)	−1.151	$^1\Sigma^{+\prime}$(III)	0.417	$^1\Sigma^-$	−0.424
$^3\Sigma^-$	−0.285	$^3\Pi$(III)	0.935	$^1\Delta$(IV)	0.117
$^1\Sigma^{+\prime}$(II)	−1.395	$^3\Delta$(I)	0.221		

[a] Positive polarity means positive charge on the hydrogen atom. From ref 42.

potential curve dissociating into an excited configuration and another repulsive $^1\Pi$ dissociating into the ground-state configuration. It was found that the $^1\Pi$ state arising from $1\sigma 2\sigma^2 1\pi$ mixes more with $^1\Pi(1\sigma^2 2\sigma 1\pi)$ at short distance than at long distance. The origin of the short-range minimum appears to be due to this mixing but it is not very large at the minimum.

The theoretical dipole moments of various electronic states of GaH are shown in Table 2. The dipole moment of the ground state of GaH in Table 2 (0.46 D) was found to be in good agreement with a SCF/SDCI/CPF value of 0.37 D obtained by Pattersson and Langhoff.[43] The CASSCF/SOCI method should provide more accurate dipole moments than SCF/SDCI. The $X^1\Sigma^+$ state has some ionic character with the positive charge on the metal atom. It is interesting to note that the dipole moment of the A state has opposite sign in comparison to the ground state.

The ground state of GaH arises from the $1\sigma^2 2\sigma^2$ configuration while the excited $^3\Pi$ and $^1\Pi$ states arise predominantly from the $1\sigma^2 2\sigma 1\pi$ configuration. The nature of the other electronic states in Table 1 is more complex. Interested readers should consult ref 42 for more details. The complex nature of the excited states of GaH such as $^1\Sigma^+$(II), $^1\Sigma^+$(III), etc. led to avoided crossings, resulting in multiple minima in the potential energy curves of these states (Figure 1).

Mulliken population analyses of the low-lying electronic states of GaH revealed that the $^1\Sigma^+$ ground state is a bit ionic with the polarity Ga^+H^- since the total gross population of the gallium atom was below 3.0. Most of the ionization was found to arise from a partial loss of the 4s electron to hydrogen since the gross p population of Ga was found to be close to 1.0.

B. GeH

The first band spectrum of GeH was observed by Kleman and Werhagen[44,45] in thermal emission in a King furnace. These authors observed two systems, which were assigned to a–X and A–X systems. Barrow et al.[46] reported bands in the UV region, although the rotational analysis of these could not be carried out due to low dispersion. However, Howell[47] estimated the rotational constants of the B state participating in the B–X system, while Klynning and Lindgren[48] carried out the rotational analysis of the A–X system. The A state was found to be predissociated, probably due to the crossing of a repulsive state dissociating into the ground-state atoms. The recent interest in GeH arises from the growth of germanium films by UV laser assisted chemical vapor deposition (CVD).[49,50] Multiphoton dissociation of the GeH_4 molecule also revealed the UV emission spectrum of GeH, which corresponds to the B–X system. The A–X system was studied by an electron impact method.[51]

TABLE 3. Theoretical Spectroscopic Properties of GeH[a]

state	R_e, Å	T_e, cm^{-1}	ω_e, cm^{-1}	D_e, eV
X $^2\Pi_{1/2}$	1.62	0	1806	2.34
$^2\Pi_{3/2}$	1.62	869	1810	2.30
a $^4\Sigma^-$	1.60	13914	1637	0.74
A $^2\Delta$	1.66	26663	1302	0.26
B $^2\Sigma^+$(II)	1.83	38528	1362	0.56
$^2\Sigma^+$(III)	1.67	46267	2107	3.06
$^2\Pi$(II)	1.59	49239	1999	
$^4\Sigma^-$(II)	1.95	49461	1567	1.84
$^2\Pi$(III)	1.81	50958	4121	1.37
$^4\Delta$	1.64	67455	1399	0.44

[a] From ref 57.

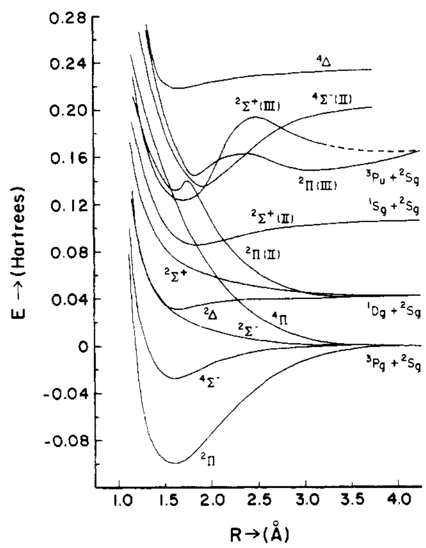

Figure 2. Potential energy curves for the electronic states of GeH (reprinted from ref 57; copyright 1988 Academic Press, Inc.). See Table 3 for assignments of known states.

The dipole moment of the ground state of GeH has been a topic of some controversy in recent years.[52–55] An experimental value of 1.24 ± 0.1 D was obtained by Brown et al.[52] using laser magnetic resonance (LMR) spectroscopy of GeH. This value was seriously questioned by four theoretical investigations,[53–55,57] all of which suggested that the dipole moment of GeH to be 0.09–0.16 D (Ge^+H^-).

The CASSCF/SOCI/RCI method of calculation was employed on 12 electronic states of GeH by Balasubramanian and Li.[57] Ten bound low-lying electronic states were found for GeH. The three experimentally observed bands (a–X, A–X, B–X) were assigned, and the uncertainties in the experimental T_e and ω_e values of these states were resolved. The D_e of GeH obtained with a CASSCF/SOCI calculation employing a large Gaussian basis set (2.81 eV) did not agree with an experimental D_e of ~3.3 eV obtained from the predissociation in the $A^2\Delta$ state.[48]

Table 3 shows the theoretical spectroscopic constants for nine electronic states of GeH obtained by Balasubramanian and Li.[57] The results in Table 3 were obtained with the CASSCF/FOCI method employing a 4s4p4d valence Gaussian basis set. Figure 2 shows the potential energy surfaces of 12 electronic states of GeH in the absence of the spin–orbit term. Among the states reported by Balasubramanian and Li, only four states have been observed experimentally through the a–X, A–X, and B–X systems. The a, A, and B states were assigned to $^4\Sigma^-$, $^2\Delta$, and $^2\Sigma^+$, respectively.

As uncertain experimental T_e value of 16 747 cm^{-1} for the a state is a bit high in comparison with the theoretical calculations, which yielded a T_e of about 14 000 cm^{-1}. The R_e value of 1.60 Å for the a state compared well with an approximate experimental value of 1.58 Å.

The experimental band origin of the A ↔ X system occurred at 25 197 cm^{-1}, in accord with experimental T_e and R_e values of the A$^2\Delta$ state, which are 25 454 cm^{-1} and 1.611 Å, respectively. As seen from Table 3, the theoretical T_e and R_e values for the A$^2\Delta$ state are 26 663 cm^{-1} and 1.66 Å, respectively, in good agreement with these values. The earlier assignment of the A–X system to the $^2\Delta$–$^2\Pi$ transition thus appears to be correct. The experimental ω_e value of the A state is uncertain due to the predissociation of the observed bands. The ω_e value of 1185 cm^{-1} listed in Huber and Herzberg[32] is somewhat low in comparison to the theoretical ω_e (1302 cm^{-1}).[57] Since the theoretical ω_e of the ground state, 1807 cm^{-1}, was found to be within 1% of the experimental result, it was believed that the theoretical ω_e of the $^2\Delta$ state should be reasonable. Klynning and Lindgren[48] reported a somewhat more accurate ω_e value of 1437 ± 24 cm^{-1} from the rotational analysis.

The experimentally observed system designated as B ← X was tentatively assigned to the $^2\Sigma^+$–$^2\Pi$ system.[48] The bands in the B ← X system could not be resolved completely presumably since these bands were predissociated. An approximate experimental T_e value of 41 074 cm^{-1} for this state was found to be, however, in reasonable agreement with the theoretical T_e value of 38 528 cm^{-1} for the $^2\Sigma^+$(II) state. As seen from Figure 2, the first $^2\Sigma^+$ state is repulsive and dissociates into Ge(^{1}D) + H(^{2}S). The B state was assigned to the second $^2\Sigma^+$ state dissociating adiabatically into Ge(^{1}S) + H(^{2}S). The theoretical R_e value of this state (1.83 Å) was noted to be considerably longer than the R_e of the X$^2\Pi$ ground state. The recommended R_e and ω_e values for the R state are 1.79 Å and 1430 cm^{-1}, respectively.[57]

Klynning and Lindgren[48] noted that the A$^2\Delta$–X$^2\Pi$ bands were predissociated probably due to the crossing of a repulsive curve dissociating into the ground-state atoms. These authors hypothesized that the $^4\Pi$ state is responsible for predissociation. As seen from Figure 2, the $^4\Pi$ repulsive curve crosses with the $^2\Delta$ curve, confirming the Klynning and Lindgren hypothesis.[48]

The D_e value of GeH calculated from predissociation of the A–X system was found to be between 22 900 and 26 600 cm^{-1}. The theoretical calculations[57] disagreed with the assumption made by Klynning and Lindgren[48] that the $^2\Sigma^+$ state dissociating into Ge(^{1}S) + H(^{2}S) would almost be repulsive. The $^2\Sigma^+$ state correlating into Ge(^{1}S) + H(^{2}S) was found to be bound; it is the B state participating in the B–X system. The $^2\Sigma^+$ state dissociating adiabatically into Ge(^{1}D) + H(^{2}S) was found to be repulsive. The best theoretical calculations gave a D_e of 2.81 eV in comparison to the lower and upper bounds of the experimental values of 2.84 and 3.30 eV. Since a comparable theoretical calculation on SeH gave a D_e value of 3.18 eV in comparison to an experimental value of 3.22 eV obtained from photoionization studies for SeH (see section III.D), a D_e value of 2.85 ± 0.05 eV was recommended by Balasubramanian and Li[57] for GeH.

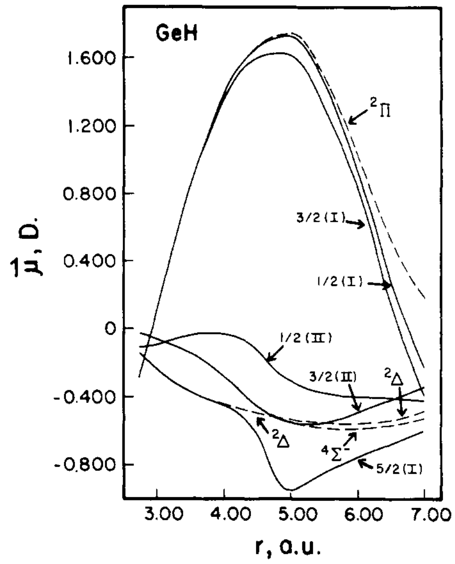

Figure 3. RCI dipole moment curves for low-lying electronic states of GeH. The positive dipole moments mean Ge$^+$H$^-$ polarity (reprinted from ref 55; copyright 1988 American Institute of Physics).

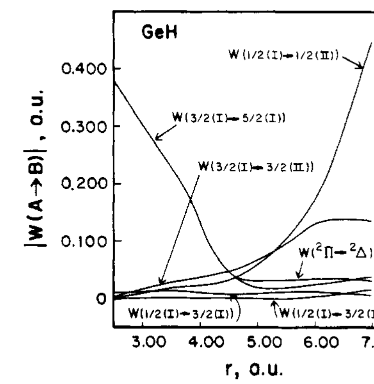

Figure 4. Electronic transition moment curves between low-lying states of GeH (reprinted from ref 55; copyright 1988 American Institute of Physics).

The dipole moments and transition moments of GeH have been the topics of discussions in many recent investigations. An experimental value of 1.24 D obtained by Brown and co-workers[52] for the dipole moment of GeH was seriously questioned by many theoretical investigators[53–55,57] who obtain a value near 0.09 D for the dipole moment of GeH. The electronegativity and periodicity arguments seemed to support the theoretical results.

Figure 3 shows the RCI dipole moment curves for the electronic states of GeH obtained by Chapman et al.[55] It is interesting to note that the curves including the spin–orbit effects are parallel to the X$^2\Pi$ dipole moment curve obtained without the spin–orbit term. Note that μ_e reaches a maximum ($^2\Pi$) and changes sign at long distance. In section VI, the dipole moment curves of GeH are compared with those of SnH and PbH. The transition moments of the various electronic transitions are shown in Figure 4. The transition labeled 1/2 → 1/2(II) corresponds to the a$^4\Sigma^-_{1/2}$ ← X$^2\Pi_{1/2}$ transition. In the absence of the spin–orbit term this transition is forbidden. Even for GeH, the transition moment for this transition becomes large at distances >4.5 bohr, indicating the importance of relativistic effects in this region. Experimentally, the a$^4\Sigma^-$–X$^2\Pi$ transition leads

TABLE 4. Spectroscopic Constants of AsH[a]

	R_e, Å		ω_e, cm^{-1}		T_e, cm^{-1}		D_e, eV		
state	theory	expt	theory	expt	theory	expt	theory	expt	μ_e,[c] D
$X^3\Sigma^-$	1.528	[1.534]	2194	2130	0	0	2.60[b]	2.80	0.178
$^1\Delta$	1.525		2190		9968		3.03		0.205
$^1\Sigma^+$	1.522		2197		17114		3.02		0.185
$A^3\Pi$	1.577	[1.58]	1398	1208	32244	[30000]	0.26		0.779
$^1\Pi$	2.467		441		36608				0.211
$^3\Pi$(II)	2.187		1386		41461				-1.315
$^1\Pi$(II)	2.561		710		44319				-0.225
$^1\Pi$(III)	1.603		3606		63288				-1.872
$^3\Pi$(III)	1.875		3264		67848				0.717
$^1\Delta$(II)	1.553		2042		72881				0.525
$^1\Sigma^+$(II)	1.552		2059		75312				0.523

[a] All theoretical values are from ref 61. All experimental values are from ref 58 except the $D_0{}^0$(AsH), which is from ref 312. [b] A superior value of 2.71 eV is obtained including 4f functions.[314] [c] Positive polarity means As^-H^+ polarity.

to the red bands of GeH. Kleman and Werhagen[44,45] have identified two bands with origins near 15370 and 16245 cm^{-1} for GeH. These bands corresponded to the $a^4\Sigma^-_{1/2}$–$X^2\Pi_{1/2}$ and $^4\Sigma^-_{3/2}$–$^2\Pi_{3/2}$ transitions of GeH. The intensity ratio of the 3/2(I) → 3/2(II):1/2(I) → 1/2(II):1/2(I) → 3/2(II) transitions was theoretically found to be 1:0.4:0.01 for GeH, in good agreement with the experimental intensity ratios of the (0–0) bands without the rotational line strength factors.

C. AsH

There are very few experimental investigations of AsH.[58-60,312] The known experimental information and tentative assignments as suggested by these authors and Huber and Herzberg[32] are shown in Table 4. The only theoretical investigation is on the ground state of AsH. Pettersson and Langhoff[43] have made SCF/SDCI/CPF calculations on the spectroscopic constants of the ground state of AsH. Balasubramanian and Nannegari[61] have completed CASSCF/SOCI calculations on AsH. Results of these calculations are summarized in Table 4.

Most of the information on the $^3\Pi$ excited states of AsH was obtained from the A ← X transition with band origins near 29282, 29822, and 30518 cm^{-1}. These bands have been tentatively assigned to the $^3\Pi_2$–$X^3\Sigma^-$, $^3\Pi_1$–$X^3\Sigma^-$, and $^3\Pi_{0^+}$–$X^3\Sigma^-$ systems. On the basis of theoretical calculations on the isoelectronic SbH[158] and BiH,[180,181] I predict that there should be $^1\Delta$, $^1\Sigma^+$, $^5\Sigma^-$ (repulsive), $^3\Pi$, and $^1\Pi$ low-lying electronic states for AsH. The author and Nannegari[61] have carried out CASSCF/SOCI calculations on these states of AsH.

Berkowitz[312] deduced an accurate D_0(AsH) to be 64.6 kcal/mol recently using high-temperature photoionization mass spectrometric methods. In this investigation and in a more recent investigation, Berkowitz and Cho[313] studied the related species AsH_2, AsH_3, etc. The singlet–triplet energy separation of $AsH_2{}^+$ was also crudely estimated.

The present author[314] carried out CASSCF/SOCI calculations employing large Gaussian basis sets that included 4f-type functions on the ground state of AsH, as well as electronic states of AsH_2, $AsH_2{}^+$, $SbH_2{}^+$, and $BiH_2{}^+$. The CASSCF/SOCI calculations yielded R_e = 1.528 Å and D_e = 62.4 kcal/mol. The theoretical D_e(HAs–H) = 69.1 kcal/mol, in excellent agreement with an experimental D_0(HAs–H) = 66.5 kcal/mol deduced by Berkowitz.[312]

The author and Nannegari[61] have completed CASSCF/SOCI calculations employing a (4s4p4d) valence Gaussian basis set on 16 low-lying electronic states of AsH. Among these, 11 bound states were found for which spectroscopic constants were calculated. The experimentally observed predissociation and Λ-doubling[58] in the A–X system were explained based on computed potential energy curves. The dipole moment curves for the low-lying states of AsH were also obtained. The theoretical spectroscopic constants for the $X^3\Sigma^-$ ground state of AsH (R_e = 1.528 Å, ω_e = 2194 cm^{-1}, D_e = 2.71 eV, μ_e = 0.18 D As^-H^+) were found to be in excellent agreement with experimental values (R_e = 1.535 Å, ω_e = 2130 cm^{-1}, D_e = 2.80 eV).

D. SeH and SeH$^+$

Radford[62] obtained the first EPR spectrum of SeH and determined the rotational and spin–orbit constants for the ground state, which were further refined by Carrington and co-workers.[63] Lindgren[64] observed diffuse spectra of SeH and SeD in the 3000–3250-Å region by employing flash photolysis of SeH_2. The observed bands in this region were tentatively assigned to an $A^2\Sigma$–$X^2\Pi_i$ transition. Donovan et al.[65] observed bands at ~55866, 66800, 69589, and 71174 cm^{-1} attributed to Rydberg transitions. These authors calculated the ionization potential of SeH to be 9.8 eV. Smyth et al.[66] and Bollmark et al.[67] obtained the spin–orbit constant of the ground state of SeH.

More recently, the vacuum-UV spectra of SeH,[70] the far-infrared laser magnetic spectrum of SeD ($X^2\Pi_{3/2}$),[71] and the fine transitions in the LMR spectrum of SeH[70-72] have been studied. These studies have yielded refined R_e and spin–orbit and spin–rotation constants for SeH. Gibson et al.[73] reported the photoionization yield curves of SeH, the dissociation energy D_0 for the SeH–H system, the dissociation energy for SeH, and the ionization potential of SeH.

The theoretical investigations on SeH to date are the CNDO/2-FPP calculations on the polarizability,[74] the SCF/SDCI calculations of Pettersson and Langhoff[43] on the ground state, and the relativistic calculations of Balasubramanian et al.[75] on SeH and SeH$^+$.

In the latest investigation on SeH,[75] CASSCF/SOCI/RCI calculations were made on the $X_1{}^2\Pi_{3/2}$, $X_2{}^2\Pi_{1/2}$, $A^2\Sigma^+_{1/2}$, 3/2(II), and 5/2 states of SeH. Spectroscopic properties of the bound states (R_e, T_e, ω_e) were computed for the electronic states of SeH. The calculated dissociation energy for the ground state including spin–orbit effects was 3.18 eV. The spin–orbit splitting constant for the ground state was calculated to be −1934 cm^{-1}. The 5/2 and 3/2(II) excited states of SeH (which

TABLE 5. Spectroscopic Properties of Low-Lying States of SeH and SeH⁺ [a]

		R_e, Å		T_e, cm⁻¹		ω_e, cm⁻¹		D_e, eV	
system	state	theory	expt	theory	expt	theory	expt	theory	expt
SeH	$X_1{}^2\Pi_{3/2}$	1.467	1.464	0.0	0.0	2371	(2400)[b]	3.18	3.22
SeH	$X_2{}^2\Pi_{1/2}$	1.467	—	1934	1764	2374	—	2.94	—
SeH	$^2\Pi$	1.466	—	1063	—	2376	—	3.19	—
SeH	$A(^1/_2(II))$	1.65	—	32 872	(31 500)[b]	2285	—	—	—
SeH	$^2\Sigma^+$	1.641	—	32 965	—	2407	—	—	—
SeH⁺	$X^3\Sigma^-_{0^+}$	1.58	—	0.0	—	2084	—	2.33	—
SeH⁺	$^1\Delta_2$	1.57	—	11 990	—	2143	—	0.84	—
SeH⁺	$^1\Sigma^+_{0^+}$	1.57	—	23 391	—	2135	—	1.63	—
SeH⁺	$^3\Pi_{0^+}$	1.73	—	31 978	—	1548	—	0.64	—

[a] μ_e(SeH) = −0.587 D (Se^-H^+).[43] All other theoretical spectroscopic constants in this table are from ref 75. [b] Experimental values are uncertain.

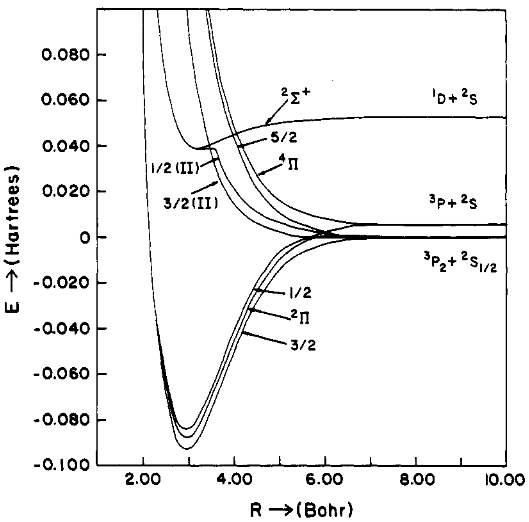

Figure 5. Potential energy curves of low-lying electronic states of SeH (reprinted from ref 75; copyright Elsevier Science Publishers B.V.). See Table 5 for assignments of known states.

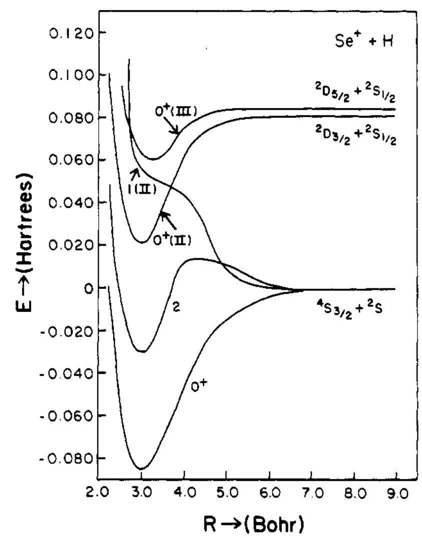

Figure 6. Potential energy curves of low-lying electronic states of SeH⁺ (reprinted from ref 75; copyright 1987 Elsevier Science Publishers B.V.). See Table 5 for assignments of known states.

are yet to be observed) exhibited interesting avoided crossings. The RCI calculations were also carried out on five low-lying electronic states of SeH⁺.[75]

Table 5 shows the theoretical and available experimental spectroscopic properties of the low-lying bound electronic states of SeH and SeH⁺. Figures 5 and 6 show the potential energy curves of the low-lying states of SeH and SeH⁺, obtained by using the SOCI and RCI methods, respectively. As seen from Table 5, the calculated R_e, ω_e, and D_e values of the ground state are in very good agreement with the experimental values, although the experimental ω_e is somewhat uncertain since the $A^2\Sigma^+$–$X^2\Pi_i$ spectral bands were found to be diffuse. The $^2\Pi_{3/2}$–$^2\Pi_{1/2}$ spin–orbit splitting was calculated[75] to be 1934 cm⁻¹, in comparison to the experimental value[71] of 1764 cm⁻¹. The diffuse spectra observed by Lindgren[64] led to an experimental estimate of the T_e value of the upper state (31 500 cm⁻¹). The theoretical T_e value[75] for the $^2\Sigma^+_{1/2}$ state was found to be 32 872 cm⁻¹, in good agreement with this estimate. The earlier tentative assignment of observed bands in this region to the $^2\Sigma^+_{1/2}$–$^2\Pi_{3/2}$ transition was thus confirmed by Balasubramanian and co-workers.[75]

Lindgren[64] obtained an approximate D_0 = 3.2 ± 0.2 eV for SeH by extrapolating the predissociated bands to Se(^{1}D) + H(^{2}S). A more definitive D_e of 3.22 eV was obtained by Gibson et al.[73] using photoionization techniques. The theoretical D_e of 3.18 eV was found to be in excellent agreement with these values.[75]

It appears that the 1/2(II)–X_2(1/2) transition has not been observed, which was predicted to be in the region of 30 938 cm⁻¹.[75] In order to observe this transition, the X_2(1/2) state should be populated appreciably. This transition cannot probably be observed in emission since the 1/2(II) state was found to be predissociated.

The theoretical adiabatic ionization energy of SeH was found to be 9.05 eV while the corresponding SeH–SeH⁺ separation at long distance was calculated as 8.86 eV.[75] The long-distance separation corresponded to the ionization potential of the Se atom, which is experimentally known to be 9.75 eV.[306] Thus, the theoretical atomic IP was found to be in 9% error in comparison to the experimental result. The corrected theoretical IP of 9.88 eV for SeH was found to be in excellent agreement with an adiabatic IP of 9.845 ± 0.003 eV reported by Gibson et al.[73]

The ground state of SeH was found to be predominantly $^2\Pi(1\sigma^2 2\sigma^2 1\pi^3)$ at near-equilibrium distances. At larger internuclear separations (R = 7.00 bohr), mixing with other configurations such as $1\sigma^2 2\sigma 3\sigma 1\pi^3$, $1\sigma^2 3\sigma^2 1\pi^3$, etc. increases. The spin–orbit mixings with other λ–s states such as $^4\Sigma^-_{3/2}$ became significant at larger internuclear distances. The 1/2(II) and 5/2 states exhibited interesting avoided crossings. At short distances the 1/2(II) state was found to be predominantly $^2\Sigma^+(1\sigma^2 2\sigma 1\pi^4)$, while at 5.00 bohr this state became predominantly $^4\Sigma^-_{1/2}(1\sigma^2 2\sigma^2 3\sigma 1\pi^2)$. This led to the predissociation shoulder in the 1/2(II) curve (see Figure

TABLE 6. Spectroscopic Constants for HBr[e]

state	R_e, Å theory	R_e, Å expt[c]	ω_e, cm^{-1} theory	ω_e, cm^{-1} expt	$\bar{\mu}$,[a] D theory	$\bar{\mu}$,[a] D expt[c]	D_e, eV theory	D_e, eV expt[c]	T_{vert},[b] cm^{-1} theory	T_e, cm^{-1} theory	T_e, cm^{-1} expt[c]
$X^1\Sigma^+$	1.455	1.414	2645	2648	0.870	0.819[d]	3.72	3.76	0	0	0
$b^3\Pi_2$	1.488	[1.473]	2445	—	−1.057	—	3.04	—	68300	67862	[67663.0]
$b^3\Pi_1$	1.489	1.442	2496	[2444]	−1.752	—	2.74	—	71154	70276	67180
$b^3\Pi_{0^+}$	1.470	[1.455]	2518	[2452]	−1.036	—	2.44		73042	72646	68998
$C^1\Pi_1$	1.51	1.46	2512	2552	−1.951	—	—	—	74889	73963	70578

[a] Dipole moments are tabulated at R_e for the respective states. Positive value of $\bar{\mu}$ indicates polarity of H^+Br^-. [b] T_{vert} is the vertical transition energy measured from r_e of the ground state. [c] From ref 32; numbers in square brackets are not certain. [d] Reference 85. [e] All the theoretical values are from ref 94.

5). This explained why the experimental $A^2\Sigma^+$–$X^2\Pi_i$ absorption bands were found to be diffuse.[64] The 5/2 state was found to be predominantly $^2\Delta_{5/2}$ at short distances but was mainly $^4\Pi_{5/2}$ at intermediate and long distances. However, this avoided crossing did not lead to a sudden change in the shape of the 5/2 curve. The 3/2(II) state was found to be predominantly $^4\Sigma^-_{3/2}$ at short distance. At long distance, however, the $^4\Pi$ and $^2\Pi$ states arising from the $1\sigma^2 2\sigma 3\sigma 1\pi^3$ configuration dominated.[75]

The $^3\Sigma^-_{0^+}$ ground state of SeH^+ was found to be almost a pure $^3\Sigma^-$ state at R_e. The 2 state of SeH^+ exhibited an interesting avoided crossing. At near R_e the 2 state was found to be $^1\Delta$, while at 5.00 bohr the $^5\Sigma^-$ state crosses with $^1\Delta$. This led to the avoided crossing of $^1\Delta_2$ with $^5\Sigma^-_2$. Thus at long distances the 2 state became $^5\Sigma^-_2$. This led to the barrier in the potential energy surface of the 2 state (see Figure 6). The 0^+(III) and 1(II) states of SeH^+ exhibited interesting trends as a function of distance. The inflections in the 1(II) surface were attributed to the changes in the contributions of various λ–s states as a function of distance.[75]

E. HBr and HBr⁻

The spectroscopic investigations of low-lying electronic states of the HBr molecule have been the subjects of many experimental investigations.[75–94] The vacuum-UV absorption spectra of HBr were studied by Price[76] and by Barrow and Stamper.[77,78] Ginter and Tilford[79,80] reexamined the absorption spectra of HBr in the 66000–79500-cm^{-1} region and assigned the observed bands to transitions from the ground state to the upper states that originated from the $(5s\sigma)\pi^3$, $(5p\sigma)\pi^3$, and $(5p\pi)\pi^3$ excited configurations.

The absorption continua near 56500 cm^{-1} were attributed mainly to transitions between the ground state and the repulsive $A^1\Pi$ state, arising from the $(\sigma^*\pi^3)$ configuration. Mulliken[82,83] analyzed the electronic spectra of heteropolar diatomic molecules.

The ground state of HBr has been studied experimentally and theoretically.[89–94] Ab initio spectroscopic constants,[91] dissociation energies, and electric dipole moments[90,91] of the ground state have been obtained which were found to be in excellent agreement with known experimental results.

The HBr^- anion and other halide ions have been the subjects of a large number of studies[95–121,123–129] since they can be formed by electronic attachment. The mechanisms that govern the HBr^- production and electron attachment processes are not entirely clear. In the fixed-finite dipole model,[110] an infinite number of bound states of an electron are predicted for attachment of an electron into a dipole field that exceeds 1.625 D,

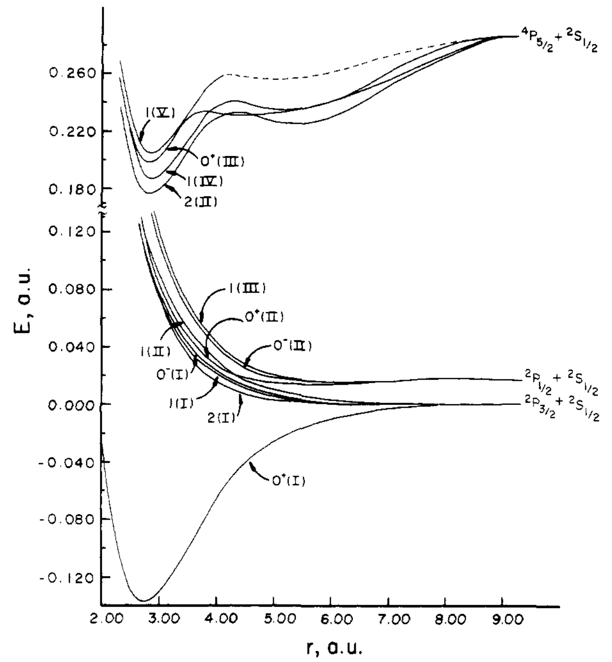

Figure 7. Potential energy curves for the low-lying electronic states of HBr (reprinted from ref 94; copyright 1987 Elsevier Science Publishers B.V.). See Table 6 for assignments of known states.

while no bound states of the electron are predicted for attachment into dipole fields below this value. In the absence of nonadiabatic effects, HBr^- (μ = 0.82 D) was predicted to be unstable with respect to autodetachment of the electron since its dipole moment is known to be below the critical value of 1.625 D.

The formation of H^- ions by dissociative attachment between 3 and 9 eV was observed in HBr and HI. The ^2P ground states of the halogen atoms are split by spin–orbit coupling into the $^2P_{3/2}$ and $^2P_{1/2}$ atomic states, providing two exit channels for H^- production. The upper $^2\Sigma^+$ and $^2\Pi$ states of HBr^- and HI^- are similarly split up by the spin–orbit coupling into their components ($^2\Sigma^+_{1/2}$, $^2\Pi_{3/2}$, and $^2\Pi_{1/2}$). The $^2\Sigma^+_{1/2}$ and $^2\Pi_{3/2}$ components should dissociate into the lower $H^-(^1S_0)$ + $X(^2P_{3/2})$ limit, while the $^2\Pi_{1/2}$ state should dissociate into the upper $H^-(^1S_0)$ + $X(^2P_{1/2})$ asymptote. The excited $^2\Sigma^+_{1/2}$ state of HBr^- was suggested to dissociate through both the $H^-(^1S_0)$ + $Br(^2P_{3/2})$ and $H^-(^1S_0)$ + $Br(^2P_{1/2})$ channels.

While there are many ab initio calculations on HCl^-, this is not the case for HBr^-. Chapman et al.[129] carried out accurate CASSCF/SOCI calculations employing large diffuse Gaussian basis sets on HBr^- and HI^-.

The theoretical SCF/RCI spectroscopic constants[94] for the electronic states of HBr and the corresponding experimental values are given in Table 6. The actual

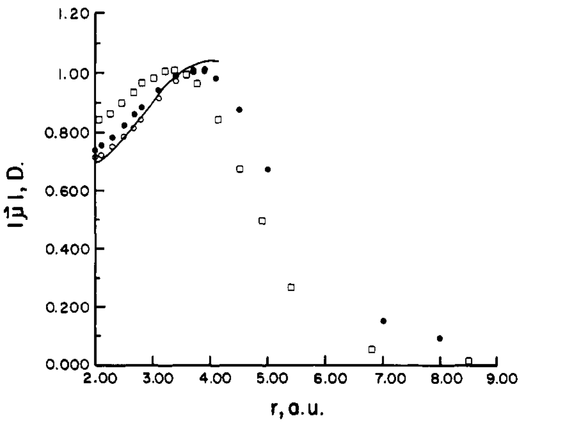

Figure 8. Comparison of the dipole moments obtained using SCEP/CEPA(0),[91] RCI (●),[94] and MCSCF[92] (□) methods with the experimental curve (—) (reprinted from ref 94; copyright 1989 Elsevier Science Publishers, B.V.).

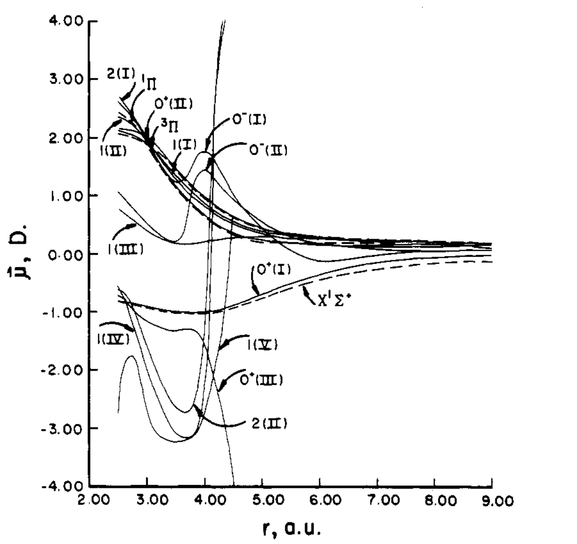

Figure 9. Dipole moment curves for the excited electronic states of HBr (reprinted from ref 94; copyright 1987 Elsevier Science Publishers B.V.).

potential energy curves of 12 electronic states of HBr obtained by Chapman et al.[94] are shown in Figure 7. Figure 8 shows the dipole moment curves for the $X^1\Sigma^+$ ground state of HBr obtained by using three different theoretical methods and the plot of known experimental values. Figure 9 shows the dipole moment curve for the excited electronic states of HBr.

As seen from Figure 8, the ECP dipole moment curve exhibits the correct behavior between 2 and 3.8 bohr. The experimental μ becomes divergent from theoretical results for $R > 3.7$ bohr, while there are no CEPA μ for long distances. The RCI curve and the MCSCF curve of Ogilvie et al.[92] exhibit a maximum. The ECP dipole moments of HBr are within 6% of the all-electron CEPA results.[91]

The theoretical spectroscopic constants in Table 6 are in excellent agreement with available experimental results. It is clear from Table 6 and Figure 7 that the ground state is well separated from the other bound states of HBr. Most of the other states that can possibly be seen near visible–UV regions were found to be repulsive (Figure 7).

As is well known, the ground state of HBr arises from the $1\sigma^2 2\sigma^2 1\pi^4$ configuration. The bromine–hydrogen bond results primarily from interactions between the

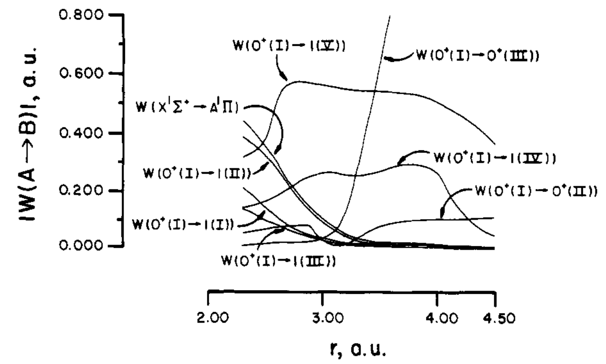

Figure 10. Electronic transition moment curves for HBr (reprinted from ref 94; copyright 1987 Elsevier Science Publishers B.V.).

Br $4p_z$ and H 1s orbitals to form the 2σ orbital. The 1σ orbital is predominantly of Br 4s character. The π electrons are localized on Br and are essentially nonbonding; promotion of a π electron into the lowest virtual antibonding σ orbital (3σ) gives rise to $^3\Pi_i$ and $^1\Pi$ λ–s states, which are split by spin–orbit interaction into 2, 1, 0^+, 0^-, and $1(^1\Pi)$ ω–ω states. These states form the repulsive manifold of the curves shown in Figure 7. The excitation of a 2σ electron from the ground-state configuration into the virtual 3σ orbital results in the $^1\Sigma^+$ and $^3\Sigma^+$ states. The $^1\Sigma^+$ state dissociates into the ionic species ($Br^- + H^+$), while the $^3\Sigma^+$ state dissociates into the ground-state limit. (See the 0^-(II) and 1(III) curves of Figure 7.) Between the ground state and the terms that arise from the $1\sigma^2 2\sigma^2 3\sigma 1\pi^3$ and $1\sigma^2 2\sigma 3\sigma 1\pi^4$ ($^3\Sigma^+$) configurations, one spectral band was found experimentally.[32] The absorption continuum with a maximum near 56 500 cm^{-1} was assigned to the $A^1\Pi \leftarrow X$ absorption.[94] The A state corresponds to the 1(II) curve in Figure 7. The calculated verticle transition energy to the 1(II) state was 57 100 cm^{-1},[94] in good agreement with experiment.

The 0^+(II), 1(I), 1(II), 1(III), 0^-(I), 0^-(II), and 2(I) ω–ω states were found to be opposite in polarity (Br^+H^-) to the ground state (Br^-H^+). Thus, these states may be characterized as charge-transfer states that arise from excitation into the antibonding 3σ orbital. Figure 10 shows electronic transition moment curves for the parallel $0^+(I) \rightarrow 0^+(II)$ and perpendicular $0^+(I) \rightarrow 1(I)$, $0^+(I) \rightarrow 1(II)$, and $0^+(I) \rightarrow 1(III)$ transitions. The transition moments without the spin–orbit terms for the $A^1\Pi \leftarrow X^1\Sigma^+$ transitions are also shown in Figure 10. The transition moment $W(0^+(I) \rightarrow 1(II))$ is much larger than the other moments $W(0^+(I) \rightarrow 1(I))$, $W(0^+(I) \rightarrow 0^+(II))$, and $W(0^+(I) \rightarrow 1(III))$ at the ground state R_e. At this distance, comparison of the transition moments with and without the spin–orbit coupling term ($W(0^+(I) \rightarrow 1(II))$, $W(X^1\Sigma^+ \rightarrow A^1\Pi)$) gives the magnitude of spin–orbit contamination in the 1(II) state (Figure 9). At 2.73 bohr, the 1(II) wave function was found to be 64% $^1\Pi_1$ from the $1\sigma^2 2\sigma^2 3\sigma 1\pi^3$ configuration and 11% $^3\Pi_1$. Consequently, the transition moment $W(0^+(I) \rightarrow 1(II))$ is lowered by about 5% relative to $W(X^1\Sigma^+ \rightarrow A^1\Pi)$ due to singlet–triplet mixing in the 1(II) state. This state exhibited interesting behavior at long distances. Up to 5.00 bohr, this state was found to be predominantly $^1\Pi_1(1\sigma^2 2\sigma^2 3\sigma 1\pi^3)$; near 7.00 bohr, however, the $^1\Pi_1$ curve underwent an avoided crossing with the $^3\Sigma_1^+$ state from the $1\sigma^2 2\sigma 3\sigma 1\pi^4$ configuration. Thus, for distances larger than 7.00 bohr, the 1(II) state be-

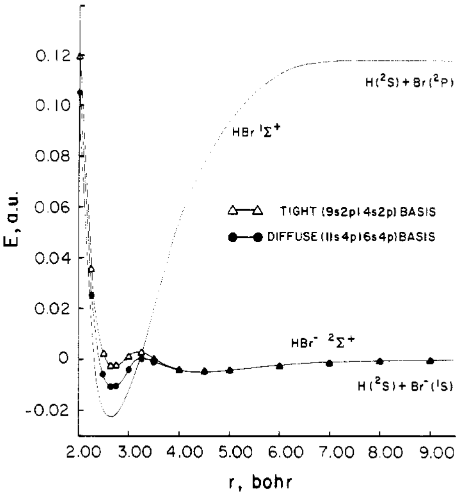

Figure 11. CASSCF/SOCI potential energy curves of the ground states of HBr and HBr⁻ obtained using two basis sets (reprinted from ref 129; copyright 1988 American Institute of Physics).

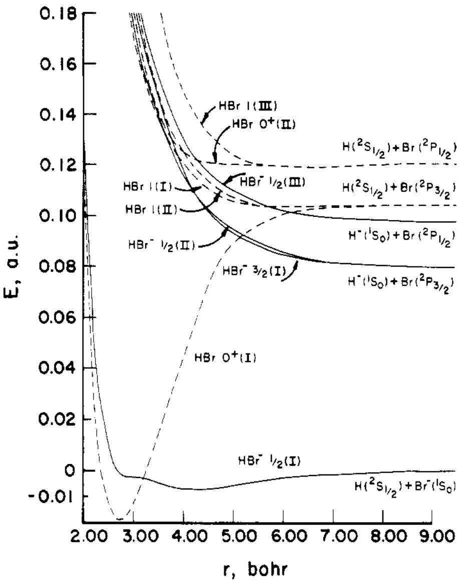

Figure 12. RCI potential energy curves of the low-lying electronic states of HBr and HBr⁻ (reprinted from ref 129; copyright 1988 American Institute of Physics).

came predominantly $^3\Sigma_1^+$, while at these distances the 1(III) state became predominantly $^1\Pi_1$. This is reflected in the transition moment curves.

The excitation of a π-electron from the ground-state configuration of HBr into the 5σ Rydberg orbital generates $^3\Pi_i$ and $^1\Pi$ λ–s states. These curves correspond to the 2(II), 1(IV), 0⁺(III), and 1(V) curves (Figure 7). Ginter and Tilford[79] discussed transitions from the ground state of HBr into the $^3\Pi_i$ and $^1\Pi$ states derived from a $(5s\sigma)\pi^3$ configuration, which were designated as the $b^3\Pi_i \leftarrow X^1\Sigma^+$ and $C^1\Pi \leftarrow X^1\Sigma^+$ bands. The ω–ω states arising from the $1\sigma^2 2\sigma^2 5\sigma 1\pi^3$ configuration dissociate into the $(^4P_{5/2} + {}^2S_{1/2})$ asymptote at long distances. The calculated $^2P_{3/2}$–$^4P_{5/2}$ splitting[94] of 63 154 cm^{-1} was found to be in excellent agreement with the experimental value of 63 529 cm^{-1}.[306] Since the $J = 3/2$ and 1/2 states of ^4P are only within 3447 cm^{-1} of $^4P_{5/2}$, states dissociating into these limits could mix strongly.

The theoretical spectroscopic constants for the 2(II), 1(IV), 1(V), and 0⁺(III) states are in Table 6. The theoretical constants are in generally good agreement with the experimental values although the 1(V) wave function was not considered to be very reliable past 4.50 bohr by Chapman et al.[94]

In Figure 10, the electronic transitions labeled 0⁺(I) → 1(IV), 0⁺(I) → 0⁺(III), and 0⁺(I) → 1(V) correspond to the $b^3\Pi_1 \leftarrow X^1\Sigma^+$, $b^3\Pi_{0^+} \leftarrow X^1\Sigma^+$, and $C^1\Pi_1 \leftarrow X^1\Sigma^+$ transitions assigned by Ginter and Tilford.[79]

The intensity estimates for the (0–0) bands of the $b^3\Pi_2 \leftarrow X^1\Sigma^+$, $b^3\Pi_1 \leftarrow X^1\Sigma^+$, $b^3\Pi_{0^+} \leftarrow X^1\Sigma^+$, and $C^1\Pi_1 \leftarrow X^1\Sigma^+$ transitions of HBr were presented by Ginter and Tilford.[79] The ratio of the intensities of $C^1\Pi_1 \leftarrow X^1\Sigma^+$ (0–0) to $b^3\Pi_1 \leftarrow X^1\Sigma^+$ (0–0) bands was found to be 5:1, while the relative intensity of the (0–0) bands of $b^3\Pi_1 \leftarrow X^1\Sigma^+$ to $b^3\Pi_{0^+} \leftarrow X^1\Sigma^+$ was found to be 1:0.02 without rotational line strengths. The ratio of theoretical intensities for transitions 0⁺(I) → 1(V) to 0⁺(I) → 1(IV) is 4.6:1, in good agreement with experiment. The intensity ratio for the (0–0) bands of 0⁺(I) → 1(IV) and 0⁺(I) → 0⁺(III) near R_e for these states was found to be approximately 1:0.01,[94] again a reasonable agreement with experiment.

Figure 11 shows the CASSCF/SOCI curves for the $^2\Sigma^+$ state of HBr⁻ and the $^1\Sigma^+$ state of HBr obtained by Chapman et al. Figure 12 shows the RCI potential curves for the 1/2(I), 1/2(II), 1/2(III), and 3/2(I) states of HBr⁻ and the potential curves for their probable parent HBr states.

As seen from Figure 11, the HBr⁻ (SOCI) curve crosses at 3.25 bohr (tight basis), while the RCI HBr/HBr⁻ crossing occurs near 3.20 bohr. The overall effect of the diffuse basis in the SOCI calculations was to move the curve crossings toward shorter distances by 0.05 bohr. The RCI HBr⁻ 1/2(I) D_e was calculated as 0.14 eV.

The electron affinity of HBr ($EA_{AD} = E[HX(R_e^{HX})] - E[HX^-(R_e^{HX^-})]$) was calculated as −0.326 eV (RCI) while the SOCI results gave a value of −0.485 eV. Both results indicated that the HBr⁻ anion should be unstable with respect to electron autodetachment.

The formation of H⁻ ions by dissociative electron attachment between 5 and 10 eV in HBr has been the topic of some investigations. The potential energy curves for the upper $^2\Sigma_{1/2}^+$, $^2\Pi_{3/2}$, and $^2\Pi_{1/2}$ states of HBr⁻ were obtained from these experimental data. The 1/2(II), 3/2(I), and 1/2(III) curves in Figure 12 correspond to the $^2\Sigma_{1/2}^+$, $^2\Pi_{3/2}$, and $^2\Pi_{1/2}$ states, respectively. The 0⁺(II), 1(I), 1(II), and 1(III) curves of HBr correspond to the $a^3\Pi_{0^+}$, $a'^3\Pi_1$, $A^1\Pi_1$, and $^3\Sigma_1^+$ states, respectively.

The HBr⁻ 1/2(II), 3/2(I), and 1/2(III) curves cross the HBr 0⁺(I) curve at $R > 5.00$ bohr (Figure 12). The electron affinity of hydrogen (6082 cm^{-1}) was found to exceed the $^2P_{3/2}$–$^2P_{1/2}$ atomic splitting of bromine (3685 cm^{-1})[306] and, consequently, the H⁻($^1S_0$) + Br($^2P_{3/2}$, $^2P_{1/2}$) limits lie below the neutral H($^2S_{1/2}$) + Br($^2P_{3/2}$) asymptote. It was noted that, although the HBr⁻ resonances are essentially repulsive, the splitting between the H⁻($^1S_0$) + Br($^2P_{3/2}$, $^2P_{1/2}$) limits at 15.00 bohr was 3591 cm^{-1}, which suggested that the negative-ion curves become very slightly attractive at longer distances due to the dispersion-type interactions. At the Franck–Condon region of the HBr ground state, the HBr⁻ 1/2(II), 3/2(I), and 1/2(III) curves were found to lie slightly above or within the manifold of 1(I), 1(II), and 0⁺(II) states arising from the neutral $1\sigma^2 2\sigma^2 3\sigma 1\pi^3$ configuration.

TABLE 7. Spectroscopic Constants for InH[a]

state	R_e, Å	T_e, cm^{-1}	ω_e, cm^{-1}	μ_e, D	D_e, eV
$X^1\Sigma^+$	1.838 (1.820)	0	1476 (1524)	(0.460)	2.48 (2.60)
$a^3\Pi_{0^-}$	1.776	16230	[1303]		
$a^3\Pi_{0^+}$	1.779	16278	1459		
$a^3\Pi_1$	1.768	16942	1415		
$a^3\Pi_2$	1.753	17800	[1301]		
$A^1\Pi$	[2.09]	22655	[142]		

[a] Experimental values are from ref 32. Theoretical values in parentheses are from ref 141. The dipole moment was obtained from a theoretical CASSCF/SOCI calculation of Balasubramanian.[141] The numbers in square brackets are uncertain.

F. InH

There are no theoretical calculations on the electronic states of InH, although Kim and Balasubramanian[141] completed CASSCF/SOCI calculations on the spectroscopic constants of the $^1\Sigma^+$ ground state of InH. Table 7 shows the experimental spectroscopic constants for InH collected by Huber and Herzberg[32] together with these theoretical constants[141] for the ground state. In summary, there are many experimental works[130-140] on InH that have led to the observation of the a–X and A–X transitions. The a and A states were both found to be predissociated. The $D_0°$ value of 2.48 eV was estimated from the predissociation of the A–X and a–X bands. The theoretical SOCI D_e value of InH was found to be 2.60 eV.[141] The Λ-type doublings were found in some of the electronic states of InH.

Veseth and Lofthus[139] suggested the existence of a $^3\Sigma^+$ state that was presumed to be repulsive and responsible for the anomalies seen in the Λ-doubling of the $a^3\Pi_1$ component. The $^3\Sigma^+$ state was also suggested as being responsible for the predissociation of all the $a^3\Pi$ components. On the basis of the selection rules for predissociation, the $^3\Sigma^+_{0^-}$ and $^3\Sigma^+_1$ states can interact with the $^3\Pi_{0^-}$ and $^3\Pi_1$ components through spin–orbit coupling. Thus the $^3\Sigma^+$ state can predissociate these components. The predissociation of $^3\Pi_2$ and $^3\Pi_{0^+}$ through $^3\Sigma^+$ cannot occur unless the molecule is rotating. Consequently, if $^3\Pi_2$ and $^3\Pi_{0^+}$ states are predissociated by $^3\Sigma^+_1$, they should show dependence of predissociation rate on the rotational J quantum number. On the basis of the earlier calculations of Kim and Balasubramanian,[42] I conclude that there is certainly a $^3\Sigma^+$ curve for InH that dissociates into the ground-state atoms. For GaH, the $^3\Sigma^+$ curve was found to be repulsive and lies above the $a^3\Pi$ and $A^1\Pi$ curves. The possibility of $^3\Sigma^+_1$–$a^3\Pi_1$, $^3\Sigma^+_1$–$A^1\Pi_1$, and $^3\Sigma^-_0$–$^3\Pi_{0^-}$ mixings in InH should be nonnegligible due to the spin–orbit coupling term. Kim and Balasubramanian are at present carrying out CASSCF/SOCI/RCI calculations on many electronic states of InH with the objective of understanding these riddles.

Bahnmaier et al.[315] have recently obtained the infrared spectrum of InH in its $^1\Sigma^+$ ground state using a diode laser spectrometer. A total of 83 transitions were measured, yielding the most accurate Dunham parameters for the ground state and an improved R_e = 1.83776 Å.

G. SnH

The early electronic spectra of SnH were recorded by Watson and Simon[142,143] in 1939–1940. The spectra contained bands in the red and two red-degrading bands in the violet. The red bands and the violet bands were assigned to $^2\Sigma^+$–$^2\Pi$ and $^2\Delta$–$^2\Pi$ transitions, respectively ($^2\Pi$ is the ground state). Kleman[131] reinterpreted the red bands as due to a $^4\Sigma^-$–$X^2\Pi$ transitions by analogy to lighter group IV hydrides. Klynning and co-workers[145,146] also recorded the absorption spectra of SnH and SnD. Energy expressions for these bands were fitted. Centrifugal distortion of the spin-orbit and spin–rotation interaction for several states of SnH was considered. Theoretical analysis of the spin–orbit splitting of the $A^2\Delta$ and $a^4\Sigma^-$ states was considered by Veseth.[151] The experimental works and their analysis of SnH are contained in ref 142 to 152.

TABLE 8. Spectroscopic Properties of SnH[a]

		T_e, cm^{-1}	A or 6λ, cm^{-1}	R_e, Å	ω_e, cm^{-1}
$X^2\Pi$	theory	0	2376	1.83	1600
	expt	0	2179	1.78	1715
$a^4\Sigma^-$	theory	13265	328	1.78	1560
	expt	15580	270	1.77	1521
$A^2\Delta$	theory (5/2)	26460		1.96	700
	expt	23790	(20)	1.85	1080

[a] Theoretical results are from ref 152. Experimental constants are from ref 32.

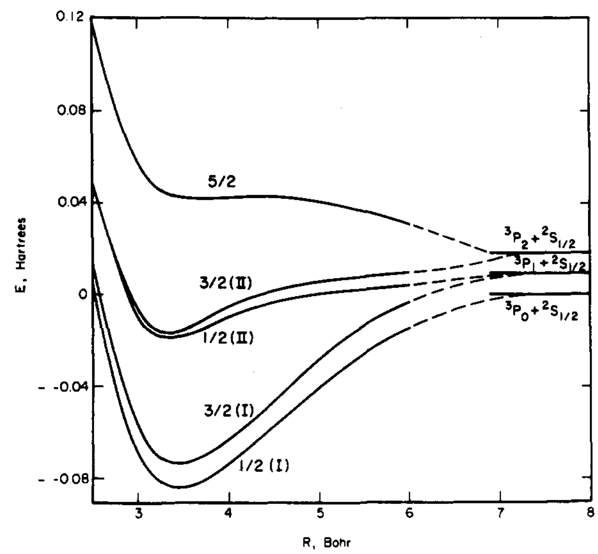

Figure 13. SCF/RCI potential energy curves of the electronic states of SnH (reprinted from ref 152; copyright 1984 Academic Press, Inc.). See Table 8 for assignments of known states.

Balasubramanian and Pitzer[152] made relativistic SCF/RCI calculations including the spin–orbit term for eight low-lying electronic states of SnH. The spectroscopic constants and the potential energy curves for these states were calculated by using this method employing a double-ζ STO basis set. Chapman et al.[55] in a later investigation employed a more accurate triple-ζ STO basis as well as CASSCF/SOCI method in conjunction with large valence Gaussian basis sets. The dipole moment curves for the electronic states of SnH in addition to the transition moment curves as a function of internuclear distance have now been obtained.[55] Table 8 shows the spectroscopic constants of SnH and comparison with known experimental results. Figure 13 shows the SCF/RCI potential energy curves of the low-lying electronic states of SnH. As seen from Table 8, the agreement between theory and experiment is very good at the level of calculations employed. The calculated total excitation energy to the $^4\Sigma^-$ term is within 15% of the observed value.

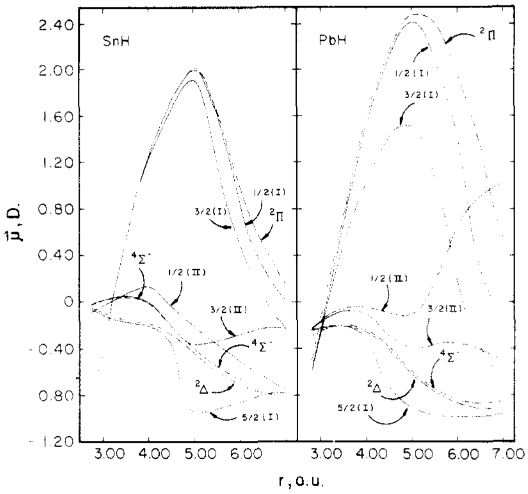

Figure 14. RCI dipole moment curves for the electronic states of SnH and PbH (refprinted from ref 55; copyright 1988 American Institute of Physics).

The $A^2\Delta$–$X^2\Pi$ bands of SnH exhibited[145] predissociation with line broadening beginning at the energy of 25 177 cm^{-1}. The SCF/RCI calculations of Balasubramanian and Pitzer[152] indicated that the 5/2 state (shown as the uppermost curve in Figure 13) is predominantly $^2\Delta_{5/2}$ at a bond distance of 3.4 bohr but that it has a broad maximum (Figure 13) arising from an avoided crossing with the $^4\Pi_{5/2}$ state. Thus some quantum tunneling was anticipated, which should result in line broadening to a lower energy for SnH than for SnD. Huber and Herzberg[32] reported an upper estimate for $D_0°$ of SnH as 2.73 eV obtained if dissociation to the $^3P_2$ + $^2S_{1/2}$ atoms was assumed. The calculations of Balasubramanian and Pitzer[152] revealed a potential maximum substantially above that energy. Hence the dissociation energy of SnH was estimated as 2.3 eV.[152]

A more recent and sophisticated CASSCF/SOCI investigation of the electronic states of SnH was carried out by Chapman et al.[55] The RCI ω_e value obtained for the ground state of SnH using a triple-ζ STO basis was found to be 1689 cm^{-1}, agreeing well with the experimental value in Table 8 (1715 cm^{-1}). The RCI ω_e values for the excited states of SnH also did not differ significantly from the earlier results.[152] The dipole moment (μ_e) of the SnH molecule in the $^2\Pi_{1/2}$ ground state was calculated to be 0.398 D, while the corresponding μ_e for the $^2\Pi_{3/2}$ state was calculated as 0.393 D. The dipole moment of the ground state of SnH was calculated by Pettersson and Langhoff[53] using the SCF/SDCI method as 0.357 D with Sn^+H^- polarity.

The calculated dipole moment curves of the various electronic states of SnH and PbH are shown together in Figure 14. Figure 15 shows the electronic transition moment curves as a function of the internuclear distance for SnH and PbH as obtained by Chapman et al.[55] Note that the dipole moment curves of the $^2\Pi_{1/2}$ and $^2\Pi_{3/2}$ states of both SnH and PbH reach a maximum, eventually reaching zero at long distance. As seen from Figure 14, the spin–orbit effects on the dipole moments of the $^2\Pi_{3/2,1/2}$ components of PbH are substantially larger.

Comparison of the transition moment curves in Figure 15 with the corresponding curves in Figure 4 for GeH clearly demonstrates the large relativistic effects in PbH. In particular, note the dramatically large transition moment for the 1/2(I) → 1/2(II) transition of PbH. The intensity ratios of the 3/2(I) → 3/2(II):1/2(I) → 1/2(II):1/2(I) → 3/2(II) transitions were calculated as 1:0.5:0.01 for the (0–0) bands of SnH without the rotational line strength factors.

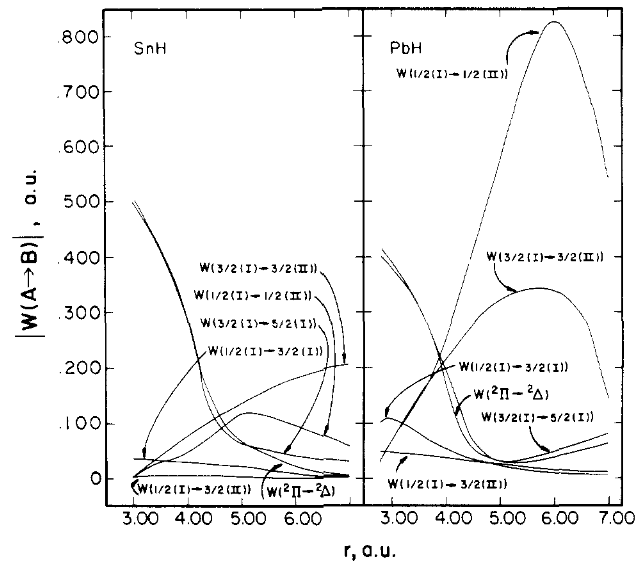

Figure 15. Electronic transition moment curves of SnH and PbH (reprinted from ref 55; copyright 1988 American Institute of Physics).

The observed red bands of SnH were resolved into two components by Klynning et al.;[145] the first of these was assigned to $^4\Sigma^-_{3/2} \leftarrow {}^2\Pi_{3/2}$ while the second was assigned to the $^4\Sigma^-_{1/2} \leftarrow {}^2\Pi_{1/2}$ transition. The theoretical transition energies for the SnH bands (14 122, 12 479 cm^{-1})[55] agreed with the interpretation of Klynning et al.[145]

H. SbH

The SbH molecule was studied in the flash photolysis of SbH_3.[153–155] Bollmark and Lindgren[153] obtained the absorption bands of SbH in the 3300–3450-Å region, which were assigned to the $A^3\Pi$–$X^3\Sigma^-$ systems. The rotational constant and R_e of the ground state were obtained from rotational analysis. Basco and Yee[154] studied the $A^3\Pi$–$X^3\Sigma^-$ system and noted that only the $A^3\Pi_{0^+}$–$X^3\Sigma^-$ system has rotational structure. Bollmark and Lindgren[155] carried out the rotational analysis of the absorption spectra of SbH and calculated the spin–orbit splitting of the ground state (0^+–1 splitting) as 660 cm^{-1}. These authors proposed that there should be $B0^+$ and $C0^+$ states that cause perturbation to the $^3\Pi_{0^+}$ bands, leading to predissociation of the $^3\Pi$ state. The other experimental works on SbH can be found in ref 156 and 157.

Balasubramanian, Tanpipat, and Bloor[158] made relativistic SCF/RCI calculations on nine low-lying ω–ω and four λ–s states (without spin–orbit coupling) of SbH. A double-ζ STO basis with the 14-electron RECPs was employed for the antimony atom. These calculations were useful in the interpretation of the experimentally observed bands.

Table 9 shows the spectroscopic constants of the low-lying electronic states of SbH while Figures 16 and 17 show the potential energy curves of the electronic states of SbH with and without the spin–orbit term, respectively.

TABLE 9. Spectroscopic Properties of SbH[a]

	R_e, Å		T_e, cm^{-1}		ω_e, cm^{-1}	
state	theory	expt	theory	expt	theory	expt
X_1 0^+(I)	1.81	1.72	0	0	1763	—
X_2 1	1.81	—	696	655	1762	—
2	1.81	—	9362	—	1784	—
0^+(II)	1.80	—	15772	—	2061	—
A_3 0^+(III)	1.87	[2.03]	30788	30116	1085	—
0^+(IV)	—	—	34891	—	—	—
$^3\Sigma^-$	1.81	—	919	—	1768	—
$^1\Delta$	1.81	—	9607	—	1786	—
$^1\Sigma^+$	1.79	—	17876	—	1804	—

[a] All theoretical results are from ref 158.

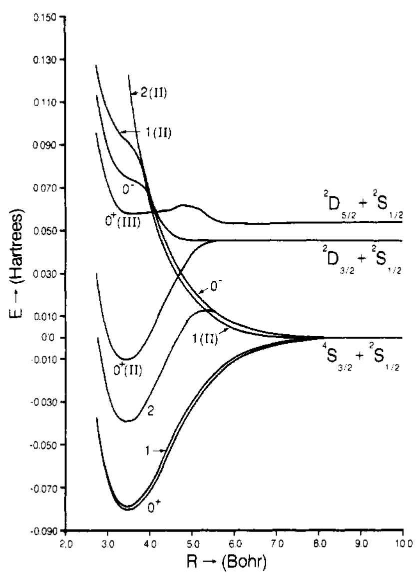

Figure 16. Potential energy curves of the low-lying electronic states of SbH including the spin–orbit term (reprinted from ref 158; copyright 1987 Academic Press, Inc.). See Table 9 for assignments of known states.

The A–X system observed in absorption was assigned to the 0^+(III) ($^3\Pi_{0^+}$) ← X(0^+) transition. The theoretical and experimental T_e values are in very good agreement (Table 9). The spin–orbit splitting (0^+–1 splitting) of the ground state was calculated as 696 cm^{-1} [158] in comparison to a value of 660 cm^{-1} obtained by Bollmark and Lindgren[155] from the rotational analysis.

Theoretical calculations of Balasubramanian et al.[158] predicted the spectroscopic properties of a number of states (1, 2, 0^+(II), 0^+(IV)) of SbH that are yet to be observed. The 0^+(II)–0^+(I) system corresponds to a $^1\Sigma^+_{0^+}$–$^3\Sigma^-_{0^+}$ transition and should be observable since the spin–orbit effects were found to be nonnegligible. Theoretical calculations predicted this transition in the region of 15770 cm^{-1}.[158] Similarly, the 0^+(IV)–X0^+(I) transition should be observable in the 35000-cm^{-1} region. Bollmark and Lindgren[155] observed a C state that perturbed the bands in the $A^3\Pi_{0^+}$–X0^+ system with a T_0 value of 30566 cm^{-1}. Thus, the 0^+(IV) state could possibly be the C state.

The theoretical dissociation energy of the SbH radical was calculated as 2.26 eV.[158] There is no experimental D_e value for the SbH radical at present. Since SCF/RCI calculations yield 85% of the experimental D_e value due to neglect of higher order correlation corrections, it was predicted that the D_e of SbH should be 2.7 ± 0.2 eV.[158]

The electronic states of SbH exhibited avoided crossings analogous to those of BiH, which resulted in

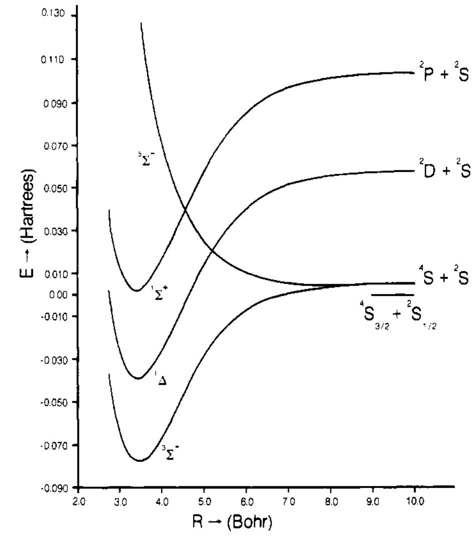

Figure 17. Potential energy curves of four electronic states of SbH without the spin–orbit term (reprinted from ref 158; copyright 1987 Academic Press, Inc.).

TABLE 10. Spectroscopic Constants of Low-Lying States of TeH[a]

	T_e, cm^{-1}		R_e, Å		ω_e, cm^{-1}		D_e, eV	
state	theory	expt	theory	expt	theory	expt	theory	expt
X_1 3/2	0.0	0.0	1.767	1.74	1839	—	2.31	—
X_2 1/2	3989	3830	1.77	—	1845	—	1.81	—
$^2\Pi$	2449	—	1.77	—	1855	—	2.35	—

[a] All theoretical values are from ref 161.

exotic shapes of potential curves. For example, the barrier in the 2 curve is due to the avoided crossing of $^1\Delta_2$ with $^5\Sigma^-_2$. Similarly, the 0^- state became predominantly $^5\Sigma^-_{0^-}$ at long distances.

The fact that only the $A^3\Pi_{0^+}$–$^3\Sigma^-_{0^+}$ system shows rotational structure can be explained based on theoretical calculations of Balasubramanian et al. As seen from Figures 16 and 17, the $^5\Sigma^-$ curve, which dissociates into the ground-state atom, is repulsive. This state contains Ω = 2, 1, and 0^- components. Consequently, only the $^3\Pi_{0^+}$ state cannot interact with $^5\Sigma^-$ repulsive state. This should explain the experimental findings that only the A–X system shows rotational structure among the $^3\Pi$ Ω components.

I. TeH

Little et al.[159] studied the vacuum-UV spectra of TeH, although the resolution was insufficient to resolve the rotational structure. The spin–orbit constant for the ground state of TeH was obtained from the ESR spectra. Freidhoff et al.[160] studied the negative-ion photodetachment spectra of TeH^-, which revealed the electron affinity of TeH.

Balasubramanian, Han, and Liao[161] carried out relativistic SCF/RCI calculations on five low-lying electronic states of TeH. The spectroscopic constants and the potential energy curves of the low-lying states of TeH were obtained.

Table 10 shows the theoretical spectroscopic constants together with available experimental data on the low-lying states of TeH. Figure 18 shows the calculated potential curves of the 3/2, 1/2, 3/2(II), 1/2(II), 5/2, $^2\Pi$, and $^4\Pi$ states. There are no experimental ω_e values for the 3/2 and 1/2 states. The calculated dissociation

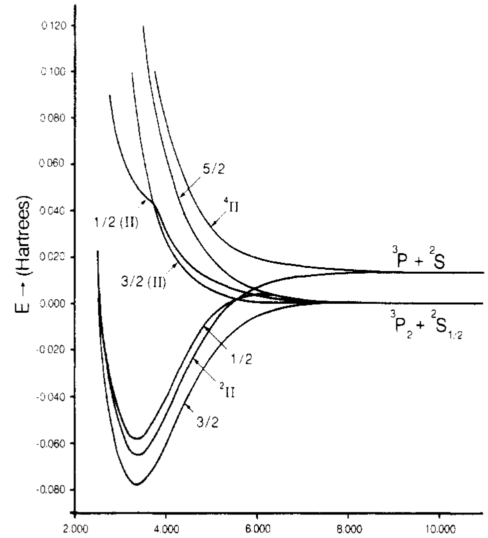

Figure 18. Potential energy curves of low-lying electronic states of TeH without the spin–orbit term (reprinted from ref 161; copyright 1987 American Institute of Physics). See Table 10 for assignments of known states.

energy of the $X_1(3/2)$ ground state is (2.31 eV) 0.04 eV lower than the corresponding $^2\Pi$ λ–s state. The D_e value of the 1/2 state is, however, much lower (1.81 eV), due to the significant spin–orbit splitting and contamination of this state. We predicted that the D_e value of the ground state should be 2.75–3.00 eV, although the experimental D_e is not known at present.

Since the 1/2(II), 3/2(II), and 5/2 curves are repulsive (Figure 18), transitions from the two spin–orbit components (X_1, X_2) of the ground state to these states can be seen only in absorption. This is consistent with the known experimental spectra of TeH. There are four absorption bands below 55 000 cm^{-1}, which are labeled $B \leftarrow X_1$, $C \leftarrow X_1$, $C \leftarrow X_2$, and $D \leftarrow X_1$. Balasubramanian, Han, and Liao[161] calculated the vertical separations of the 3/2(II), 1/2(II), and 5/2 states at 3.25 bohr (near R_e of $3/2(X_1)$). These splittings are 28 568, 39 000, and 52 010 cm^{-1}, respectively. The 1/2(II)–1/2 splitting at this distance is 24 563 cm^{-1}. On the basis of this splitting, the $B \leftarrow X_1$ transition was tentatively assigned to the 3/2(II) ← 3/2 transition.

The 1/2(II) and 5/2 states of TeH exhibited interesting avoided crossings. At short distances the 1/2(II) state was found to be predominantly $^2\Sigma^+(1\sigma^2 2\sigma 1\pi^4)$. At about 4.00 bohr, it became predominantly $^4\Sigma^-(1\sigma^2 2\sigma^2 3\sigma 1\pi^2)$, although other states such as $^2\Sigma^-$, $^2\Sigma^+$, etc. also made appreciable contributions. This avoided crossing led to the shoulder in the 1/2(II) curve (Figure 18). The 5/2 state was found to be predominantly $^2\Delta_{5/2}$ at short distances but became mainly $^4\Pi_{5/2}$ at intermediate and long distances. The 3/2(II) state was found to be predominantly $^4\Sigma^-_{3/2}$ at short distances. At long distances, however, the $^4\Pi$ and $^2\Pi$ states arising from the $1\sigma^2 2\sigma 3\sigma 1\pi^3$ configuration dominated.

J. HI and HI⁻

Among the heavy hydrogen containing molecules, HI and HBr have been the most studied species for a number of years.[76–129,162–166] The electronic spectra of HI basically consisted of continuous absorption bands near 23 000, 46 000, and 55 555 cm^{-1}. The UV continuum spectrum of HI contained a maximum at 45 000

TABLE 11. Spectroscopic Properties of Low-Lying States of HI[a]

	T_{vert},[b] cm^{-1}		R_e, Å		ω_e, cm^{-1}	
state	theory	expt[c]	theory	expt	theory	expt
X 0⁺(I)	0.0	0.0	1.66	1.61	2939	2309
a 0⁺(II)	49 605	43 000	—	—	—	—
a 1(I)	46 532	39 500	—	—	—	—
A 1(II)	54 763	47 000	—	—	—	—

[a] All theoretical results are from ref 122. [b] T_{vert} is the vertical separation of the excited states from the ground state at the minimum R value. [c] Approximate values obtained from measurements taken near the probable absorption curve maxima.

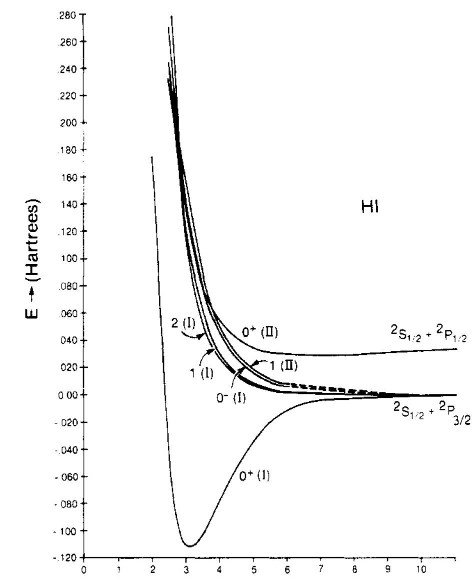

Figure 19. Potential energy curves for six low-lying states of HI (reprinted from ref 122; copyright 1985 Elsevier Science Publishers B.V.). See Table 11 for assignments of known states.

cm^{-1} and was found to be broad and featureless. Mulliken[82,83] interpreted the observed spectra of HI as due to $^3\Pi_{0^+} \leftarrow {}^1\Sigma^+_{0^+}$, $^3\Pi_1 \leftarrow {}^1\Sigma^+_{0^+}$, and $^1\Pi_1 \leftarrow {}^1\Sigma^+_{0^+}$ transitions. Clear et al.[164] carried out a photofragmentation investigation of HI.

The first ab initio relativistic SCF/RCI calculation on the electronic states of HI was made by Chapman, Balasubramanian, and Lin.[122] In this investigation a double ζ + polarization STO basis set was used for the iodine atom in conjunction with the RECPs. The potential energy curves of seven low-lying electronic states dissociating into $I(^2P_{1/2})$ + H and $I(^2P_{3/2})$ + H were obtained.

The spectroscopic constants for the electronic states of HI are summarized in Table 11. Figure 19 shows the potential energy curves for six low-lying states of HI including the spin–orbit term as obtained by Chapman, Balasubramanian, and Lin.[122] The atomic $^2P_{3/2}$–$^2P_{1/2}$ splitting of the iodine atom calculated by these authors (6971 cm^{-1}) was found to be in very good agreement with the experimental splitting of 7603 cm^{-1}. As seen from Table 11, the agreement between the theoretical constants for the ground state and the experimental values is also very good. The theoretical D_e value for the 0⁺(I) ground state of HI (3.03 eV) was found to be almost in exact agreement with an experimental value of 3.05 eV.

The experimental vertical transition energies listed in Table 11 are from ref 164. Clear et al.[164] demon-

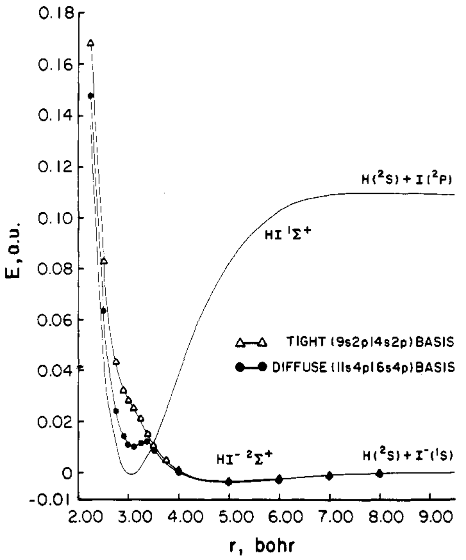

Figure 20. CASSCF/SOCI potential energy curves of HI and HI$^-$ (reprinted from ref 129; copyright 1988 American Institute of Physics).

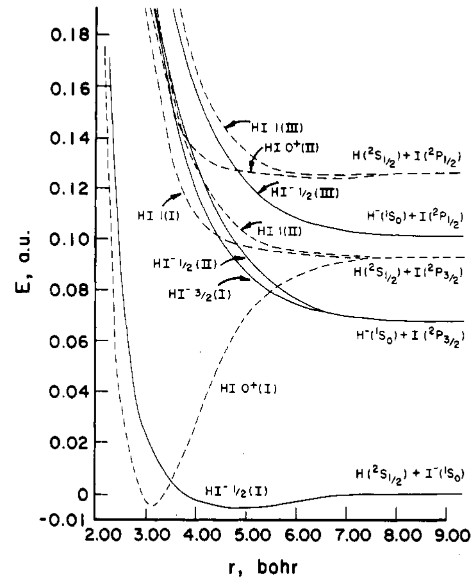

Figure 21. Potential energy curves of many electronic states of HI$^-$ and HI (reprinted from ref 129; copyright 1988 American Institute of Physics).

strated the composite nature of the observed absorption continuum of HI, which was attributed to three overlapping transitions (1 ← X, 0$^+$(II) ← X, 1(II) ← X) whose maxima were found to be located at approximately 39 500, 43 000, and 47 000 cm^{-1}, respectively. Table 11 shows these values compared with the theoretical results. In general, theoretical results are expected to be a bit higher due to limitations in basis sets and electron correlation effects.

As mentioned in reviewing HBr$^-$ calculations, Chapman, Balasubramanian, and Lin[129] carried out both SCF/RCI and CASSCF/SOCI calculations employing a large Gaussian basis set on HI$^-$ and comparable calculations on the ground state of HI. The HI molecule was predicted to have a slightly positive adiabatic electron affinity in comparison to −0.485 eV for HBr. I have briefly reviewed earlier (section III.E) the importance of theoretical study of HBr$^-$ and HI$^-$ to understand the mechanisms that govern the electron attachment and halide anion production processes.

Figure 20 shows the potential energy curves for the ground state of HI and HI$^-$. The diffuse Gaussian basis sets yielded the first minimum in the HI$^-$ ground state, which was found to be absent when a tight basis set was used (Figure 20). The HI/HI$^-$ curves cross at 3.45 bohr (CASSCF/SOCI). The $^2\Sigma^+_{1/2}$ ground state of HI$^-$ was found to be 0.1–0.2 eV bound at 5 bohr. The theoretical RCI electron affinity of the halogen atom was found to be 2.83 eV in comparison to an experimental value of 3.06 eV. The CASSCF/SOCI calculations yielded a slightly better EA of 2.99 eV for the iodine atom.

The theoretical positive electron affinity for HI was found to be consistent with the mass spectrometric investigations of Spence et al.[128] in which evidence for the stability of HI$^-$ was found. Spence et al.[128] suggested that the $^2\Sigma^+$ curve should be deep and broad enough to support at least one vibrational level below the HI $^1\Sigma^+$ curve. On the basis of this, these authors concluded that the electron affinity of HI is positive and should exceed 0.007 eV.

The exceptionally large rate constant for thermal electron attachment of HI observed by Adams et al.[96] was explained by Chapman et al.[129] using the Langevin model. The attachment rate constant data were found to exhibit a temperature dependence (β = (3.3 ± 1) × 10^{-12} cm^3 s^{-1} at 300 K; β = (2.8 ± 1) × 10^{-10} cm^3 s^{-1}) at 510 K for HBr, while the rate coefficients for HI remained constant (β = (3.5 ± 1) × 10^{-7} cm^3 s^{-1}) at 300 and 510 K. These data suggested that the attachment process was governed by two different mechanisms in HBr and HI. The thermal-averaged Langevin rate constant is given by

$$k_L(\epsilon) = 2\pi e(\alpha/m)^{1/2}$$

where α represents the electronic polarizability of the neutral molecule and m the mass of the electron. The calculated k_L's for HBr and HI were found to be of the same order (10^{-7} cm^3 s^{-1}) as the experimental β values for HI.

The potential energy curves of the excited states of HI$^-$ and HI are shown in Figure 21. Le Coat et al.[97,98] deduced the potential energy curves for some of the excited states of HI$^-$ (1/2(II), 3/2, 1/2(III)) from dissociative electron attachment experiments. The spin–orbit effects are more important for HI$^-$ since the $^2P_{3/2}$–$^2P_{1/2}$ spin–orbit splitting of I (7603 cm^{-1})[306] exceeds the electron affinity of the hydrogen atom. Consequently, the crossings of ionic and neutral curves differ for HI$^-$ substantially in comparison to HBr$^-$. The H$^-$ + I($^2P_{3/2}$) limit is below the H + I ($^2P_{3/2}$) neutral asymptote. The HI$^-$ 1/2(II) and 3/2(I) curves are the only curves that crossed with the ground-state curve of HI.

The nature of the HI$^-$ curves can be understood if one compares the parent (HI) electronic states. The 1(III) state of HI was found to be predominantly of $^3\Sigma^+_I(1\sigma^2 2\sigma 3\sigma 1\pi^4)$ character, while the HI$^-$ 1/2(II) state was found to be predominantly $^2\Sigma^+_{1/2}(1\sigma^2 2\sigma 3\sigma^2 1\pi^4)$. Hence, electron attachment to the 3σ orbital of the neutral $^3\Sigma^+_I$ state could generate the negative ion in the 1/2(II) state. The 1/2(II) state of HI$^-$ was found to lie below the neutral 1(II) curve (Figure 21) leading to the 1/2(II) state as a Feshbach resonance. On the contrary, the 3/2(I) and 1/2(III) states are components of the $^2\Pi(1\sigma^2 2\sigma^2 3\sigma^2 1\pi^3)$ states, which were found to lie above their parent $^3\Pi,^1\Pi(1\sigma^2 2\sigma^2 3\sigma 1\pi^3)$ states, and conse-

TABLE 12. Spectroscopic Constants for TlH[a]

state	R_e, Å theory	R_e, Å expt	T_e, cm^{-1} theory	T_e, cm^{-1} expt	ω_e, cm^{-1} theory	ω_e, cm^{-1} expt	D_e, eV theory	D_e, eV expt
X 0$^+$(I)	1.99	1.87	0	0	1300	1391	1.81	1.97
0$^-$(I)	1.95	—	16600	—	795	—	0.24	—
A 0$^+$(II)	1.91	1.91	17100	17723	1000	760	0.61	0.74
2	1.90	—	21800	—	740	—	0.04	—
C 1(II)	3.1	2.9	23400	24180	200	140	—	—

[a] All theoretical values are from ref 28.

quently the 3/2(I) and 1/2(III) states cannot be considered as Feshbach resonances.

K. TlH

The thallium hydride molecule has been the subject of many relativistic theoretical calculations[28,167,168] since it is the simplest sixth-row p-block hydride and has a $^1\Sigma^+$ closed-shell ground state. Lee, Ermler, and Pitzer[167] carried out relativistic SCF calculations in ω–ω coupling for TlH. In a subsequent study Christiansen and Pitzer[168] made MCSCF LCAS-MS spinor calculations on TlH. Christiansen, Balasubramanian, and Pitzer[28] carried out the first RCI calculations on TlH that included spin-orbit effects and electron correlation corrections simultaneously in a RCI scheme. In this investigation Christiansen, Balasubramanian, and Pitzer considered the spectroscopic properties and potential energy curves for six electronic states of TlH.

The experimental spectroscopic constants on five electronic states of TlH were obtained through the electronic spectrum obtained in both absorption and emission.[169–172] Grundström and Valberg[169] as well as Neuhaus and Muld[171] studied the A ↔ X systems. Larsson and Neuhaus[172] obtained several bands with origins at 23556 and 23655 cm^{-1}, which were attributed to D ← X and C ← X systems, respectively. Ginter and Battino[37] obtained two potential curves for TlH from the experimental data.

Table 12 shows the spectroscopic constants for TlH obtained from the theoretical calculations of Christiansen, Balasubramanian, and Pitzer[28] and the experimental values for comparison. Figure 22 shows a comparison of the RCI potential energy curves and the curves deduced from the Rydberg–Kein–Rees (RKR) method of fitting experimental data. As seen from Figure 22 the overall shapes of the potential curves are very similar. The experimental curve is deeper, with the R_e being shorter. The behavior of the 0$^+$(II) state is especially interesting and compares remarkably well with experiment. Figure 23 shows the potential energy curves of six electronic states of TlH. The 0$^-$, 1, 2, and 0$^+$(II) states were found to be predominantly components of a $^3\Pi$ state near the inner well, while the 1(II) state was found to be predominantly composed of a $^1\Pi$ state.

The 0$^+$ and 0$^+$(II) states of TlH were found to exhibit avoided crossings. At short distances the 0$^+$ state was found to be predominantly $^1\Sigma^+$, while it became $^3\Pi_{0^+}$ at longer distances. The reverse behavior was found to be true for the A0$^+$(II) state. That is, at short distances A0$^+$(II) was found to be $^3\Pi_{0^+}$ and became $^1\Sigma^+_{0^+}$ at long distances. The inner wells in the 0$^-$, 1, and 2 states are results of an avoided crossing. In the outer region the metal atom was described by the 6s^{2}6p configuration, while in the inner region there was considerable 6s6p^2

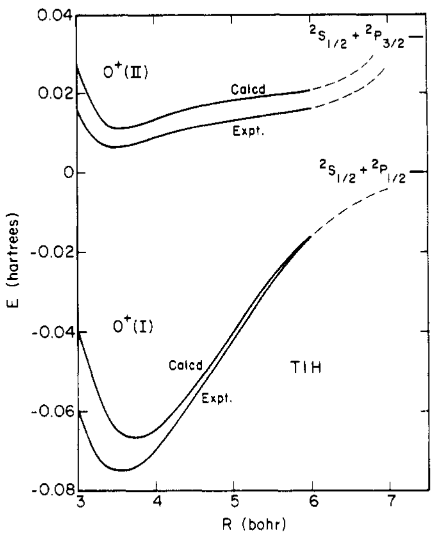

Figure 22. Comparison of the theoretical and experimental potential energy curves of two electronic states of TlH (reprinted from ref 28; copyright 1982 American Institute of Physics). See Table 12 for assignments of known states.

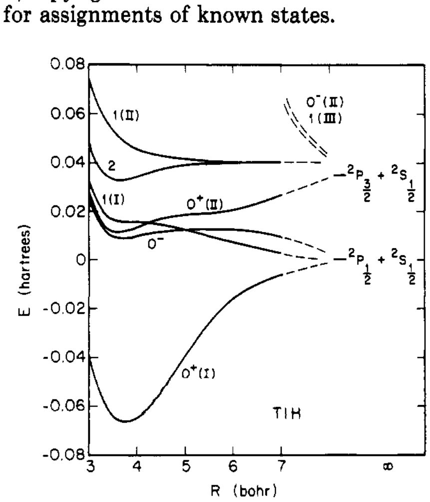

Figure 23. Theoretical potential energy curves of six electronic states of TlH (reprinted from ref 28; copyright 1988 American Institute of Physics). Experimental curves for the 0$^+$(I) and 0$^+$(II) states were derived by Ginter and Batino[37] using the RKR method. See Table 12 for assignments of known states.

character, allowing a σ bond between 6s of Tl and H 1s. A number of spectral lines observed by Larsson and Neuhaus[172] were tentatively assigned to the 2–X and C1(II)–X transitions. The approximate R_e and ω_e values of the 1(II) state were deduced as 2.9 Å and 140 cm^{-1} (see Table 12).

The merging (crossing) of the 1(II) and 2 curves (Figure 23) supported the hypothesis of Larsson and Neuhaus,[172] who assigned some of the spectral lines to the 2 ← 0$^+$ transition as a result of perturbation with the 1(II) state. The low-potential maxima were found in the 2 and 1(II) states.

L. PbH

Watson[173] was the first to observe complex red and near-infrared bands for PbH. Watson and Simon[142,143] assigned these bands to A–X and B ← X systems, although the ground state of PbH was then regarded as $^2\Sigma^+_{1/2}$. However, now it is clearly established that the ground state of PbH is X$^2\Pi_{1/2}$. Gerö[174] reassigned the A and B states to two $^2\Sigma^+_{1/2}$ states, although later Kleman[131] argued that these should be components of a $^4\Sigma^-$

TABLE 13. Spectroscopic Properties of a Few Low-Lying Bound States of PbH

	R_e, Å		T_e, cm^{-1}		ω_e, cm^{-1}	
state	theory	expt	theory	expt	theory	expt
X 1/2(I)	1.95	1.84	0.0	0.0	1418	1564
3/2(I)	1.92		6846		1457	
A 1/2(II)	2.68	(2.36)	17213	17590	391	500
B 3/2(II)	2.44	(2.60)	20341	18030	442	479

[a] All theoretical results are from ref 175.

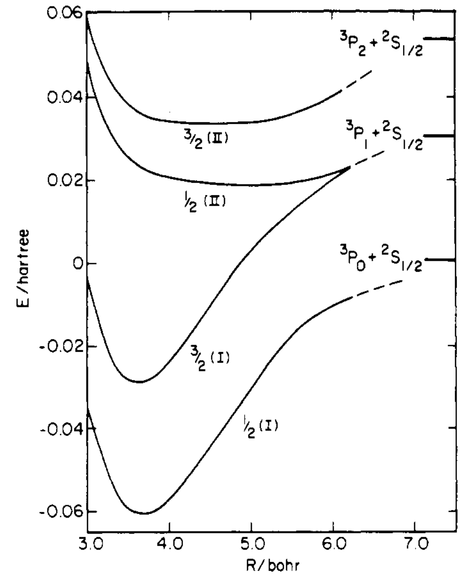

Figure 24. RCI potential energy curves of four electronic states of PbH (reprinted from ref 175; copyright 1984 American Chemical Society). See Table 13 for assignments of known states.

state. Howell[47] reported the C ← X system in the region of 26 200 cm^{-1}, although these bands have not yet been fully analyzed.

Balasubramanian and Pitzer[175] made relativistic SCF/RCI calculations on five electronic states of PbH employing a double-ζ STO basis with 14e RECPs for the lead atom. The calculated RCI spectroscopic constants are summarized in Table 13 and compared with experimental values when available. Figure 24 shows the RCI potential energy curves of PbH. The ground state of PbH was found to be clearly $^2\Pi_{1/2}$, confirming Howell's[47] reinterpretation of Watson's spectra.[173]

The excited A1/2(II) and B3/2(II) states were found to be predominantly $^4\Sigma^-_{1/2}$ and $^4\Sigma^-_{3/2}$ at near R_e distances of these states. The dissociation energy of PbH was calculated as 1.64 eV,[175] in very good agreement with an experimental value of 1.59 eV[32] obtained from the predissociation in the B state assuming dissociation into $^3P_1$ + ^2S.

Chapman et al.[55] calculated the dipole moment of PbH in the $X^2\Pi_{1/2}$ ground state as 0.937 D employing a double-ζ STO basis set. The dipole moment of the $^2\Pi_{3/2}$ state was found to be 0.673 D (Pb^+H^-). The transition moment curves and the electronic dipole moment curves of PbH were also obtained and compared with those of SnH (see Figures 14 and 15).

Schwerdtfeger et al.[316] have recently studied the ground states of PbH^+, PbH, PbH_2, and PbH_4 using semiempirical relativistic and nonrelativistic pseudopotentials and the CISD method for inclusion of electron correlation. The calculated R_e(PbH) = 1.839 Å was found to be almost in exact agreement with the experimental value. The ground state of PbH^+ was found to be the $^1\Sigma^+$ state, analogous to the ground state of TlH.

Balasubramanian studied the $^1A_1$–$^3B_1$ energy separations of GeH_2, SnH_2, and PbH_2 in a recent investigation.[317] He found that the geometry of the $^3B_1(A_1)$ state changed substantially due to the spin–orbit effects via mixing of $^3B_1(A_1)$ with the $^1A_1(A_1)$ ground state.

M. BiH and BiH+

The BiH molecule is one of the most complex and thoroughly investigated (theoretically) species among the heavy hydrides.[180,181] Balasubramanian[181] in a preliminary theoretical investigation studied four low-lying electronic states of BiH. In a subsequent detailed study[180] the spectroscopic constants and potential energy curves of ten low-lying ω–ω states and five λ–s states of BiH were investigated. BiH is the most complex among the main-group hydrides both because of the $6s^26p^3$ open-shell configuration of the Bi atom and the large spin–orbit effects. Consequently, there are many low-lying electronic states for BiH.

The experimental spectroscopic investigations of BiH date back to the early 1930s.[176–179] In particular, Heimer,[178,179] Khan and Khan,[157] Neuhaus,[177] and Lindgren and Nilsson[156] have investigated the electronic spectra of BiH. These investigations yielded information on the B → X, B → A, D → C, and E ← X systems of BiH. The rotational analyses of the E ← X system were made by Khan and Khan[157] and Lindgren and Nilsson.[156] The abrupt disrupture of the bands in the E ← X system clearly indicated that the E state must be predissociated; it was hypothesized that a repulsive L state dissociating into Bi($^2D_{3/2}$) + H(^2S) should be responsible for this predissociation. An upper bound for the D_e of BiH ground state was estimated by assuming the predissociation of E ← X into Bi($^2P_{3/2}$) + H. From the hyperfine structure of the A state, the spin–orbit constant of the $^3\Sigma^-$ ground state of BiH was deduced to be 4917 cm^{-1}. Bopegedera et al.[333] have recently recorded diode laser spectra of BiH and BiD. From the rotational line positions these authors have determined the R_e value of BiH accurately as 1.80867 Å.

The spin–orbit effects were found to be substantial for BiH, leading to many avoided crossings. As shown by Balasubramanian,[180] these avoided crossings resulted in shoulders, barriers, multiple minima, and other exotic features in the potential energy curves of the excited states of BiH.

The ground state of BiH was found to be a $^3\Sigma^-_{0^+}$ state arising from the $1\sigma^22\sigma^21\pi^2$ configuration, where the 2σ orbital should be the bonding Bi($6p_z$) + H(1s) orbital, while the 1π orbital should be a nonbonding Bi 6p orbital. Thus, the spin–orbit splitting of the $^3\Sigma^-$ state arising from this configuration should be large. Balasubramanian carried out SCF/RCI calculations on BiH employing a STO basis set.[180,181] Ramos et al.[334] have also carried out relativistic calculations on a few sixth-row diatomic hydrides including BiH. However, these authors obtain a poorer D_e for most of these hydrides since electron correlation effects are not addressed properly in these much smaller CI expansions.

Table 14 shows the spectroscopic constants of BiH obtained from the RCI calculations including the

TABLE 14. Spectroscopic Properties of Low-Lying States of BiH[a]

state	R_e, Å theory	R_e, Å expt	T_e, cm^{-1} theory	T_e, cm^{-1} expt	ω_e, cm^{-1} theory	ω_e, cm^{-1} expt
X 0^+(I)	1.90	1.81	0.0	0.0	1619	1636
A 1	1.89	1.79	5737	4917	1630	1669
2	1.89	—	13469	—	1630	—
B 0^+(II)	1.88	1.78	26286	21263	1585	1643
2(II)	2.58	—	23450	—	1529	—
E 0^+(IV)	2.51	2.18	38780	32940	1000	1106
$^3\Sigma^-$	1.88	—	8013	—	1687	—
$^1\Delta$	1.92	—	16494	—	1296	—
$^1\Sigma^+$	1.86	—	25670	—	1705	—
$^1\Sigma^+(\pi^4)$	1.74	—	—	—	1890	—

[a] All theoretical values are from ref 180.

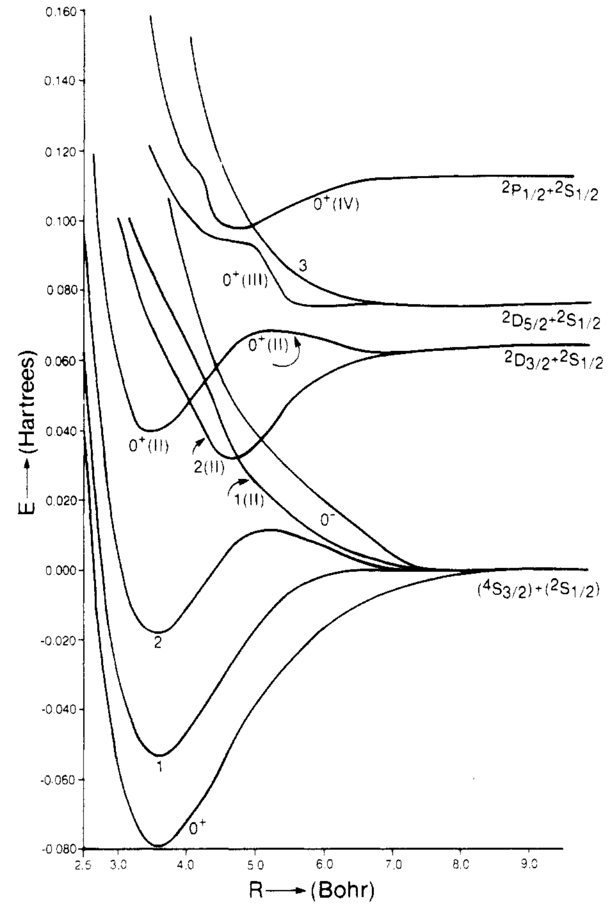

Figure 25. RCI potential energy curves of ten low-lying states of BiH (reprinted from ref 180; copyright 1986 Academic Press, Inc.). See Table 14 for assignments of known states.

spin–orbit term. The experimental results are also included for some of the states for which there is experimental information. Figure 25 shows the potential energy curves of BiH including the spin–orbit effects. Figure 26 shows comparable potential energy curves without the spin–orbit term. In Figure 26 although the ^4S state of the Bi atom (dissociation limit) is not split by the spin–orbit term, it can interact with $^2D_{3/2}$ when spin–orbit integrals are included. Thus, the limit labeled $^4S_{3/2}$ + $^2S_{1/2}$ (Figure 26) includes spin–orbit integrals while ^4S + ^2S does not include these integrals.

The RCI calculations of Balasubramanian[180] enabled the assignment of the experimentally observed X, A, B, and E states to the 0^+, 1, 0^+(II), and 0^+(IV) states, respectively. Among these the 0^+ and 1 states are type-c analogues of $^3\Sigma^-_{0^+}$ and $^3\Sigma^-_1$ at near-equilibrium geome-

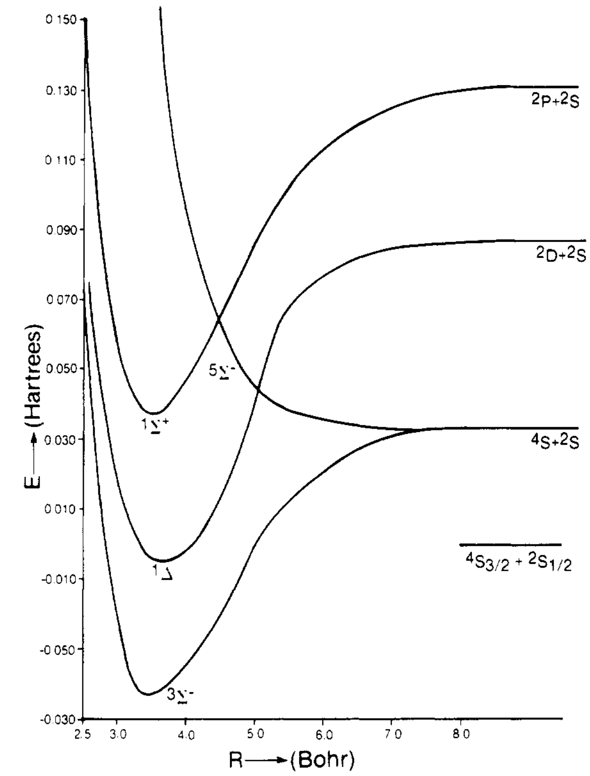

Figure 26. Potential energy curves of BiH without the spin–orbit term (reprinted from ref 180; copyright 1986 Academic Press, Inc.).

tries. The 0^+(IV) state (E) exhibited avoided crossing of $^3\Pi_{0^+}(\sigma^2\sigma^*\pi)$ with $^1\Sigma^+_{0^+}(\sigma^2\pi^2)$ among other avoided crossings. The $^1\Sigma^+(\sigma^2\pi^2)$ state would dissociate into ^2P(Bi) + ^2S(H) atoms in the absence of spin–orbit interactions. The $^3\Pi$ state, however, dissociates into ^2D(Bi) + ^2S(H) and is a repulsive state. The ^2P(Bi) state is much higher than the ^2D(Bi) state. Thus these two states cross in the absence of spin–orbit interactions, and therefore their 0^+ components exhibited avoided crossings.

The repulsive 1(II) state, which dissociates into ground-state atoms, crosses the 2(II) state close to the equilibrium bond distance (see Figure 25). The 1(II) state also crosses with the 0^+(II) state, but at a considerably longer distance than the R_e value of the 0^+(II) state. The 2(II) state is thus predissociated and should be short-lived. The 0^+(II) and 2 states have barriers as a result of avoided crossings. The $^3\Sigma^-$ and $^3\Pi$ states, which dissociate to the Bi(^2D) state, cross $^1\Sigma^+$, which dissociates to the ^2P state. In the presence of spin–orbit interactions this led to avoided crossings. Thus 0^+(II), which is predominantly $^1\Sigma^+(\sigma^2\pi^2)$ at near-equilibrium geometries, is forced to dissociate into $^2D_{3/2}$(Bi) + $^2S_{1/2}$(H) as a result of avoided crossings. The barrier in the 2 state arises from the avoided crossing of the bound $^1\Delta_2$ with the repulsive $^5\Sigma^-_2$ dissociating into the ground-state atoms.

The 0^+(III) state, which has not been experimentally characterized yet, is repulsive but at long distance (6.0 bohr) has a shallow minimum. At 3.5 bohr the 0^+(III) state is 73% $^3\Pi_{0^+}(\sigma\pi^3)$, 13% $^1\Sigma^+_{0^+}(\sigma^2\pi^2)$, and 4% $^3\Sigma^-_{0^+}(\sigma^2\pi^2)$. Thus it is predominantly $^3\Pi_{0^+}$ in type-c coupling. The X(0^+) state was found to be 76% $^3\Sigma^-_{0^+}(\sigma^2\pi^2)$ and 16% $^1\Sigma^+_{0^+}(\sigma^2\pi^2)$. Thus the 0^+(III) ← X(0^+) transition is a type-c analogue of the $^3\Pi$ ← $^3\Sigma^-$ transition at the same distance. This transition is an allowed case a transition in the perpendicular direction. Also, mixing of $^3\Sigma^-_{0^+}$ and $^1\Sigma^+_{0^+}$ in the 0^+(III) state should contribute to the z component of the transition moment indirectly since $^3\Pi_{0^+}$ mixes with $^1\Sigma^+_{0^+}$. For the isoelectronic NH molecule the $^3\Pi(\sigma\pi^3)$ state is bound and is observed both in emission and in absorption (A ↔ X) at 29 820 cm^{-1}.[32] The theoretical separation of the 0^+(III) state with respect to the X(0^+) state is about 43 895 cm^{-1} at 3.5 bohr.

The experimental E0^+ ← X0^+ absorption bands break off abruptly, which was attributed by Lindgren and Nilsson[156] to the predissociation of the E0^+ state caused by the crossing of a repulsive 1 state with the E0^+ state at a distance longer than the equilibrium geometry to cause predissociation in the v = 2 level. These authors suggested that the most probable candidate for this predissociation is the repulsive $^5\Sigma^-_1$ state. The 1(II) state (Figure 25) is predominantly $^5\Sigma^-_1$ at distances longer than 4.5 bohr. Since the predissociation of the E0^+ state occurs at about 5 bohr, it is unlikely that this is caused by the $^5\Sigma^-_1$ state. This is because the 1(II) state is much too low in energy at this distance to cross the 0^+(IV) state. Balasubramanian[180] suggested that the predissociation of the E0^+ state should be attributed to crossing of the 1(III) or 1(IV) curves, which dissociate into $^2D_{3/2}$ + $^2S_{1/2}$ atoms.

The experimental dissociation energy of the BiH molecule was calculated by using the predissociation of the v = 2 vibrational band (in the E ← X system) of the E0^+ state. It was assumed that this dissociated into $^2D_{3/2}$ + $^2S_{1/2}$ atoms. The 0^+(III) state actually dissociates into $^2D_{5/2}$ + $^2S_{1/2}$ atoms and hence it will keep the E0^+(IV) state higher than the $^2D_{5/2}$ + $^2S_{1/2}$(Bi + H) atoms at all distances (see Figures 25). Thus the assumption of the predissociation limit of E0^+ as Bi($^2D_{3/2}$) + H($^2S_{1/2}$) atoms should yield a $D_0{}^{306}$ 4019 cm^{-1} [Bi($^2D_{5/2}$)–Bi($^2D_{3/2}$) splitting] higher than the true value. Consequently, the D_0 value calculated by extrapolating the v = 2 band of E0^+ to $^2D_{3/2}$ + $^2S_{1/2}$ (2.89 eV) should be corrected to 2.39 eV. The corrected value was found to be in very good agreement with Balasubramanian's[180] calculated separation of the minimum of X(0^+) with respect to the energy of X(0^+) at 9.0 bohr (2.17 eV).

Balasubramanian[180] calculated a high-lying bound $^1\Sigma^+$ state arising from the π^4 electronic configuration. This state was found to lie about 83 160 cm^{-1} above the ground state for the iso-valence-electronic NH.[32] The calculated R_e and ω_e values are shown in Table 14. This state should be in the far-ultraviolet region by comparing with iso-valence-electronic NH. Electronic spectra of the BiH molecule in the ultraviolet and far-ultraviolet regions have not been studied at all.

The BiH molecule is one of the most fascinating candidates to exemplify the important impacts of the spin–orbit coupling on the electronic states. The nature of the electronic states of BiH was investigated by analyzing the RCI wave functions. The squares of the coefficients of the various λ–s states in the RCI wave functions of the electronic states of BiH were collected and plotted against R. The plots of two very interesting states, namely, 0^+(II) (B0^+) and 0^+(IV) (E0^+), are shown in Figures 27 and 28, respectively. I describe below the nature of various electronic states of BiH.

The ground state X(0^+) was found to be a mixture of $^3\Sigma^-_{0^+}$ (76%) and $^1\Sigma^+_{0^+}$ (16%) near the equilibrium bond

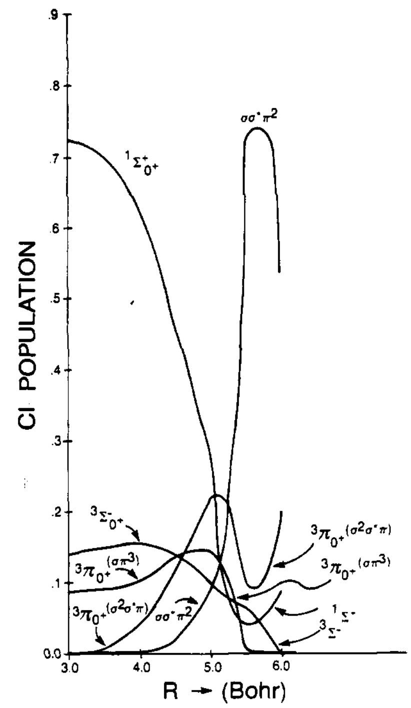

Figure 27. CI weights of the 0^+(II) B0^+ state of BiH as a function of internuclear distance (reprinted from ref 180; copyright 1986 Academic Press, Inc.).

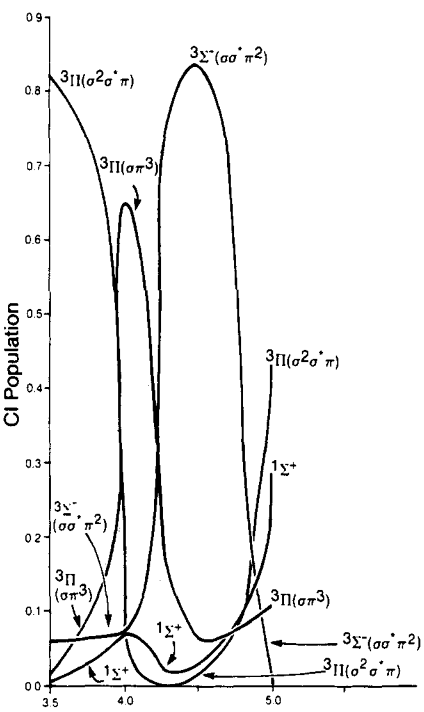

Figure 28. CI weights of the 0^+(IV) E0^+) state of BiH as a function of internuclear distance (reprinted from ref 180; copyright 1986 Academic Press, Inc.).

distance. At an intermediate distance (6.0 bohr) the 0^+(I) state became 54% $^3\Sigma^-_{0^+}$, 12% $^1\Sigma^+_{0^+}$, 14% $^3\Sigma^-_{0^+}(\sigma^{*2}\pi^2)$, 3% $^1\Sigma^+_{0^+}(\sigma^{*2}\pi^2)$, 6% $^3\Pi_{0^+}(\sigma^2\sigma^*\pi)$, and 5% $^3\Sigma^-_{0^+}(\sigma\alpha\sigma^*\alpha\pi_x\beta\pi_y\beta-\sigma\beta\alpha^*\beta\pi_x\alpha\pi_y\alpha)$.

The 0^+(II) state (B0^+) exhibited an interesting behavior (see Figure 27).[180] As seen from Figure 27, at near-equilibrium geometries this state is predominantly $^1\Sigma^+_{0^+}$ (70%). The $^3\Sigma^-_{0^+}$ and $^3\Pi_{0^+}(\sigma\pi^3)$ configurations account for 15 and 8% of the weight, respectively. At 6.0

TABLE 15. Spectroscopic Properties of BiH^+ [a]

state	R_e, Å	T_e, cm^{-1}	ω_e, cm^{-1}	D_e, eV
X 1/2(I)	1.89	0.0	1608	1.05
3/2(I)	1.87	11384	1653	1.37
1/2(II)	2.24	17388	801	0.48
3/2(II)	2.37	24537	504	0.25
$^2\Pi$	1.87	9846	1751	2.17

[a] All results are from ref 182.

bohr, this state became 39% $^3\Sigma^-_{0^+}$ (arising from $\sigma\alpha\sigma^*\alpha\pi_x\beta\pi_y\beta$ and $\sigma\beta\sigma^*\beta\pi_x\alpha\pi_y\alpha$), 20% $^3\Pi_{0^+}(\sigma^2\sigma^*\pi)$, 10% $^1\Sigma^+_{0^+}(\sigma^2\pi^2)$, 8% $^3\Pi_{0^+}(\sigma\pi^3)$, 9% $^3\Pi_{0^+}(\sigma\sigma^{*2}\pi)$, and 2% $^3\Sigma^-_{0^+}(\sigma^2\pi^2)$. At 9.0 bohr it is 67% $^3\Sigma^-_{0^+}(\sigma\alpha\sigma^*\alpha\pi_x\beta\pi_y\beta-\sigma\beta\sigma^*\beta\pi_x\alpha\pi_y\alpha)$, 5% $^1\Sigma^+_{0^+}(\sigma^2\pi^2)$, 8% $^3\Pi_{0^+}(\sigma^2\sigma^*\pi)$, and 10% $^3\Pi_{0^+}(\sigma\sigma^{*2}\pi)$.

The 1(I) (A1) state of BiH was found to be 88% $^3\Sigma^-_1$ and 2% $^3\Pi_1$. At long distances the $^5\Sigma^-_1(\sigma\sigma^*\pi^2)$ made a substantial contribution. At 6.0 bohr the 1 state was found to be 46% $^3\Sigma^-_1$, 18% $^5\Sigma^-_1$, 8% $^3\Pi_1(\sigma\pi^3)$, and 13% $^3\Sigma^-_1(\sigma^{*2}\pi^2)$. The 2 state was found to be 90% $^1\Delta_2$ near the equilibrium distance, while at 6.0 bohr it became 54% $^5\Sigma^-_2$, 7% $^1\Delta_2$, 4% $^3\Pi_2(\sigma^2\sigma^*\pi)$, and 12% $^3\Pi_2(\sigma\pi^3)$. Thus $^5\Sigma^-_2$ dominated at long distances, which explains the barrier in this state. The 2(II) state exhibited an opposite behavior. It was found to be 40% $^5\Sigma^-_2$ and 44% $^3\Pi_2(\sigma\pi^3)$ at 4.25 bohr. At 4.5 bohr it was found to be 50% $^5\Sigma^-_2$ and 35% $^3\Pi_2$. The second avoided crossing arises from the crossing of $^1\Delta$ with $^5\Sigma^-$. At 6.0 bohr the 2(II) state was found to be 55% $^1\Delta_2$, 23% $^5\Sigma^-_2$ and 0.7% $^3\Pi_2$.

The 0^- state was found to be 54% $^3\Pi_{0^-}(\sigma^2\sigma^*\pi)$, 28% $^5\Sigma_{0^-}(\sigma\sigma^*\pi^2)$, 9% $^3\Sigma^+_{0^-}(\sigma\sigma^*\pi^2)$, and 4% $^3\Pi_{0^-}(\sigma\sigma^{*2}\pi)$ at 4.0 bohr. At 6.0 bohr it became 62% $^5\Sigma^-_{0^-}(\sigma\sigma^*\pi^2)$, 12% $^3\Pi_{0^-}(\sigma^2\sigma^*\pi)$, 15% $^3\Sigma^+_{0^-}(\sigma\sigma^*\pi^2)$, and 9% $^3\Pi_{0^-}(\sigma\sigma^{*2}\pi)$. Thus the 0^- state exhibited not only an avoided crossing but also a large spin–orbit contamination at long distances.

The 0^+(III) and 0^+(IV) ($E0^+$) states exhibited several interesting relativistic avoided crossings. The CI weight of the 0^+(IV) state is shown in Figure 28. At 3.5 bohr the 0^+(III) state was found to be 73% $^3\Pi_{0^+}(\sigma\pi^3)$, 13% $^1\Sigma^+_{0^+}(\sigma^2\pi^2)$ and 4% $^3\Sigma^-_{0^+}(\sigma^2\pi^2)$. However, at 4.0 bohr it became 73% $^3\Pi_{0^+}(\sigma^2\sigma^*\pi)$, 16% $^1\Sigma^+_{0^+}(\sigma^2\pi^2)$, and 1% $^3\Pi_{0^+}(\sigma\pi^3)$. Thus at this distance the 0^+(III) state exhibited an avoided crossing of $^3\Pi_{0^+}(\sigma^2\sigma^*\pi)$ with $^3\Pi_{0^+}(\sigma\pi^3)$. This results in the first shoulder in the potential energy curve of 0^+(III) in Figure 25. At 4.0 bohr 0^+(IV) was predominantly $^3\Pi_{0^+}(\sigma^2\sigma^*\pi)$, and at 4.25 bohr it became predominantly $^3\Pi_{0^+}(\sigma\pi^3)$. At 5.0 bohr the 0^+(III) state was found to be 84% $^3\Sigma^-_{0^+}(\sigma\alpha\sigma^*\alpha\pi_x\beta\pi_y\beta-\sigma\beta\sigma^*\beta\pi_x\alpha\pi_y\alpha)$, 6.4% $^3\Pi_{0^+}(\sigma\pi^3)$, and 3% $^3\Sigma^-_{0^+}(\sigma^2\pi^2)$.

Thus at 5.0 bohr the 0^+(III) curve has a second shoulder as a result of the avoided crossing of repulsive $^3\Sigma^-_{0^+}(\sigma\sigma^*\pi^2)$ with $^3\Pi_{0^+}(\sigma^2\sigma^*\pi)$. At 6.0 bohr the 0^+(III) has a shallow minimum, and at this distance it is 42% $^3\Sigma^-_{0^+}(\sigma\sigma^*\pi^2)$, 12% $^3\Sigma^-_{0^+}(\sigma^2\pi^2)$, 15% $^3\Pi_{0^+}(\sigma\pi^3)$, and 11% $^3\Pi_{0^+}(\sigma^2\sigma^*\pi)$. The experimentally observed $E0^+$ exhibits several avoided crossings (see Figure 25).

Although the BiH^+ ion has not been investigated experimentally at all, the spectroscopic constants and the potential energy curves of many electronic states of the ion were obtained by Balasubramanian.[182] The SCF/RCI calculations of Balasubramanian[182] revealed the existence of eight low-lying ω–ω states and five λ–s states of BiH^+. The ionization potential of BiH was calculated by the RCI method to be 8.1 eV.

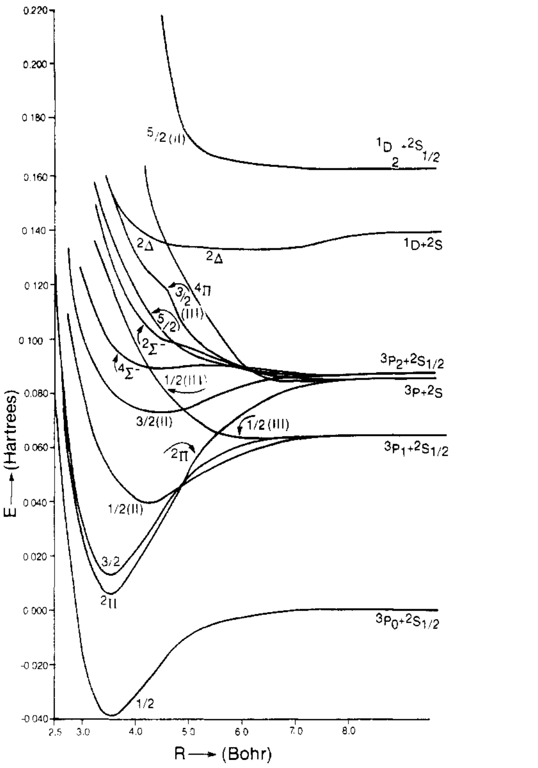

Figure 29. RCI potential energy curves of the low-lying states of BiH^+ (reprinted from ref 182; copyright 1986 American Chemical Society).

Table 15 shows the RCI spectroscopic constants of the BiH^+ ion. Figure 29 shows the RCI potential energy curves of BiH^+. Since the ground state of the neutral BiH molecule is $^3\Sigma^-(0^+)$ arising from $1\sigma^22\sigma^21\pi^2$, the ionization of the highest occupied nonbonding 1π orbital of BiH should lead to a $^2\Pi_{1/2}$ ground state for BiH^+ arising from the $1\sigma^22\sigma^21\pi$ configuration. The removal of one of the 2σ electrons should result in a large array of states arising from the $1\sigma^22\sigma1\pi^2$ configuration ($^4\Sigma^-$, $^2\Delta$, $^2\Sigma^-$, $^2\Sigma^+$, etc.). All these states were investigated by Balasubramanian.[182]

The ionization potential of the Bi atom was also calculated by Balasubramanian[182] as 6.98 eV, in very good agreement with an experimental value of 7.29 eV.[306] Further using the asymptotic separations of X(1/2)–3/2, 1/2–5/2, and 1/2–5/2(II) states, Balasubramanian[182] calculated the $^3P_0$–$^3P_1$, $^3P_0$–$^3P_2$, and $^3P_0$–$^1D_2$ splittings of the Bi^+ ion as 13937, 19138, and 36038 cm^{-1}, respectively. These values were found to be in very good agreement with the corresponding experimental values[306] of 13324, 17030, and 33939 cm^{-1}, respectively.

The D_e of BiH^+ was calculated as 1.05 eV.[182] This is much smaller than the D_e value of the 0^+ state of BiH, which was calculated as 2.2 eV.[180] Since the π orbital of BiH is essentially nonbonding, it was expected that the ionization of the π shell should not alter the D_e value too much. Thus the difference in the D_es of BiH and BiH^+ was puzzling. However, at dissociation limits the spin–orbit stabilizations of the electronic states of the neutral atom and ion are substantially different. The Bi neutral atom has a ^4S ground state that cannot be split by spin–orbit interaction but is lowered by 0.03266 hartree. The Bi^+ ion has a ^3P l–s state that is split apart into $^3P_0$, $^3P_1$, and $^3P_2$. Balasubramanian's calculations[182] indicated that the $^3P_0$ state is 0.0859 hartree lower than ^3P. Thus the $^3P_0$ state of Bi^+ is lowered considerably in comparison to Bi as well as BiH^+. This appears to be the reason for the lower D_e for BiH^+ (since Bi^+ is more stabilized by spin–orbit interaction than BiH^+). This is further justified if one compares the D_e value of the $^3\Sigma^-$ state of BiH with that of the $^2\Pi$ state of BiH^+ calculated without spin–orbit integrals. The D_e value of $^3\Sigma^-$ is 2.06 eV in comparison to the $^2\Pi$ state of BiH^+, which is 2.17 eV. Thus it is clear that the spin–orbit interaction reduces the D_e of BiH^+.

IV. Spectroscopic Properties and Potential Energy Curves of Heavy Halides

The interest[183–232] in heavy metal and other halides arises from a number of reasons, one of which is that many of the halides such as MF, MCl, etc. are generated in chemiluminescent reactions of the following type:

$$M + X_2 \rightarrow MX^* + X$$

Some of the heavier halides have been investigated by Parson and co-workers[214] recently. In the chemiluminescent reactions of $M + X_2$, the MX_2 triatomic (C_{2v}) is generated, which eventually forms MX^* in the excited state. The excited MX chemiluminesces, emitting photons. Thus many of the heavy main-block halides and chalconides have been investigated as candidates for chemical lasers.

The photoionization of nonvolatile materials such as thallous halides has been the topic of many investigations.[185–191] Berkowitz and Chupka[185] have examined the ion-pair processes in thallous halides and the high-energy processes that ionize the molecule. The electronic spectra of some of these species are not completely understood due to the complexities of the electronic states. The potential energy curves of these species exhibit peculiar shapes such as barriers.

There are many recent experimental investigations[318–323] on group IIIA halides, and in particular InCl. In the most recent investigation on InCl, Hoeft and Nair[318] obtained the rotational spectra of InCl. From these data, the vibrational constants and Dunham potential constants are derived for InCl.

Glenewinkel-Meyer et al.[324] have studied the emission spectra of ten group IIIA monohalide ions, MX^+ (M = B, Al, Ga, In; X = F, Cl, Br) in the visible and near-UV regions. The emission spectra of all these species were obtained through the following chemiluminescent reaction:

$$M^+ + X_2 \rightarrow MX^{+*} + X$$

On the basis of the observed spectra, these authors concluded that the excited states of these ions are considerably displaced compared to the ground states. For six of the ten species studied, these authors observed narrow-band systems which they assigned to $C^2\Pi$–$X^2\Sigma^+$. The narrow features that accompanied this system for $GaCl^+$, $GaBr^+$, and $InBr^+$ were attributed to $D^2\Sigma^+$–$X^2\Sigma^+$ transitions. All these results were compared with existing ab initio calculations on AlF^+.[325] The potential energy curves of the $X0^+$, $A0^+$, and B1 states of the InI diatomic have been recently constructed from experimental data and rotational analyses.[327–329]

TABLE 16. Calculated Spectroscopic Properties of Low-Lying Bound States of TlF and Available Experimental Values[a]

	R_e, Å		T_e, cm^{-1}		ω_e, cm^{-1}	
state	theory	expt	theory	expt	theory	expt
X 0+(I)	2.04	2.08	0	0	592	477
A 0+(II)	2.12	2.05	40462	35186	462	436
0−(I)	2.10	—	40891	—	345	—
B 1(I)	2.12	2.08	42612	36863	326	366
C 1(II)	2.69	—	45164	45546	396	346
2(I)	2.10	—	46245	—	340	—
2(II)	2.92	—	49700	—	264	—
0−(II)	2.90	—	50053	—	279	—

[a] All theoretical results are from ref 198.

Although there are many experimental investigations on halides such as GeF, GeCl, SnF, etc., we have restricted the present review to those heavy halides that have been investigated theoretically also so that comparison between theory and experiment is possible. Since at present theoretical calculations are available only on TlF, PbF, BiF, PbCl, and SnCl, our review of this topic is restricted to these five species. The emphasis is on the spectral properties, potential energy curves, and discussion of agreements and differences between theory and experiment.

A. TlF

The spectroscopic investigations on TlF include those of Boizova and Butkow,[193] Howell,[194] and Barrow and co-workers.[192] These investigations have revealed the existence of three excited states of TlF, $^3\Pi_{0^+}$, $^3\Pi_1$, and $^1\Pi_1$, in addition to the closed-shell $^1\Sigma^+_{0^+}$ ground state. The rotational analyses of the A–X and B–X systems have also been carried out. The microwave spectra, the Stark–Zeeman spectra, and the rotational spectra of TlF have also been obtained.[195,196]

The photoionization studies of the vapors of thallous halides have been considered by Trenin and co-workers[183,184] and Berkowitz and Chupka.[185] The vaporization reactions of thallous halides have been investigated by Cubicciotti.[186] The dimeric and tetrameric species of thallous halides have been detected in the vapor phase. The infrared spectra and the structure of matrix-isolated Tl_2F_2 and Tl_2Cl_2 species have been investigated by Brom and Fransen.[188] These authors proposed a linear structure for Tl_2F_2 (F–Tl–Tl–F).

Murad, Hildenbrand, and Main[190] calculated the dissociation energies of group IIIA halides using high-temperature mass spectroscopic methods. On the basis of the fact that the thermodynamic D_es are lower than the spectroscopically derived D_es for TlF, these authors suggested that there should be barriers in the excited potential energy curves of TlF. This was also supported by the photoionization mass spectroscopic investigation of Berkowitz and Walter,[191] who examined TlF, TlCl, and TlBr. The threshold for the formation of Tl^+ was used to calculate the D_es of these species in this method.

Balasubramanian[198] carried out SCF/RCI calculations on nine low-lying ω–ω states and the corresponding λ–s states of TlF. The spectroscopic properties and the potential energy curves of these states were calculated. Table 16 shows the spectroscopic constants of TlF obtained by Balasubramanian[198] and the experimental data when available. Figures 30 and 31 show the theoretical potential energy curves[198] of the low-

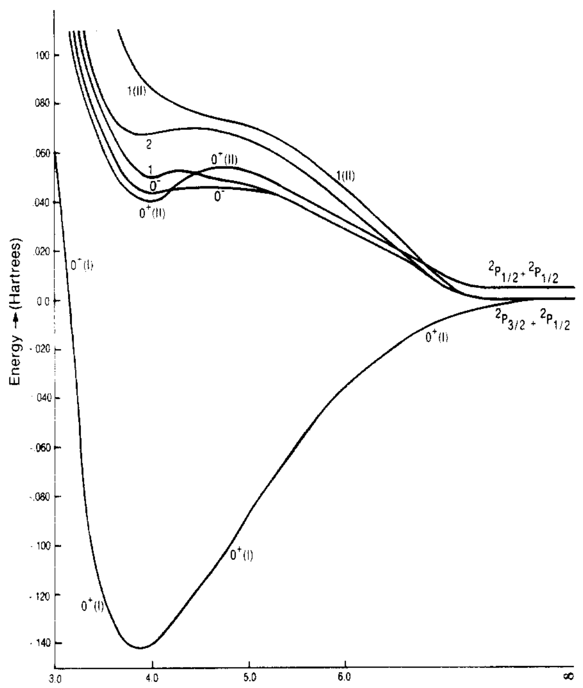

Figure 30. Potential energy curves of some low-lying states of TlF (reprinted from ref 198; copyright 1985 American Institute of Physics). See Table 16 for assignments of known states.

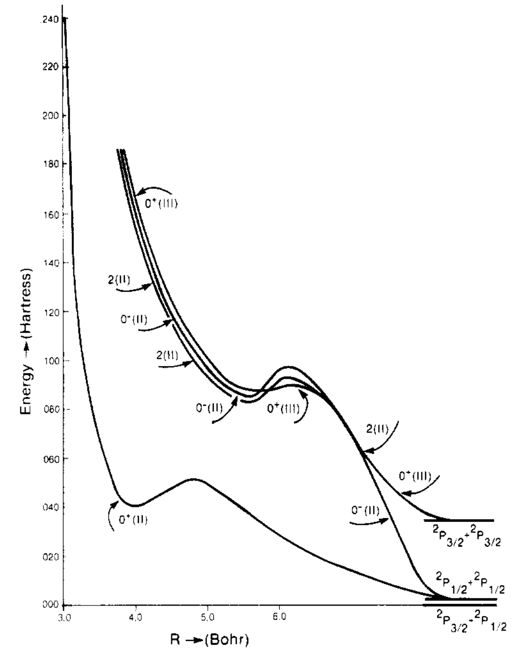

Figure 31. Potential energy curves of the excited states of TlF (reprinted from ref 198; copyright 1985 American Institute of Physics). See Table 16 for assignments of known states.

lying electronic states of TlF.

The ground state of TlF arises from the $1\sigma^2 2\sigma^2 3\sigma^2 1\pi^4$ configuration where the 1σ and 2σ orbitals arise from Tl(6s) and F(2s), while the 3σ orbital is a mixture of Tl($6p_z$) with F($2p_z$). The 1π orbital is predominantly F(2p). Thus the 2π orbital is predominantly the Tl(6p) nonbonding orbital. The low-lying excited electronic states of TlF arise from the $1\sigma^2 2\sigma^2 3\sigma^1 1\pi^4 2\pi^1$ configuration, which leads to ω–ω states of the $^3\Pi$ and $^1\Pi$ states.

As seen in Table 16, theoretical calculations confirmed the earlier assignment of the X, A, and B states of TlF to 0^+, 0^+(II), and $1(^3\Pi_1)$ states, respectively. The 1(II) state in Table 16 is the C state in the C → X(0^+) emission system.

Absorption continua in the region of 45 400 cm^{-1} and above 50 000 cm^{-1} were assigned to the 0^+(IV) state, which was found to be predominantly $^1\Sigma^+(\text{II})_{0^+}$ arising from $\sigma^2\pi^3\pi^*$, which was mixed significantly with $\sigma^2\pi^3\pi^*(^3\Sigma^-_{0^+})$. There are also several 1 states arising from $\sigma^2\pi^3\pi^*$ configurations. These states could also be attributed to those continua of bands in the region above 50 000 cm^{-1}.

In the $^3\Pi_{0^+}$–X system no bands higher than $v' = 3$ for $^3\Pi_{0^+}$ [0^+(II)] were observed. Howell[194] postulated the existence of a repulsive state that crosses with $^3\Pi_{0^+}$ and $^3\Pi_1$ so as to produce predissociation in both $^3\Pi_{0^+}$ and $^3\Pi_1$. As seen from Figure 30, the $^3\Pi_{0^-}$ [i.e., 0^-(I)] crosses with 0^+(II) and 1 (the crossing with 0^+(II) is at a shorter distance in comparison to the crossing with the 1 state). Thus the 0^-(I) state may be responsible for the predissociation in $^3\Pi_1$. However, predissociation via a tunneling mechanism through the small barrier or via rotationally induced coupling to $B^3\Pi_1$ should not be ruled out. Howell's[194] observed spectra showed the continuum to be of lower intensity in comparison to the bands in these systems.

Rao and Rao[199] reported band spectra of TlF in the 28 500–29 500-cm^{-1} region that were abruptly cut off. The vibrational frequency of the upper state calculated by these authors was about 194 cm^{-1}, suggesting that this is a shallow minimum. This was attributed to a possible long-distance shallow minimum by Balasubramanian.[198]

The existence of maxima in the potential energy curves of the excited Π states of TlF was predicted by many authors.[190,191] This prediction was based on the higher spectroscopic dissociation energies obtained from Birge–Sponer extrapolation of the excited Π states. The spectroscopic dissociation energies for these molecules were thus higher than the thermochemical values. As seen in Figures 30 and 31, the excited Π states, 0^+(II), 0^-, 1, 2, and 1(II), and the 0^-(II), 0^+(III), and 2(II) states have maxima in their potential curves. These states are bound but their dissociation limits are way down, and thus they have to go through maxima.

Howell[194] misassigned the A and B states of TlF to $^3\Pi_{0^+}$ and $^3\Pi_1$ arising from the $\sigma^2\pi^3\sigma^*$ configuration. Balasubramanian's[198] SCF calculations indicated that the σ^* orbital is very highly antibonding while the π^* orbital is the nonbonding thallium 6p orbital. The CI calculations confirmed that the $^3\Pi$ state arising from $\sigma^2\pi^3\sigma^*$ is much higher in energy in comparison to $^3\Pi$ arising from the $\sigma\pi^4\pi^*$ configuration. Thus the A0$^+$ and B1 states are $^3\Pi_{0^+}$ and $^3\Pi_1$, arising from the $\sigma\pi^4\pi^*$ configuration. On the basis of the electronic properties of isoelectronic BF and AlF molecules, Murad, Hildebrand, and Main[190] correctly concluded that the lowest-lying $^3\Pi$ and $^1\Pi$ states should arise from the $\sigma\pi^4\pi^*$ configuration.

The theoretical dissociation energy for the 0^+(I) state of 3.86 eV[198] was found to be in reasonable agreement with the photoionization mass spectrometric value of Berkowitz and Walter (4.57 eV).[191]

B. PbF

The early investigations (1930s)[200,201] of the band spectrum of PbF showed conflicting evidence on the

 Chemical Reviews, 1989, Vol. 89, No. 8

TABLE 17. Calculated and Available Experimental Spectroscopic Properties of PbF[a]

	R_e, Å		T_e, cm^{-1}		ω_e, cm^{-1}		D_e, eV	
state	theory	expt	theory	expt	theory	expt	theory	expt
$X_1{}^2\Pi_{1/2}1/2(I)$	2.08	2.06	0	0	540	503	3.75	3.69 ± 0.09
$X_2{}^2\Pi_{3/2}3/2(I)$	2.06	2.03	7895	8264	547	520	2.78	—
$A^2\Sigma^+_{1/2}1/2(II)$	2.13	2.16	24510	22557	502	[395][c]	0.78	—
$^4\Sigma^-_{3/2}3/2(II)$	2.53	—	34440	—	267	—	0.38	—
$B^2\Sigma^+_{1/2}$[b]	1.99	1.98	35941	35664	724	606	—	—
$^4\Sigma^-_{1/2}$	2.37	—	35998	—	239	—	0.28	—
$^2\Pi$	2.07	—	5168	—	553	—	4.43	—
$^2\Sigma^+$	2.16	—	24218	—	487	—	2.09	—

[a] The theoretical results are from ref 208. [b] The spectroscopic properties of the $B^2\Sigma^+_{1/2}$ (Rydberg) state were calculated with an extended triple-ζ s and p basis for the lead atom and a comparison calculation for the ground state. See text for discussion. [c] Experimental value is uncertain.

ground state of PbF. The electronic spectra of PbF did not show the typical doublet-type structures of the lighter analogues of that group such as SnF. Thus the early assignments of the observed spectra were very difficult. The spin–orbit splitting of the lead atom is so large that the ground state of PbF was found to be split apart by 8000 cm^{-1}. The absorption spectra of PbF were studied by Morgan[200] and Rochester.[201] A part of the earlier analysis of the spectra of PbF was incorrect as shown by Barrow and co-workers[202] in a later investigation. The electronic spectra of PbF exhibited Λ-doubling due to the large spin–orbit coupling. Lumley and Barrow[205] carried out the rotational analyses of the observed $B-X_2$, $B-X_1$, and $A-X_1$ systems. The assignments of the A and B states remained uncertain. The other experimental works on PbF are contained in refs 203, 204, 206, and 207. Mêlen and Dubois[331] have assigned 39 unattributed electronic states of GeX, SnX, and PbX (X = F, Cl, Br, I) to Rydberg configurations. Ionization potentials and quantum defects have been derived.

Balasubramanian[208] carried out SCF/RCI calculations on six ω–ω states and five λ–s states of PbF. These calculations enabled the assignment of the observed X_1, X_2, A, and B states. In addition, the spectroscopic properties of some of states of PbF that have not been observed to date were calculated.

Table 17 shows the theoretical and experimental spectroscopic constants of PbF. Figure 32 shows the SCF/RCI potential energy curves of PbF with and without the spin–orbit coupling term. As seen from Table 17, the spin–orbit splitting of the $^2\Pi_{1/2}$–$^2\Pi_{3/2}$ states was calculated as 7895 cm^{-1} [208] in comparison to an experimental value of 8264 cm^{-1}.[32] The calculated properties of the ground state are also in excellent agreement with experiment.

The A state observed in the $A-X_1$ system was assigned to the $^2\Sigma^+_{1/2}$ state arising from the $\sigma^2\sigma^*\pi^4$ configuration. The calculated T_e and R_e values of this state confirmed this assignment. The properties of the $^4\Sigma^-_{3/2}$ and $^4\Sigma^-_{1/2}$ states are shown in Table 17. It seems that these states have not yet been observed experimentally.

Lumley and Barrow[205] discussed the possible assignments of the B state observed in the $B-X_2$ and $B-X_1$ systems. These possibilities included B to be the lowest Rydberg $^2\Sigma^+$ state, $^4\Sigma^-$, or $^2\Pi_{1/2}$. The R_e of $^4\Sigma^-_{1/2}$ is larger than the R_e of the ground state (Table 17). The experimentally observed B state has an R_e smaller than the R_e of the ground state. The calculated ω_e of the $^4\Sigma^-_{1/2}$ state (239 cm^{-1}) is quite different from the ω_e of the B state (606 cm^{-1}). The separation of $^4\Pi(\sigma^2\pi^3\pi^{*2})$ from $X^2\Pi$ at 4.0 bohr was calculated as 42227 cm^{-1} [208] and $^2\Pi(\sigma^2\pi^3\pi^{*2})$ would thus even be higher. Balasubramanian[208] calculated the properties of the first Rydberg state ($^2\Sigma^+_{1/2}$) arising from the $\sigma^2\sigma_R\pi^4$ configuration with a triple-ζ Pb s and p basis set. The T_e value calculated for this Rydberg state agreed with the experimental value. Thus the B state was assigned to a $^2\Sigma^+{}_{1/2}$ Rydberg state.

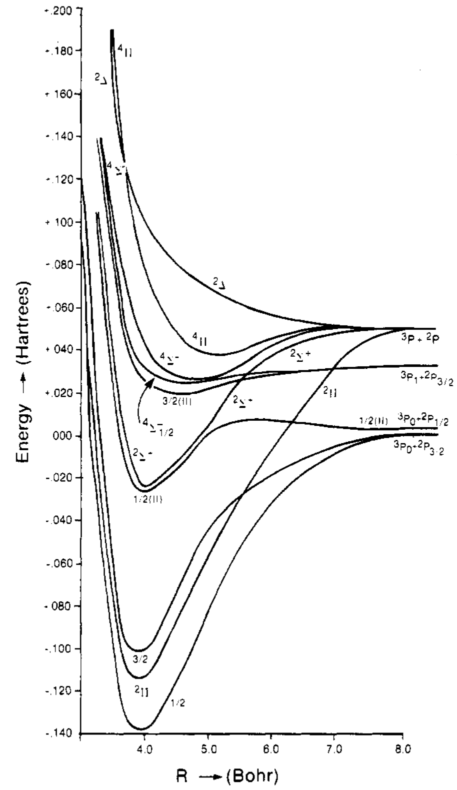

Figure 32. Potential energy curves of low-lying electronic states of PbF (reprinted from ref 208; copyright 1985 American Institute of Physics). See Table 17 for assignments of known states.

C. BiF

The BiF molecule appears to be the most studied among the p-block sixth-row fluorides. There are some 18 references on this topic to date.[215–232] The first spectrum of BiF was recorded in emission by Howell,[215] while Morgan[216] studied BiF in absorption. The A–X emission system observed by Howell[215] was studied by many authors subsequently.[217–228] Kuijpers and Dynamus[229] obtained the rotational constants of the ground state of BiF through the millimeter wave spectrum of BiF.

TABLE 18. Spectroscopic Properties of BiF[a]

state	R_e, Å theory	R_e, Å expt	T_e, cm^{-1} theory	T_e, cm^{-1} expt	ω_e, cm^{-1} theory	ω_e, cm^{-1} expt
$X0^+$	2.087	2.052	0	0	502	511
1	2.075	—	7280	9216	501	535
2	2.075	—	14595	—	511	—
$A0^+$(II)	2.076	2.15	25931	22960	467	381
$^3\Sigma^-$	2.068	—	9441	—	514	—
$^1\Delta$	2.06	—	18247	—	496	—
$^1\Sigma^+$	2.06	—	23544	—	537	—

[a] All theoretical results are from ref 232.

Balasubramanian[232] carried out SCF/RCI calculations employing a double-ζ basis set on the low-lying electronic states of BiF. The theoretical calculations were not consistent with Jones and McLean's[230] suggestion of a 0^+ excited state in the 9216-cm^{-1} region. Further, theoretical calculations on BiF indicated that the bands observed by Avasthi,[226] Chakko and Patel,[228] and Murthy et al.[227] in the 5800–6600-Å region were misassigned by these authors. The correct assignments of these bands were made by Balasubramanian.[232]

The rotational analyses of the A–X and B–X systems were done by Jones and McLean,[230] who pointed out the difficulties in the rotational analyses as a result of predissociation and perturbation of the levels arising from the interaction of two 0^+ states in this region. These authors attempted to assign the bands in the 5800–6000-Å region by comparing the BiF molecule with the isoelectronic well-characterized SbF molecule. They suggested the existence of a $b0^+$ state about 9216 cm^{-1} above the ground state which was designated as $X0^+$.

Table 18 shows the theoretical[232] and known experimental spectroscopic properties of the low-lying states of BiF. Figure 33 shows the theoretical potential energy curves of BiF.[232] The properties of the $^3\Sigma^-$, $^1\Delta$, and $^1\Sigma^+$ λ–s states calculated without the spin–orbit term are also reported in Table 18. The $X0^+$ ground state was found to be a mixture of $^3\Sigma^-_{0^+}$ and $^1\Sigma^+_{0^+}$ states, whereas the 1(I) state was found to be the 1 component of the $^3\Sigma^-$ state. The 2 state was predominantly $^1\Delta_2$ at near-equilibrium geometries while the 0^+(II) state was found to be a mixture of $^1\Sigma^+$, $^3\Sigma^-$, and $^3\Pi(\sigma^2\sigma^*\pi^4\pi^*)$, with the $^1\Sigma^+$ state making a predominant contribution. The vibrational frequency of the 0^+(II) state was found to be considerably influenced by avoided crossings.

The second 0^+ state (0^+(II)) was found to be about 25 900 cm^{-1} above the ground state, and no excited state of 0^+ symmetry was found below this state. Thus the assignment of the b state to 0^+ by Jones and McLean[230] as well as Chakko and Patel,[228] who designate the b state by the X_3 state, was shown to be incorrect.[232] The experimental b or X_3 state was found to be 9216 cm^{-1} above the ground state. The only state with a T_e value in this region is the 1(I) state (Table 18). The electronic bands around 6600 Å observed by Avasthi[226] and the electronic bands around 6200 Å observed by Murthy et al.[227] were assigned to the A'–$X_2(2)$ and A_1–$X_2(2)$ transitions, where the X_2 state was assumed to be a 2 state above the ground state. Jones and McLean[230] called this the a(2) state with a T_e value of about 6000 cm^{-1}. The theoretical calculations revealed that there is no such state (Table 18). Balasubramanian[232] suggested, based on the calculated properties of low-lying states of BiF, that the electronic bands observed by

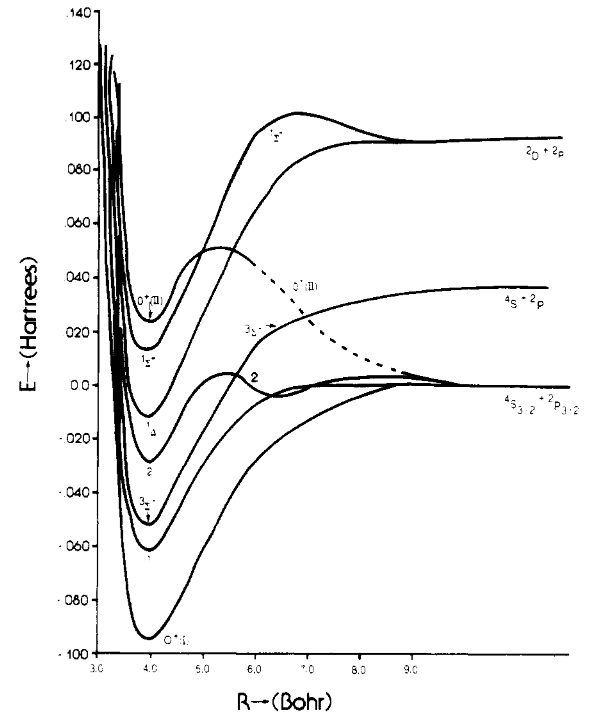

Figure 33. Potential energy curves of BiF (reprinted from ref 232; copyright 1986 Elsevier Science Publishers B.V.). See Table 18 for assignments of known states.

Avasthi,[226] Murthy et al.,[227] and Chakko and Patel[228] may all be due to the same electronic transition.

Jones and McLean[230] designated the 0^+ and 1 states arising from $^3\Sigma^-(\sigma\pi^4\pi^{*2})$ as the X_1 and X_2 states, while the $^1\Delta_2$ state was designated a; the b state was assigned to $^1\Sigma^+(b0^+)$ arising from the electronic configuration $\sigma^2\pi^4\pi^{*2}$. The experimentally observed b state is 9216 cm^{-1} above the ground state. Balasubramanian's[232] calculations indicated that the $^1\Sigma^+(0^+)$ (0^+(II)) state was 25 900 cm^{-1} above the ground state. The bands observed by Chakko and Patel[228] as well as Murthy et al.[227] in this region were assigned to the $0^+(\mathrm{II}) \rightarrow 1$ transition by Balasubramanian.[232] The difference in the calculated T_e values of these two states (18 650 cm^{-1}) was found to be in good agreement with an experimental value of 16 570 cm^{-1}.[228] Thus the lowest excited electronic state above the ground state is a 1 state and is 7280 cm^{-1} above the ground state. Consequently, Balasubramanian[232] showed that the hypothesis of an X_2 state (a2) below this state is false. The experimentally observed A state in the A–X system was assigned to the 0^+(II)–0^+(I) transition. The A state was found to be a mixture of $^1\Sigma^+(\sigma^2\pi^4\pi^{*2})$ and $^3\Sigma^-(\sigma^2\pi^4\pi^{*2})$.

Theoretical calculations supported the existence of a B state very close to the $A0^+$(II) state that perturbed the bands in the A–X system, making rotational analysis of this system difficult. The 0^+(II) state was found to exhibit an avoided crossing within a bohr from its equilibrium geometry. This avoided crossing resulted from the crossing of a $^3\Pi(\sigma^2\sigma^*\pi^3\pi^{*2})$ state with $^1\Sigma^+(\sigma^2\pi^4\pi^{*2})$. Thus the theoretical and experimental R_e and ω_e values of the A state are not in very good agreement. It seems that a more accurate rotational analysis of the A state should be pursued.

The theoretical D_e value of BiF was found to be about 2.63 eV.[232] An upper limit for the D_e of 3.63 eV for the ground state was obtained by Jones and McLean[230] by extrapolating the $v' = 6$ vibrational level to the predissociation limit of the A state. Gaydon[231] reported a D_0 value of 2.65 ± 0.3 eV for BiF. This value was found to be in more reasonable agreement with the theoretically calculated value of 2.63 eV.[232]

The excited states of BiF exhibited avoided crossings.[232] As seen from Figure 33, the 2 and 0^+(II) curves contain barriers that are due to these avoided crossings. The potential energy curve of the 2 state also contains a second shallow minimum.

These features in the potential energy curves of BiF are best understood by considering the weights of various λ–s states in the RCI wave function of BiF as a function of distance.

The highest occupied σ orbital of BiF was found to be a bonding orbital of Bi 6s,6p_z and F 2p_z, with F 2p_z making the dominant contribution. The occupied π orbital was found to be mostly on the fluorine atom. The π^* orbital was predominantly on the Bi atom but the fluorine p orbitals made a nonnegligible contribution. The contribution of the spin–orbit interaction to the electronic states arising from the lowest $\sigma^2\pi^4\pi^{*2}$ electronic configuration should thus be quite high, since the π^* orbital is predominantly on Bi.

At 4.25 bohr, the RCI wave function of the 0^+(I) state consisted of 66% $^3\Sigma^-$, 20% $^1\Sigma^+$, and 5.5% $^3\Pi$. At longer distances, contributions from $^3\Sigma^-(\sigma\sigma^*\pi^4\pi^{*2})$ and $^3\Sigma^-(\sigma^{*2}\pi^4\pi^{*2})$ became important. The 0^+(II) (A) state consisted of 23% $^3\Sigma^-$, 58% $^1\Sigma^+$, 5% $^3\Pi(\sigma^2\sigma^*\pi^4\pi^*)$, and 2% $^3\Pi(\sigma\pi^4\pi^{*3})$ at 4.0 bohr. On the contrary, at 5.0 bohr the 0^+(II) state was found to be 18% $^1\Sigma^+$, 12% $^3\Sigma^-$, 14% $(\sigma^2\sigma^*\pi^3\pi^{*2})$, 18% $^3\Pi(\sigma^2\sigma^*\pi^4\pi^*)$, and 9% $^3\Sigma^-(\sigma^2\sigma^*\pi^4\pi^{*2})$. At 5.5 bohr, this state became predominantly $\sigma^2\sigma^*\pi^3\pi^{*2}$. The 2 state was 79% $^1\Delta_2$ and 5% $^3\Pi_2(\sigma^2\sigma^*\pi^4\pi^*)$ at 4.0 bohr. However, at 6.0 bohr it became 8% $^1\Delta_2$, 3% $^3\Pi_2(\sigma^2\sigma^*\pi^4\pi^*)$, 17% $^3\Pi(\sigma\pi^4\pi^{*3})$, 52% $^5\Sigma_2^-(\sigma\sigma^*\pi^4\pi^{*2})$, and 8% $^1\Delta(\sigma\sigma^*\pi^4\pi^{*2})$, and at longer distances, $^5\Sigma_2^-$ dominated. The barrier and the second minimum in the 2 state were attributed to this avoided crossing.

D. PbCl

The electronic spectroscopy of lead halides has been the topic of a number of investigations for many years.[200,201,205,206,233–237] Analogous to the spectra of PbH, the band spectra of lead halides showed conflicting evidence for the nature of the ground state since these spectra did not exhibit doublet character typical of the lighter analogues.

The absorption spectrum was studied by Morgan,[200] who assigned the observed spectra to the A ↔ X_1 system. The vibrational analysis of this system yielded the ω_e and T_e values for the A state. Rochester[201] studied the band spectrum of PbCl, which facilitated the calculation of the vibrational frequencies of both the X_1 and A states.

The B–X_1 system in the ultraviolet region was first observed by Wieland and Newburgh,[233] although the bands were diffuse and predissociated. These authors extrapolated these bands to predict the D_e of PbCl as 3.05 and 3.40 eV, where the latter value was considered somewhat improbable by these authors.[233] Rao and Rao[235] carried out the rotational analysis of four bands designated by these authors as (4,0), (6,0), (1,1), and (3,1). The rotational constants obtained from this analysis, however, were inconsistent with the theoretical calculations of Balasubramanian,[238] which suggested that a revised rotational analysis was necessary for PbCl. The electron impact study of $PbCl_2$ provided the ionization potential and electron affinity for PbCl.[236] Cordes and Gehrke[234] carried out the revised vibrational analysis for the B–X_1 system.

TABLE 19. Spectroscopic Properties of PbCl[a]

state	R_e, Å theory	R_e, Å expt	T_e, cm^{-1} theory	T_e, cm^{-1} expt	ω_e, cm^{-1} theory	ω_e, cm^{-1} expt
$X_1{}^2\Pi_{1/2}$	2.61	—	0	0	304	304
$X_2{}^2\Pi_{3/2}$	2.58	—	8473	8272	313	322
$A^2\Sigma^+_{1/2}$	2.84	—	22916	21865	220	229
3/2(II)	2.97	—	29915	—	199	—
$^2\Pi$	2.59	—	5640	—	313	—

[a] All theoretical results are from ref 238.

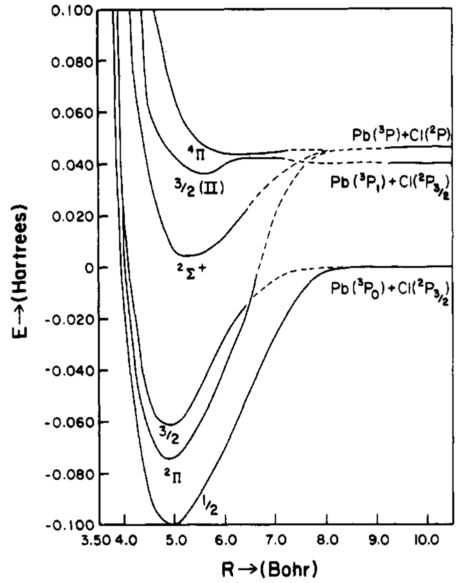

Figure 34. Potential energy curves of low-lying electronic states of PbCl (reprinted from ref 238; copyright 1988 Academic Press, Inc.). See Table 19 for assignments of known states.

Balasubramanian[238] carried out the first SCF/RCI calculations on six low-lying ω–ω states and five λ–s states ($^2\Pi$, $^2\Sigma^+$, $^2\Delta$, $^4\Sigma^-$, $^4\Pi$) of PbCl. The spectroscopic constants and the potential energy curves of these states were calculated.

Table 19 shows the theoretical spectroscopic properties of bound low-lying states of PbCl and the corresponding available experimental values. Figure 34 shows the potential energy curves of the low-lying electronic states of PbCl.

As seen from Table 19, the vibrational frequencies (ω_e) of the low-lying bound electronic states are in excellent agreement with the known experimental values for the X_1, X_2, and A states. The ground-state spin–orbit splitting of 8473 cm^{-1} was found to be in excellent agreement with an experimental value of 8272 cm^{-1}.[32]

An unambiguous assignment of the A state observed in the A–X_1 system was not possible since many electronic states could be candidates for the A state. The A state could be $^2\Sigma^+_{1/2}(1\sigma^22\sigma^23\sigma^24\sigma1\pi^4)$, $^4\Sigma^-_{1/2}(1\sigma^22\sigma^23\sigma1\pi^42\pi^2)$, or $^2\Sigma^\pm_{1/2}(1\sigma^22\sigma^23\sigma1\pi^42\pi^2)$. Balasubramanian's theoretical calculations[238] revealed that the $^4\Sigma^-$ and $^2\Sigma^\pm$ electronic states arising from $1\sigma^22\sigma^23\sigma1\pi^42\pi^2$ are not very strongly bound. The only probable electronic state in the A–X_1 region was found to be the $^2\Sigma^+_{1/2}$ state arising from the $1\sigma^22\sigma^23\sigma^24\sigma1\pi^4$ configuration. The A–X_1 system was thus assigned by

Balasubramanian[238] to the $^2\Sigma^+_{1/2}$–$^2\Pi_{1/2}$ transition.

Although Table 19 does not report the properties of the 1/2(III) state, Balasubramanian's theoretical calculations[238] indicated the existence of a 1/2(III) state (predominantly $^4\Sigma^-_{1/2}(1\sigma^2 2\sigma^2 3\sigma 1\pi^4 2\pi^2)$ 200 cm^{-1} below the $^4\Sigma^-_{3/2}$ state. The B–X system observed in the ultraviolet region was found to be analogous to the B–X system of PbF (see section IV.B). The T_e value of the B state of PbF was calculated to be about 35 941 cm^{-1},[238] which agreed well with an experimental value of 35 664 cm^{-1}.[32] The B–X system of PbCl was observed in the same (35 199 cm^{-1}) region as PbF. On the basis of the earlier calculations on PbF,[208] Balasubramanian[238] concluded that the B state of PbCl also should be a Rydberg state arising from the $1\sigma^2 2\sigma^2 3\sigma^2 5\sigma 1\pi^4$ configuration.

The tentative rotational analysis of the bands in the A–X_1 system made by Rao and Rao[235] was found to be incorrect by Balasubramanian.[238] Rao and Rao[235] reported R_e values obtained from the rotational analysis for the X_1 and A states as 2.195 and 2.338 Å, respectively. However, as seen from Table 19, the theoretical equilibrium bond lengths of the X_1 and A states are much longer; for the X_1 state there is a difference of about 0.41 Å between the value reported by Rao and Rao[235] and the theoretical results. Huber and Herzberg[32] considered the results of Rao and Rao[235] as only tentative and did not report their results for R_e. Accurate experimental results are available for the isoelectronic (SnF, SnCl) as well as (SiF, SiCl) pairs.[32] Balasubramanian[238] compared the bond lengths of the ground states of SnF (1.944 Å), SnCl (2.361 Å), SiF (1.60 Å), and SiCl (2.06 Å), which suggested a difference of about 0.42–0.46 Å between the bond lengths of fluorides and chlorides. Since the bond length of PbF was established by both theoretical[208] and experimental investigations[32] to be about 2.06 Å, the R_e value of the ground state of PbCl should be at least 2.52 Å, eliminating the 2.19 Å value reported by Rao and Rao.[235] Further, the bond length of PbCl should be longer than the corresponding value for SnCl (2.36 Å). Thus it was concluded by Balasubramanian that the correct R_e value of the ground state of PbCl should be at least 2.45 Å, suggesting that a revised rotational analysis of the A–X bands should be carried out.

The D_e of PbCl was calculated by Balasubramanian[238] as 2.72 eV. The experimental D_e value of 3.0 eV was calculated by extrapolating the B–X bands since these bands were predissociated.[32] On the basis of the theoretical results of Balasubramanian,[238] it was predicted that the D_e of PbCl should be <3.0 eV.

The $X_1(1/2)$ ground state of PbCl at its equilibrium geometry was found to be 91% $^2\Pi_{1/2}(1\sigma^2 2\sigma^2 3\sigma^2 1\pi^4 2\pi)$ and 2% $^2\Sigma^+_{1/2}(1\sigma^2 2\sigma^2 3\sigma^2 4\sigma^1 \pi^4)$. The $X_2(3/2)$ state was found to be predominantly $^2\Pi_{3/2}$ at the equilibrium geometry, while the 3/2(II) state was found to be 78% $^4\Sigma^-_{3/2}$, 4% $^2\Pi_{3/2}$, 2.5% $^4\Sigma^-_{3/2}(1\sigma^2 2\sigma^2 4\sigma 1\pi^4 2\pi^2)$, and 4% $^2\Pi_{3/2}(1\sigma^2 2\sigma^2 3\sigma 4\sigma 1\pi^4 2\pi)$. At long distances, the 3/2(II) state was found to exhibit an avoided crossing; at 6.0 bohr the 3/2(II) state was 76% ($1\sigma^2 2\sigma^2 3\sigma^2 1\pi^3 2\pi^2$: $^4\Pi_{3/2}$, $^2\Pi_{3/2}$, $^2\Delta_{3/2}$), 9% ($1\sigma^2 2\sigma^2 3\sigma 1\pi^4 2\pi^2$), and 3% ($1\sigma^2 2\sigma^2 3\sigma^2 1\pi^4 2\pi$). The A state (1/2(II)) was found to be 80% $^2\Sigma^+_{1/2}(1\sigma^2 2\sigma^2 3\sigma^2 4\sigma 1\pi^4)$, 5% $^2\Pi_{1/2}$-($1\sigma^2 2\sigma^2 3\sigma^2 1\pi^4 2\pi$), and 2% $^2\Sigma^+_{1/2}$(Rydberg; $1\sigma^2 2\sigma^2 3\sigma^2 5\sigma 1\pi^4$) at its equilibrium geometry. At 6.0 bohr, this state was 66% $^2\Sigma^+_{1/2}(1\sigma^2 2\sigma^2 3\sigma^2 4\sigma 1\pi^4)$, 6% $^2\Pi_{1/2}(1\sigma^2 2\sigma^2 3\sigma^2 1\pi^4 2\pi)$, and 7% $^4\Sigma^-_{1/2}(1\sigma^2 2\sigma^2 3\sigma 1\pi^4 2\pi^2)$.

The 1/2(III) state exhibited an avoided crossing of Rydberg $^2\Sigma^+_{1/2}$ with $^4\Sigma^-_{1/2}$. At short distance (3.50–4.00 bohr) it was found to be the Rydberg state arising from $^2\Sigma^+_{1/2}(1\sigma^2 2\sigma^2 3\sigma^2 5\sigma 1\pi^4)$, while at 5.00 bohr the 1/2(III) state consisted of 63% $1\sigma^2 2\sigma^2 1\pi^4 3\sigma\alpha 2\pi^2(^3\Sigma^-_0)$, 16% $1\sigma^2 2\sigma^2 1\pi^4 3\sigma\beta\, 2\pi^2(^3\Sigma^-_1)$, 3% $^2\Sigma^+_{1/2}(1\sigma^2 2\sigma^2 3\sigma^2 4\sigma 1\pi^4)$, and 8% $^2\Sigma^+_{1/2}(1\sigma^2 2\sigma^2 3\sigma^1 1\pi^4 2\pi^2)$.

TABLE 20. Spectroscopic Properties of SnCl[a]

state	R_e, Å theory	R_e, Å expt	T_e, cm^{-1} theory	T_e, cm^{-1} expt	ω_e, cm^{-1} theory	ω_e, cm^{-1} expt	D_e, eV theory
$X_1\,^2\Pi_{1/2}$	2.479	2.361	0	0	361	357	3.34
$X_2\,^2\Pi_{3/2}$	2.477	2.356	2769	2357	360	364	2.99
$^2\Pi$	2.479	—	1607	—	359	—	3.14
$A'\,^2\Sigma^+_{1/2}$	2.62	2.619	20956	19418	259	232	—
$^2\Sigma^+$	2.62	—	20773	—	259	—	—
$A\,^4\Sigma^-_{1/2}$	2.50	—	25864	28963	308	301	—
$^4\Sigma^-$	2.49	—	25092	—	308	—	—

[a] Theoretical values are from ref 249.

E. SnCl

The electronic spectra of SnCl were observed by Jevons[239] and Ferguson[240] in the late 1920s and later by Fowler.[241] Sarma and Venkateswarlu[242] identified a band system in the 6440–4880-Å region and assigned the bands observed by Ferguson[240] and by Jevons[239] to the $^2\Delta$–$^2\Pi$ and $^2\Sigma$–$^2\Pi$ systems. Hastie et al.,[243] Oldershaw and Robinson,[244] and Richter[245] studied the absorption spectrum of SnCl in the UV region. The vibrational analyses of the C–X systems have been carried out.[245]

Chatalic et al.[246] carried out the rotational analysis of the B–X and A–X bands and questioned the earlier assignment of the systems in the 28 000-cm^{-1} region to the $^2\Delta$–$^2\Pi$ transition. They reassigned these bands to the 3/2 and 1/2 Ω components of the $^4\Sigma^-$–$^2\Pi$ system. The other experimental work on SnCl is in ref 247. Mulliken[248] in his general theoretical paper on electronic states and band spectra of diatomics interpreted the bands observed by Jevons[239] as due to the ^2S–$^2P_{1/2}$ atomic transition of Sn^+.

Balasubramanian[249] carried out SCF/RCI calculations employing a double-ζ STO basis set for the Sn and Cl atoms. Spectroscopic properties and potential energy curves of seven electronic states of SnCl were obtained.

Table 20 shows the theoretical spectroscopic constants of SnCl compared with available experimental results. Figure 35 shows the actual potential energy curves of the low-lying electronic states of SnCl. The experimental T_e value of the A′ state (19 418 cm^{-1}) was found to be in very good agreement with the theoretical T_e value of the $^2\Sigma^+_{1/2}$ state (20 956 cm^{-1}). This combined with the good agreement between the calculated and experimental R_e and ω_e values enabled the assignment of the A′ state to a $^2\Sigma^+_{1/2}$ state.

The electronic state (A) in the A ↔ X system was first assigned to a $^2\Delta$ state. Later Chatalic et al.[246] reinterpreted the observed bands in the A–X system as due to the Ω components of a $^4\Sigma^-$ state (3/2, 1/2). The theoretical results in Table 20 support Chatalic et al.'s reinterpretation of the A state. The B state in the B–X system was again assigned to a $^2\Sigma^+_{1/2}$ Rydberg state based on comparison with PbCl.

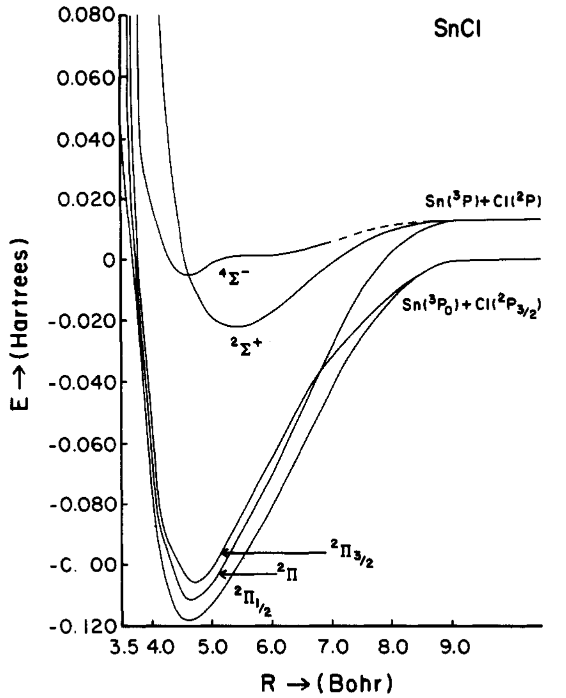

Figure 35. Potential energy curves for SnCl (reprinted from ref 249; copyright 1988 Academic Press, Inc.). See Table 20 for assignments of known states.

The theoretical dissociation energy (D_e) of SnCl was calculated as 3.34 eV. There are no experimental D_e's available for SnCl. Balasubramanian[249] predicted that the experimental D_e of SnCl should be 3.7–3.9 eV.

At the equilibrium geometry, the ground state X_1-($^2\Pi_{1/2}$) was found to be 95% $^2\Pi_{1/2}$ and 0.4% $^2\Sigma^+_{1/2}$-($1\sigma^2 2\sigma^2 3\sigma 1\pi^4$). The $A'^2\Sigma^+$ state was found to be 90% $^2\Sigma^+_{1/2}(1\sigma^2 2\sigma^2 3\sigma 1\pi^4)$ and 0.52% $^2\Pi_{1/2}$. The $^4\Sigma^-_{1/2}$(A) state was found to be 87% $^4\Sigma^-_{1/2}$ and 0.4% $^2\Sigma^+_{1/2}$-($1\sigma^2 2\sigma^2 3\sigma 1\pi^4$).

V. Spectroscopic Properties and Potential Energy Curves of Heavy Group IV Chalconides and Their Ions

The interest in heavy group IV oxides and sulfides arises from the fact that these species are generated in chemiluminescent reactions of atoms such as Pb and Sn with molecules such as N_2O, O_3, OCS, etc.[250-253] Examples of many chemiluminescent reactions of the heavy group IV atoms are shown in eq 1–5. Reactions

$$Pb + O_3 \rightarrow PbO^* + O_2 \quad (1)$$

$$Pb + N_2O \rightarrow PbO^* + N_2 \quad (2)$$

$$Sn + N_2O \rightarrow SnO^* + N_2 \quad (3)$$

$$Pb + OCS \rightarrow PbS^* + CO \quad (4)$$

$$Sn + OCS \rightarrow SnS^* + CO \quad (5)$$

1–5 were investigated for their suitabilities as chemical laser pumping reactions. Consequently, a wealth of information has accumulated on the spectroscopic properties of both the ground state and the excited electronic states of molecules such as SnO, SnS, PbO, PbS, etc.[254-270] Balasubramanian and Pitzer[271,285] studied the spectroscopic properties and potential curves of SnO and PbO. Later Balasubramanian pursued this line of study further to complete calculations on SnS, PbS, PbSe, and their positive ions.[273,285,304] The experimental photoelectron spectra of heavy group IV chalconides were also interpreted by using the results of these calculations. This section reviews both experimental and theoretical developments on these species.

TABLE 21. Spectroscopic Properties of SnO

state	T_e, cm^{-1}	R_e, Å	ω_e, cm^{-1}
X $^1\Sigma^+(0^+)$	0	1.94	800
		(1.83)	(823)
$^3\Sigma^+(0^-,1)$	18606	2.13	542
	(20622?)		(554?)
$^3\Delta(1,2,3)$	20561	2.16	493
$^3\Sigma^-(0^+,1)$	22750	2.15	530
	(20622?)		(554?)
$^1\Sigma^-(0^-)$	22890	2.14	540
A $^3\Pi(0^+,0^-,1,2)$	24100	2.06	770
B	(24333, 0^+)	(2.01, 0^+)	(555, 0^+)
	(24890, 1)	(1.99, 1)	(560, 1)
D $^1\Pi(1)$	26700	2.06	710
	(29624)	(1.95)	(574)

[a] Numbers in parentheses are experimental values from ref 32. The theoretical values are from ref 271.

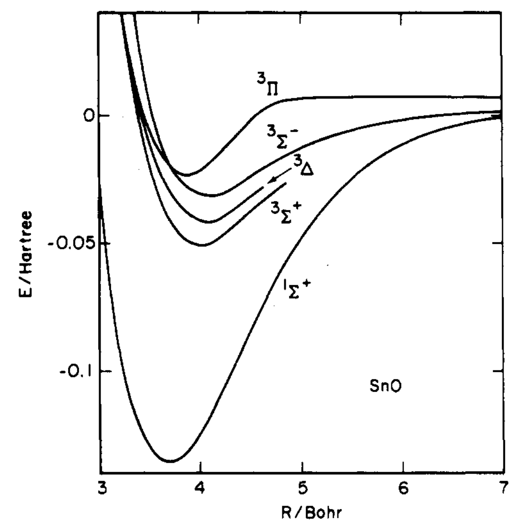

Figure 36. Potential energy curves for SnO (reprinted from ref 271; copyright 1983 Elsevier Science Publishers B.V.). See Table 21 for assignments of known states.

A. SnO and SnO^+

The spectroscopic properties, electronic dipole moments, and photoelectron spectra of SnO have been the subjects of many investigations for several years.[254-270] The chemiluminescent spectra of SnO have also demonstrated the existence of several emission systems in the visible and ultraviolet regions. The tin oxide molecule was also investigated as a candidate for chemical lasers because of the high photon yields (~ 50%) of the Sn + N_2O reaction.[262] The observed bands in the visible and near-UV regions for SnO, however, were not interpreted satisfactorily before the theoretical calculations of Balasubramanian and Pitzer.[271]

Balasubramanian and Pitzer[271] made relativistic SCF/CI calculations on seven λ–s states of SnO employing a double-ζ STO basis set. The theoretical spectroscopic constants for SnO together with available experimental data are shown in Table 21. The potential energy curves of these states are shown in Figure 36.

TABLE 22. Spectroscopic Constants of SnO^+ and Ionization Potentials of SnO[a]

		R_e, Å		T_e, cm^{-1}		ω_e, cm^{-1}	
method[b]	state	theory	expt	theory	expt	theory	expt
RCI	$^2\Pi$	2.05	2.00	0	0	695	700
RCI	$^2\Sigma^+$	1.96	—	3616	—	708	—

method[b]	splitting	IP, eV	method[b]	splitting	IP, eV
SCF	$^1\Sigma^+$–$^2\Pi$	6.73	KT	$^1\Sigma^+$–$^2\Pi$	10.15
RCI	$^1\Sigma^+$–$^2\Pi$	8.44	KT	$^1\Sigma^+$–$^2\Sigma^+$	9.79
RCI	$^1\Sigma^+$–$^2\Sigma^+$	8.76			

[a] All theoretical results are from ref 273. The experimental values are from ref 272. [b] RCI = relativistic CI; KT = Koopmans' theorem.

The SnO molecule is expected to have a closed-shell $^1\Sigma^+$ ground state arising from the $1\sigma^2 2\sigma^2 3\sigma^2 1\pi^4$ configuration where the highest occupied 3σ orbital should be a mixture of metal p_z with O p_z while the highest occupied 1π orbital should be predominantly the oxygen 2p nonbonding orbital. Thus the 2π orbital should be predominantly on the tin atom. The theoretical investigation of Balasubramanian and Pitzer[271] considered the $^1\Sigma^+$ ground state, the $^3\Sigma^+$, $^3\Sigma^-$, $^3\Delta$, and $^1\Sigma^-$ states arising from the $1\sigma^2 2\sigma^2 3\sigma^2 1\pi^3 2\pi$ configuration, and the $^3\Pi$ and $^1\Pi$ states arising from the $1\sigma^2 2\sigma^2 3\sigma 1\pi^4 2\pi$ configuration.

Deutsch and Barrow[260] observed and analyzed the emission bands from the $^3\Pi(0^+)$ and $^3\Pi(1)$ states to the $^1\Sigma^+$ state designated as the A–X and B–X systems. As seen from Table 21, the theoretical T_e values of these states are in reasonable agreement with the experimental results. Capelle and Linton[262] obtained additional bands for the system near 20 000 cm^{-1} reported earlier by Joshi and Yamdagni[261] at 19 000 cm^{-1}. Capelle and Linton[262] assigned this system to the $^3\Sigma^+(1) \rightarrow {}^1\Sigma^+$ transition. However, the experimental T_e of 20 622 cm^{-1} was found to be higher than the theoretical value of 17 650 cm^{-1} obtained by Balasubramanian and Pitzer.[271] Thus Balasubramanian and Pitzer[271] argued for the possibility of this system state as either $^3\Sigma^-(0^+)$ or $^3\Sigma^-(1)$.

The calculations of Balasubramanian and Pitzer[271] supported the earlier assignment of the D–X system ($D(T_e)$ = 29 624 cm^{-1}) to $^1\Pi(1)$ [1(V)] although the calculated T_e of 26 700 cm^{-1} was considerably lower. Balasubramanian and Pitzer[271] attributed the difference to the fact that it is the fifth excited 1 state, and thus theoretical results may not be very accurate.

The theoretical D_e of 3.70 eV was found to be considerably smaller than the experimental value[32] of 5.49 eV. This was mainly because of a single-configuration SCF followed by CI, which does not take into account all of the electron correlation effects.

The He I photoelectron spectra of the SnO molecule was recorded by Dyke et al.[272] in the X($^1\Sigma^+$) ground state. This photoelectron spectrum revealed the existence of low-lying states of SnO^+ of $^2\Pi$ and $^2\Sigma^+$ character. Dyke et al.[272] also made Dirac–Fock SCF–Xα calculations to determine the ordering of the two observed states of SnO^+.

Balasubramanian[273] carried out SCF/RCI calculations on the low-lying electronic states of SnO^+ as well as the heavier PbO^+, PbS^+, and $PbSe^+$ ions. Three low-lying states including the spin–orbit coupling were found for all these species. Table 22 shows the spectroscopic constants for SnO^+ and the ionization potentials of SnO as obtained by different methods. Figure 37 shows the potential energy curves of the two low-lying electronic states of SnO^+.

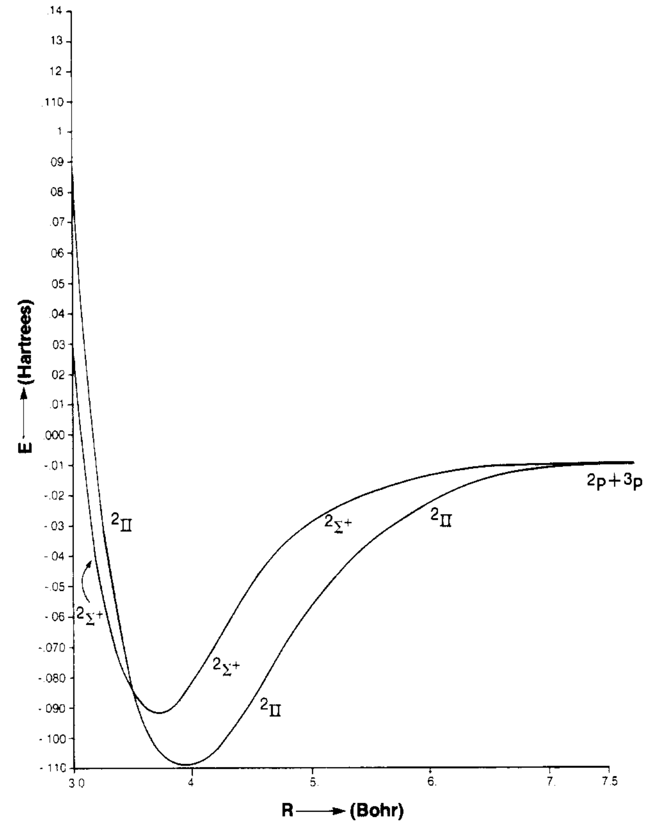

Figure 37. Potential energy curves of two electronic states of SnO^+ (reprints from ref 273; copyright 1984 American Chemical Society).

As seen from Table 22, the agreement between SCF/RCI results of Balasubramanian[273] and Dyke et al.'s[272] photoelectron spectrum is excellent. The D_e's of SnO^+ in the $^2\Pi$ and $^2\Sigma^+$ states are 2.95 and 2.50 eV, respectively, in comparison to the corresponding experimental values of 3.23 and 2.71 eV, respectively.

The vertical ionization potentials of SnO to generate SnO^+ in the $^2\Pi$ and $^2\Sigma^+$ states were calculated to be 8.44 and 8.76 eV, respectively. Agreement with the corresponding experimental values of 9.98 and 10.12 eV is not exact, but it is well-known that the IPs and EAs cannot be calculated exactly by ab initio methods. However, the SCF/RCI method predicts the correct ordering of the electronic states of SnO^+ in contrast with Koopmans' theorem, which predicts the ground state of SnO^+ to be $^2\Sigma^+$ incorrectly. Koopmans' theorem is also off in the magnitudes of the IPs of the two states. Balasubramanian[273] explained the breakdown of Koopmans' theorem based on the large orbital relaxation effects.

The potential energy curves of the $^2\Sigma^+$ and $^2\Pi$ states cross near the repulsive wall of the $^2\Pi$ state. Thus the corresponding 1/2 components undergo avoided crossings. The adiabatic splitting of the $^2\Sigma^+$–$^2\Pi$ states (0.34 eV) was found to be a bit larger than the vertical separation at the R_e of SnO molecule (0.32 eV). The bond length of the $^1\Sigma^+$ state of the SnO molecule was calculated as 1.94 Å, while the R_e of the $^2\Pi$ state of SnO^+ was calculated as 2.05 Å. Thus the bond length

TABLE 23. Spectroscopic Properties of PbO[a]

state	R_e, Å theory	R_e, Å expt	T_e, cm^{-1} theory	T_e, cm^{-1} expt	ω_e, cm^{-1} theory	ω_e, cm^{-1} expt
X $^1\Sigma^+$(I), 0^+(I)	2.02	1.92	0	0	715	721
b? $^3\Sigma^+0^-$	2.23		14 461	16 454?		441?
a 1	2.23	2.12	14 551	16 025	487	482
b? $^3\Delta_2$	2.23		15 205	16 454?	540	441?
1(II)	2.24		15 360		472	
$^1\Delta$(2(II))	2.24		16 035		451	
$^3\Pi0^-$(III)?	2.14		18 758		576	
A 0^+(II)	2.14	2.09	18 890	19 863	528	444
B 1(III)		2.07		22 285		498
C $^3\Sigma^-0^+$(III)	2.23		20 747	23 820	612	532
C′ 1(IV)				24 947		494
D $^1\Pi$(1(V))	2.14	2.05	27 215	30 199	521	530
E $^1\Sigma^+$(II) (0^+(IV))		2.18		34 454		454
$^1\Sigma^+$	2.02		682		706	
$^3\Sigma^+$	2.21		16 610		503	
$^3\Delta$	2.24		18 267		485	
$^3\Sigma^-$	2.23		20 292		600	
$^1\Sigma^-$	2.22		20 477		594	
$^3\Pi$	2.13		22 469		514	
$^1\Pi$	2.15		24 771		505	
$^1\Sigma^+$(II)	2.22		39 202		703	

[a] All theoretical results are from ref 285.

is increased by 0.11 Å when SnO is ionized.

B. PbO and PbO$^+$

The PbO molecule has been studied experimentally in both the visible and UV regions.[274-284] An intense system labeled A0$^+$ → X0$^+$ in the emission has been characterized. A few other less intense systems labeled a → X and b → X have also been observed. In addition to these, the B, C, C′, D, E, and G states of PbO have been characterized in the B ↔ X, C ← X, C′ ← X, D ↔ X, E ↔ X, F ← X, and G ← X systems. The dissociation energy of PbO was obtained by using the mass spectrometric method[279] as well as from the chemiluminescence spectra of Pb + O_3 under single-collision conditions by Oldenborg, Dickson, and Zare.[281] The experimental D_e of PbO obtained by these methods was found to be between 3.74 and 3.83 eV.

The dipole moment of the PbO molecule was measured as $\mu_{el}(v=0)$ = 4.64 D using the Stark spectra.[267] The relative intensities[309] and transition probabilities[310] of the B–X bands have also been deduced from the experimental information. The RKR potential functions have been derived for the A and X states.[280]

The theoretical calculations on PbO were made by Balasubramanian and Pitzer[285] using the SCF/RCI method which employed a double-ζ STO basis set. These authors found 11 low-lying electronic states of PbO. The spectroscopic constants of eight λ–s states were also obtained without the spin–orbit term for comparison.

Table 23 shows the spectroscopic constants of PbO together with available experimental results. Figure 38 shows the theoretical potential energy curves for PbO calculated by Balasubramanian and Pitzer.[285]

In analogy with SnO, the ground state of PbO was found to be a $^1\Sigma^+_{0^+}$ state arising from the $1\sigma^2 2\sigma^2 3\sigma^2 1\pi^4$ configuration. The excited states of PbO arise from the $1\sigma^2 2\sigma^2 3\sigma^1 1\pi^4 2\pi$ and $1\sigma^2 2\sigma^2 3\sigma^2 1\pi^3 2\pi$ configurations.

The A0$^+$–X0$^+$ bands observed in emission with a T_e of 19 863 cm^{-1} were assigned by Balasubramanian and Pitzer[285] to a $^3\Pi_{0^+}$–$X^1\Sigma^+$ system, where the theoretical T_e value of the A state was found to be 18 890 cm^{-1}. The A state was found to be actually a mixture of the $^3\Pi_{0^+}$ and $^1\Sigma^+_{0^+}$ states. The agreement between the theoretical and experimental R_e and ω_e values of the A state also appeared to be good.

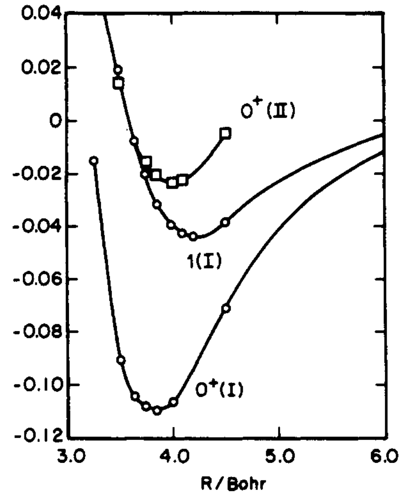

Figure 38. Potential energy curves for the electronic states of PbO (reprinted from ref 285; copyright 1983 American Chemical Society). See Table 23 for assignments of known states.

The earlier assignment of the a1 state to $^3\Sigma^+_1$ was confirmed by the calculations of Balasubramanian and Pitzer.[285] However, the spin–orbit components (0^-, 1) of the $^3\Sigma^+$ state were found to be contaminated substantially with other λ–s states. The 0^- state was found to be 75% $^3\Sigma^+_{0^-}$ and 25% $^1\Sigma^-_{0^-}$ while the 1 state was found to be a 3/4 $^3\Sigma^+_1$ and 1/4 $^3\Sigma^-_1$ mixture. In Table 23, two possible assignments for the b state ($^3\Sigma^+_{0^-}$ or $^3\Delta_2$) are suggested.

An emission system labeled B → X0$^+$ with a T_e value 22 885 cm^{-1} was assigned to $^3\Pi_1$ by several investigators. The assignment of the B state to $^3\Pi_1$ was supported by the theoretical calculations of Balasubramanian and Pitzer,[285] although this state was found to be certainly a mixture of $^3\Pi_1$, $^1\Pi_1$, and $^3\Sigma^-_1$. The C state was assigned to $^3\Sigma^-_{0^+}$. The theoretical ω_e value of C (613 cm^{-1}) was in good agreement with the experimental value. The D → X0$^+$ and E → X0$^+$ emissions have also been observed experimentally. The experimental T_e values of these states are 30 199 and 34 454 cm^{-1}. The D and E states correspond theoretically to the 1(V) and 0^+(IV) states. These states were found to be predominantly $^1\Pi_1$ and $^1\Sigma^+$(II) states.

The calculated dissociation energy of 3.0 eV[285] for the PbO molecule was found to be in reasonable agreement with the experimental value of 3.83 eV.[32] The calculated[285] R_e and ω_e values for the ground state were in good agreement with the experimental values and the values obtained by Basch, Stevens, and Krauss using a MCSCF calculation.[286] The calculated ω_e and R_e values for the excited states were found to be in good agreement with the available experimental results.

The three lowest-lying electronic states of PbO$^+$ were investigated by Balasubramanian[273] using a SCF/RCI scheme including the spin–orbit term. The ionization potentials of PbO obtained by various methods together with the theoretical spectroscopic constants are shown in Table 24. Figure 39 shows the potential energy curves for the low-lying electronic states of PbO$^+$.

As seen from Table 24, the 3/2 and 1/2 components of the $^2\Pi$ state of PbO$^+$ are nearly degenerate since the 1π orbital of PbO is predominantly the nonbonding

TABLE 24. Spectroscopic Constants for PbO^+ and Ionization Potentials of PbO[a]

method	state	R_e, Å	T_e, cm^{-1}	ω_e, cm^{-1}
RCI	3/2	2.18	0	590
RCI	1/2	2.16	46	610
RCI	1/2(II)	2.09	4979	712

method	splitting	IP, eV	method	splitting	IP, eV
SCF	$^1\Sigma^+$–$^2\Pi$	6.23	KT	$^1\Sigma^+$–$^2\Pi$	9.82
RCI	$^1\Sigma^+$–$^2\Pi$	8.10	KT	$^1\Sigma^+$–$^2\Sigma^+$	9.31
RCI	$^1\Sigma^+$–$^2\Sigma^+$	8.52			

[a] All results are from ref 273; KT = Koopmans' theorem.

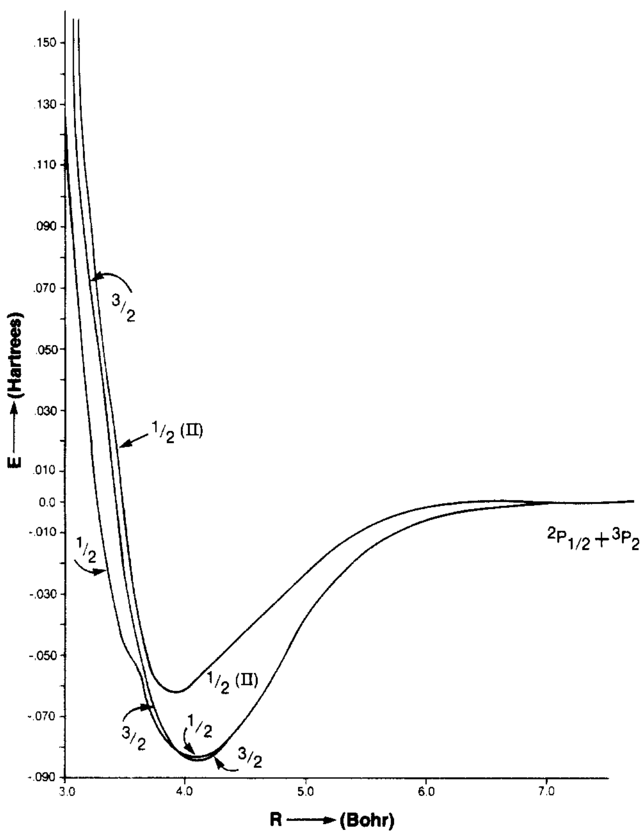

Figure 39. Potential energy curves for the low-lying electronic states of PbO^+ (reprinted from ref 273; copyright 1984 American Chemical Society).

O(2p) orbital. Since the spin–orbit splitting of the oxygen atom is small, the $^2\Pi_{3/2,1/2}$ components are close in energy.

The RCI $^1\Sigma^+$–$^2\Pi$ and $^1\Sigma^+$–$^2\Sigma^+$ neutral–ionic splittings should be about 15% lower than the experimental values due to the errors introduced by electron correlation effects. The IPs of PbO are thus predicted as 9.32 ($^2\Pi$) and 9.8 eV ($^2\Sigma^+$), respectively. There are no experimental IPs available for PbO. Koopmans' theorem, however, breaks down for PbO in that it predicted the wrong ordering for the electronic states of PbO^+.

As seen from Figure 39, the 1/2 state of PbO^+ contains a shoulder. This shoulder resulted from an avoided crossing. In the absence of the spin–orbit coupling term the $^2\Sigma^+$ and $^2\Pi$ states cross. Since both states yield one state of the same symmetry (1/2) when spin–orbit coupling is included, the 1/2 components of these states undergo an avoided crossing. Thus the 1/2 state was found to be predominantly $^2\Sigma^+_{1/2}$ at short distances but became $^2\Pi_{1/2}$ near the well and long distances. At 3.8 bohr, the 1/2 state of PbO^+ was found to be 75% $^2\Pi_{1/2}$ and 16% $^2\Sigma^+_{1/2}$.

TABLE 25. Spectroscopic Properties of SnS[a]

	R_e, Å		T_e, cm^{-1}		ω_e, cm^{-1}	
state	theory	expt	theory	expt	theory	expt
$X^1\Sigma^+$	2.32	2.21	0.0	0.0	449	487
$a^3\Sigma^+(0^-,1)$	2.55	—	21 864	18 144	356	338
$C^3\Sigma^-(0^+,1)$	2.62	—	25 632	(22 380, 0^+)	308	—
C′				(22 480, 1)		
$^3\Delta(3,2,1)$	—	—	~24 000	—	—	—
$^1\Sigma^-(0^-)$	2.62	—	25 685	—	307	—
$A^3\Pi$	2.42	—	28 658	22 021, 0^+	377	
B				23 320, 1		
$D^1\Pi$	2.48	2.36	32 707	28 337	371	331
$E^1\Sigma^+(II)$	2.63	—	41 238	33 037	336	294

[a] All theoretical results are from ref 295.

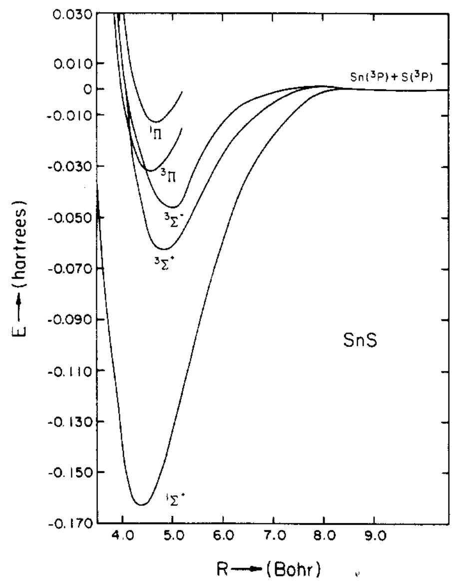

Figure 40. Potential energy curves for SnS (reprinted from ref 295; copyright 1987 Elsevier Science Publishers B.V.). See Table 25 for assignments of known states.

C. SnS

The absorption and emission spectra of SnS observed below 35 000 cm^{-1} yielded information on the a → X, A ↔ X, C′ ↔ X, D ↔ X, and E ↔ X systems.[287–294] Greenwood, Linton, and Barrow[292] studied the electronic spectrum of SnS using the Sn + OCS chemiluminescence reaction. Two electronic states excited in chemiluminescence were characterized (a, A) and assigned to a $^3\Sigma^+_1$ and $A^3\Pi_{0^+}$. These authors made rotational analyses of the bands seen in absorption, which enabled tentative assignment of these to the Ω components of $^3\Sigma^-$ and $^3\Pi_1$.

Balasubramanian[295] carried out SCF/CI calculations that employed a double-ζ STO basis on eight λ–s state of SnS. The spectroscopic constants and the potential energy curves of these states were computed. Since the SnS molecule is iso-valence-electronic with SnO, its ground state should be a $^1\Sigma^+$ state arising from the $1\sigma^2 2\sigma^2 3\sigma^2 1\pi^4$ electronic configuration. The excited states of SnS should arise from the $1\sigma^2 2\sigma^2 3\sigma^2 1\pi^3 2\pi$ and $1\sigma^2 2\sigma^2 3\sigma 1\pi^4 2\pi$ configurations.

Table 25 shows the theoretical spectroscopic constants for SnS together with experimental results. The theoretical potential energy curves of SnS are shown in Figure 40 in the absence of the spin–orbit coupling term.

The first excited $a^3\Sigma^+$ electronic state of SnS was observed by Greenwood, Linton, and Barrow[292] in chemiluminescence. The theoretical T_e values of all the excited states are about 15% higher than the experimental values since the ground state was correlated more than the excited states. If this correction is applied to all the excited states, the assignments of the observed states are possible.

The $^3\Delta_{3,2,1}$ electronic states have not yet been observed; the transitions to the 3 and 2 Ω components of this state are forbidden from the ground state. The T_e value of this state (24 000 cm^{-1}) when corrected for the differential correlation errors yielded a T_e of 20 400 cm^{-1} in the absence of spin–orbit interaction.

Greenwood, Linton, and Barrow[292] observed five systems of SnS for which rotational analyses were made. Since the transitions of systems 5 and 4 had three-branch bands, these authors assigned the upper states of systems 4 and 5 to $\Omega = 1$ components. The systems 2 and 3 were assigned to $\Omega = 0^+$. The first system with an experimental T_e value of 18 144 cm^{-1} was assigned to a $^3\Sigma_1^+$. Greenwood, Linton, and Barrow[292] assigned the bands in systems 2–5 based on a comparison to the ordering of lead compounds. System 5 (T_e = 23 320 cm^{-1}) was assigned to the $B^3\Pi_1$–$X^1\Sigma^+$ system, while system 4 (T_e = 22 480 cm^{-1}) was assigned to the $C'^3\Sigma_1^-$–$X^1\Sigma^+$ system; system 3 (T_e = 22 390 cm^{-1}) was assigned to $C^3\Sigma_{0^+}^-$–$^1\Sigma^+$, and system 2 (T_e = 22 021 cm^{-1}) to $A^3\Pi_{0^+}$–$^1\Sigma^+$. The theoretical calculations of Balasubramanian[295] when corrected for the differential correlation errors in T_e values supported all these assignments.

The vibrational frequencies of the A, B, C, and C′ states could not be calculated accurately from experimental results since the observed bands were perturbed. Further, the A0$^+$ and C0$^+$ states were found to be only 380 cm^{-1} apart, implying that mixing of $^3\Sigma_{0^+}^-$ and $^3\Pi_{0^+}$ could be large.

The calculated dissociation energy of 4.48 eV[295] for the $^1\Sigma^+$ state in the absence of spin–orbit interaction was found to be in very good agreement with the thermochemical value of 4.77 eV.[32] The approximate $D_0°$ (≤4.48 eV)[32] derived from the spectroscopic continuous absorption (assuming dissociation into ^{1}D + ^{1}D) was also not unreasonable.

D. PbS

The first electronic spectrum of PbS was obtained in absorption by Rochester and Howell[296] in the regions 2600–4500 and 3100–8000 Å. Vago and Barrow[276] later studied the UV absorption systems of PbS, while Barrow, Fry, and LeBargy[297] studied four absorption systems of PbS which they assigned to the a ← X, A ← X, B ← X, and D ← X systems. Nixon and coworkers[298,299] studied the emission and vibronic spectra of PbS in inert gas and SF_6 matrices, while Burkin et al.[300] studied the laser-induced fluorescence spectra of PbS. Greenwood, Barrow, and Linton[294] carried out a revised vibrational analysis of the a–X system as well as rotational analyses of bands of the C–X and C′–X systems. Knöckel et al.[301] recorded the microwave optical double resonance (MODR) spectra in a molecular beam of the X and A states of PbS. The dipole moment of PbS was also measured.[302,308] Maki and Lovas[330] recently recorded the infrared spectrum of PbS (Δv = 2 transitions). These spectra have provided improved Dunham constants for PbS.

TABLE 26. Spectroscopic Properties of PbS[a]

state	R_e, Å theory	R_e, Å expt	T_e, cm^{-1} theory	T_e, cm^{-1} expt	ω_e, cm^{-1} theory	ω_e, cm^{-1} expt
X 0$^+$(I)	2.40	2.29	0.0	0.0	432	429
a 1(I)	2.63	2.56	17 533	14 893	321	286
0$^-$(I)	2.64	—	17 581	—	312	—
A 0$^+$(II)	2.61	2.51	22 256	18 853	282	261
0$^-$(II)	2.55	—	24 486	—	324	—
C 0$^+$(III)	2.60	—	24 698	23 213	395	304
$^1\Sigma^+$	2.40	—	1 645	—	446	—
$^3\Sigma^+$	2.62	—	20 691	—	332	—
$^3\Sigma^-$	2.68	—	24 144	—	295	—
$^3\Pi$	2.52	—	28 377	—	340	—
$^1\Pi$	2.57	—	31 611	—	327	—

[a] All theoretical results are from ref 304.

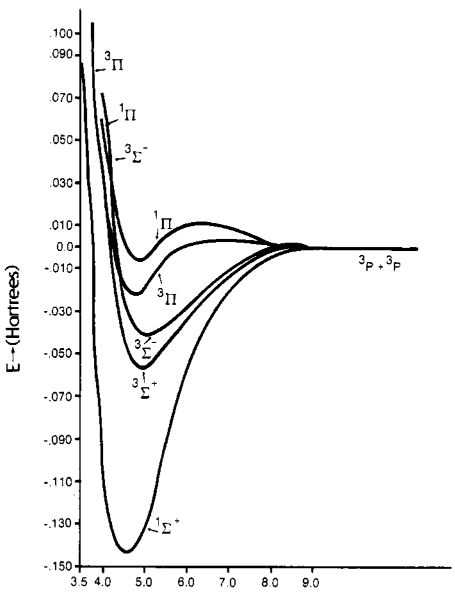

Figure 41. Potential energy curves for PbS without the spin–orbit term (reprinted from ref 304; copyright 1986 American Institute of Physics). See Table 26 for assignments of known states.

Thermodynamic studies of PbS using mass spectrometric techniques revealed the $D_0°$ values for these systems.[303] Through an analysis of experimental data, potential energy curves of some low-lying states of PbS have been constructed.[264]

Balasubramanian[304] made relativistic SCF/RCI calculations on six ω–ω states (0$^+$, 1, 0$^-$, 0$^-$(II), 0$^+$(II), 0$^+$(III)) and six λ–s states without the spin–orbit term for PbS. The spectroscopic constants of PbS calculated this way are shown in Table 26 and compared with experiments. Figures 41 and 42 show the theoretical RCI potential energy curves for the electronic states of PbS without and with spin–orbit effects, respectively.

The X ground state is a $^1\Sigma_{0^+}^+$ state arising from the $1\sigma^2 2\sigma^2 3\sigma^2 1\pi^4$ electronic configuration. The a state is the 1 component of $^3\Sigma^-$, while the A state is the second root of the 0$^+$ calculations. The A state was found to be a mixture of $^3\Pi_{0^+}$ and $^3\Sigma_{0^+}^-$, with $^3\Pi_{0^+}$ making a predominant contribution. The C state was also found to be of 0$^+$ symmetry and it corresponded to the third root of the 0$^+$ theoretical calculations.[304]

The theoretical[304] D_e value for the X0$^+$ state of PbS was 3.83 eV in comparison to an experimental thermochemical value of 3.49 eV.[32] Thus the theoretical D_e

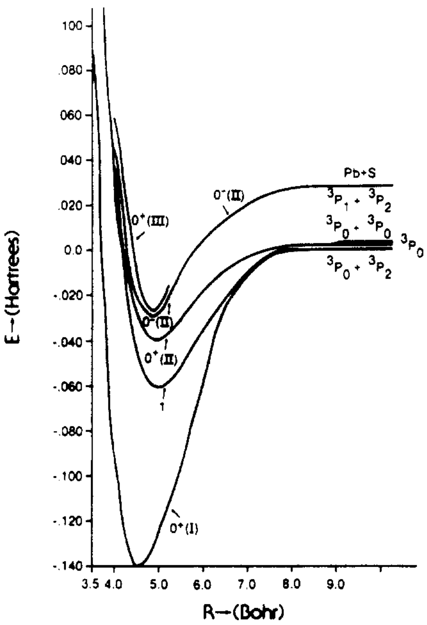

Figure 42. Potential energy curves of PbS with the spin-orbit term (reprinted from ref 304; copyright 1986 American Institute of Physics).

TABLE 27. Spectroscopic Constants of PbS^+ and Ionization Potentials of PbS[a]

method	state	R_e, Å	T_e, cm^{-1}	ω_e, cm^{-1}
RCI	3/2	2.56	0	363
RCI	1/2	2.56	506	335

method	splitting	IP, eV
RCI	$^1\Sigma^+$–$^2\Pi_{3/2}$	7.87
KT	$^1\Sigma^+$–$^2\Pi$	8.77
KT	$^1\Sigma^+$–$^2\Sigma^+$	8.98

[a] From ref 273; KT = Koopmans' theorem.

value is in very good agreement with the experimental value.

The theoretical SCF/RCI spectroscopic properties and ionization potentials of PbS^+ are shown in Table 27, while the potential energy curves of the two lowest states of PbS^+ are shown in Figure 43. Again, due to electron correlation errors, the theoretical IP should be 15% less than the experimental value, and thus the IP of PbS should be about 9 eV.

Wang et al.[326] in a joint experimental–theoretical study obtained the photoelectron spectra of PbTe, PbSe, SnTe, and SnSe. CASSCF/MRSDCI/RCI calculations including up to 200 000 configurations were also carried out on the $^1\Sigma^+$ ground states of all four species and the $^2\Pi_{3/2,1/2}$ and $^2\Sigma^+_{1/2}$ states of the positive ions. The theoretical calculations on these species facilitated interpretation of the experimental photoelectron spectra and construction of the potential energy curves. All four positive ions exhibited avoided crossings of the $^2\Pi_{1/2}$ and $^2\Sigma^+_{1/2}$ components. The theoretical RCI potential energy curves of PbTe and $PbTe^+$ are shown in Figure 44. The theoretical R_e and ω_e values were within 2–6% of the experimental values in all cases. The theoretical IPs of all these species were also found to be within 0.6–6% of the experimental results. The rather broad and diffuse nature of the observed spectral bands for the first two envelopes ($^2\Pi_{3/2} \leftarrow {}^1\Sigma^+$, $^2\Pi_{1/2} \leftarrow {}^1\Sigma^+$) in comparison to the third peak ($^2\Sigma^+_{1/2} \leftarrow {}^1\Sigma^+$) was explained by using theoretical potential energy

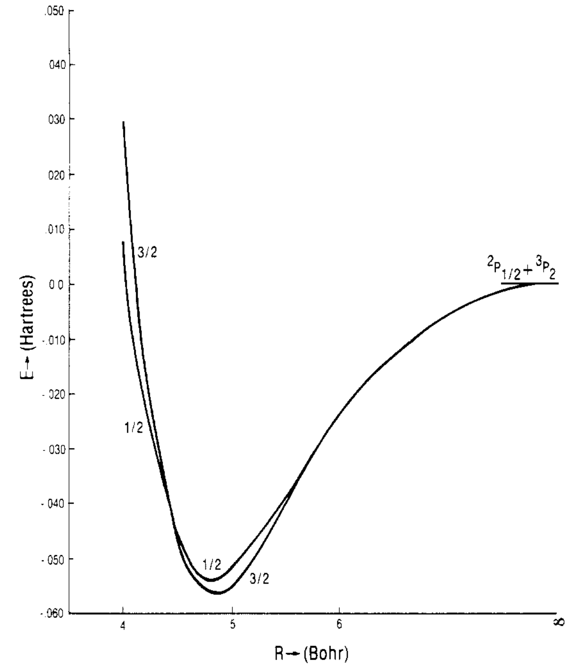

Figure 43. Potential energy curves of PbS^+ (reprinted from ref 273; copyright 1984 American Chemical Society).

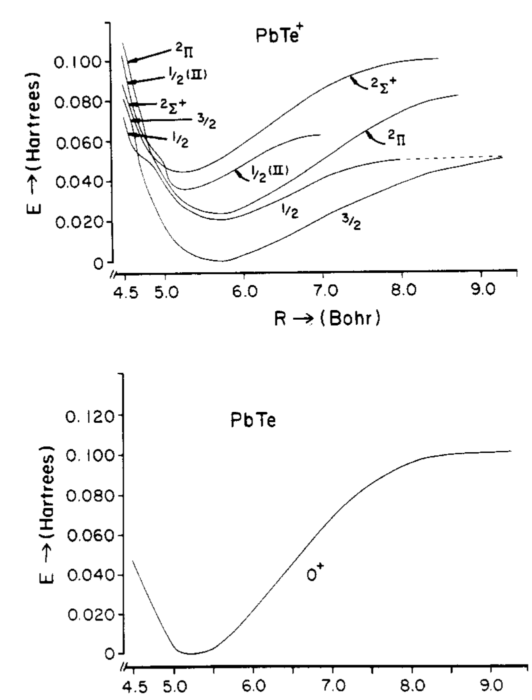

Figure 44. Potential energy curves for PbTe and $PbTe^+$. The shoulders in the 1/2 curves are due to relativistic avoided crossings (reprinted from ref 326; copyright 1989 American Institute of Physics).

curves. The experimental and theoretical spectroscopic constants for PbSe and $PbSe^+$ are shown in Table 28 as an example to illustrate the good agreement between theory and experiment.

VI. Comparison of the Spectroscopic Properties of Heavy Hydrides

In this section we compare the spectroscopic constants of heavy hydrides, obtain periodic trends, and explain the deviations observed, especially in the

TABLE 28. Spectroscopic Constants of PbSe and $PbSe^+$ [a]

		R_e, Å		ω_e, cm^{-1}		IP(ad), eV		D_e, eV		IP(vert), eV	
species	state	theory	expt	theory	expt	theory	expt	theory	expt	theory	expt
PbSe	0^+	2.447	2.40	268	278	—	—	3.5	3.1	—	—
$PbSe^+$	$^2\Pi_{3/2}$	2.66	2.58	207	210	8.72	8.67	1.38	1.7	8.82	8.8
$PbSe^+$	$^2\Pi_{1/2}$	2.67	2.55	205	210	9.04	9.00	1.07	1.44	9.14	9.1
$PbSe^+$	$^2\Sigma^+_{1/2}$	2.53	2.45	222	242	9.64	9.54	—	—	—	—

[a] All values from ref 326. The theoretical constants are from CASSCF/MRSDCI/RCI calculations; experimental results of the positive ion are from photoelectron spectra, while those of the neutral species are from ref 32.

TABLE 29. Periodic Table of the Ground-State Properties of Hydrides[a]

GaH $^1\Sigma^+$, 1.662 Å 1612 cm^{-1}, 2.81 eV μ_e = +0.46	GeH $^2\Pi_{1/2}$, 1.62 Å 1806 cm^{-1}, 2.34 eV μ_e = 0.09	AsH $^3\Sigma^-$, 1.534 Å 2130 cm^{-1}, 2.8 eV μ_e = −0.2	SeH $^2\Pi_{3/2}$, 1.467 Å 2371 cm^{-1}, 3.2 eV μ_e = −0.587	HBr $^1\Sigma^+$, 1.455 Å 2645 cm^{-1}, 3.72 eV μ_e = −0.82
InH $^1\Sigma^+$, 1.837 Å 1048 cm^{-1}, 2.48 eV μ_e = 0.675	SnH $^2\Pi_{1/2}$, 1.83 Å 1600 cm^{-1}, 2.3 eV μ_e = 0.398	SbH $^3\Sigma^-_{0^+}$, 1.72 Å 1763 cm^{-1}, 2.7 eV	TeH $^2\Pi_{3/2}$, 1.76 Å 1839 cm^{-1}, 2.31 eV	HI $^1\Sigma^+_{0^+}$, 1.66 Å 2939 cm^{-1}, 3.03 eV μ_e = −0.45
TlH $^1\Sigma^+_{0^+}$, 1.95 Å 1300 cm^{-1}, 1.81 eV μ_e = 1.231	PbH $^2\Pi_{1/2}$, 1.95 Å 1418 cm^{-1}, 1.64 eV μ_e = 0.937	BiH $^3\Sigma^-_{0^+}$, 1.81 Å 1619 cm^{-1}, 2.2 eV		

[a] The value in Å is R_e; the values in cm^{-1} and eV are ω_e and D_e, respectively. μ_e is the dipole moment in Debye, with the convention of positive value meaning the positive charge is on the heavy atom.

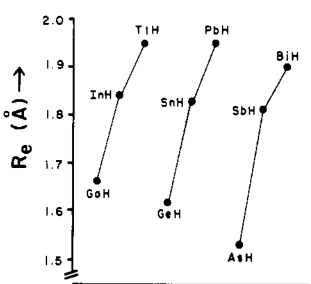

Figure 45. Plots of R_es of the GaH–TlH, GeH–PbH, and AsH–BiH triads.

sixth-row hydrides. We mainly focus on comparing the ground-state spectroscopic properties (R_e, ω_e, D_e, μ_e) and the energy separations (T_e) of select excited states with respect to the ground state.

Table 29 contains the ground-state spectroscopic constants of all the heavy hydrides considered in this review in a periodic tabular form. There are no experimental or theoretical data available on PoH and HAt mainly because there are not many stable isotopes of these elements although $^{210}Po_2$ has been studied.[32] The dipole moment of HAt is being obtained by Kim and Balasubramanian[305] to understand the periodic trends in the dipole moments of the HBr to HAt (H-Br–HAt) triad.

As seen from Table 29 interesting trends emerge in comparing the spectroscopic constants of even the ground states of these species. For example, the dissociation energies, D_e, decrease dramatically in going from the fifth row to the sixth row. The trends in R_e, D_e, μ_e, etc. are best understood by plotting these for the various groups.

Figure 45 shows the plot of R_e for each of the three groups for which a complete set of data is available. Note the upward tilt in the slope of the InH–TlH curve in comparison to the GaH–InH curve. Similar behaviors are observed in the GeH–PbH and AsH–BiH triads.

Figure 46 shows the plot of the D_e's for all three triads. The slopes tilt more downward for the D_e's in

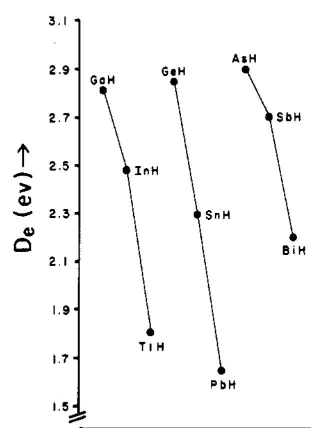

Figure 46. Plots of D_es of the GaH–TlH, GeH–PbH, and AsH–BiH triads.

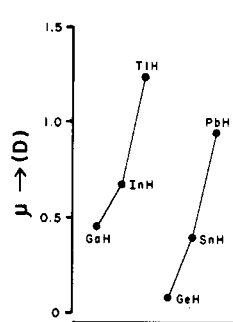

Figure 47. Dipole moments (μ_e) of the GaH–TlH and GeH–PbH triads.

moving from the fifth row to the sixth row. This trend is approximately opposite of the trend in R_e's since increases in R_e's imply weakening of the bond and thus D_e's should decrease correspondingly.

Figure 47 shows plots of the dipole moments for the GaH–TlH and GeH–PbH triads. The dipole moments of InH, TlH, and HAt were obtained by Kim and Balasubramanian[305] in an investigation that considered the periodicities in the dipole moments of these species. As

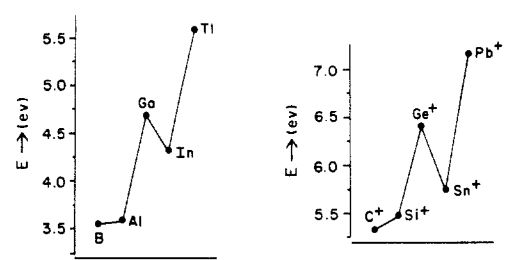

Figure 48. $(ns^2np^1)^2P$–$(ns^1np^2)^4P$ energy separations of B–Tl and C^+–Pb^+ (reprinted from ref 13; copyright 1989 American Chemical Society).

seen from Figure 47 and Table 29, there is a marked increase in the dipole moment for TlH and PbH in comparison to their lighter analogues. This clearly demonstrates the increased electropositive character of the elements in the sixth row. All the above trends can be explained based on relativistic effects and a comparison of the atomic properties of the elements in this group.

Figure 48 shows the $(ns^2np^1)^2P$–$(ns^1np^2)^4P$ energy separations for B–Tl and C^+–Pb^+. All the atomic energy separations were taken from ref 306. As seen from Figure 47, this separation increases up to Ga (Ge^+), then decreases, and again increases sharply in moving from In (Sn^+) to Tl (Pb^+). This is mainly a consequence of a phenomenon referred to as the "inert pair effect", which is actually a relativistic effect. Relativistic effects are defined as the differences in chemical, spectroscopic, and other properties arising from the difference in the true velocity of light as opposed to the assumed infinite velocity in classical mechanics. Balasubramanian[13] recently reviewed in a feature article for the *Journal of Physical Chemistry* the general impacts of relativity on chemical bonding. The very heavy elements in the bottom of the periodic table are subjected to large nuclear charges. Consequently, the inner electrons of such heavy elements acquire a considerable fraction of the speed of light. For example, it is estimated that the $1s^2$ electrons of Tl or Pb should be moving with about 65% of the speed of light. A relativistic effect called the mass–velocity correction, which is a correction to the kinetic energy arising from the variation of the mass of the electron with speed, becomes quite important for elements such as Au, Hg, Tl, Pb, etc. Although the mass–velocity effects are large in the core, they manifest themselves in the valence space to a large enough extent that they affect the valence chemical and spectroscopic properties to a considerable extent. The outer 6s orbitals of elements such as Au, Hg, Tl, etc. contract as a result of this large relativistic mass–velocity correction. This contraction of the outer valence 6s orbital of these elements leads to an enhanced stability for the $6s^2$ shell, thereby making this shell somewhat inert in comparison to the other valence ns^2 shells of the lighter p-block elements.

The enhanced stability of the $6s^2$ shell (the inert pair effect) manifests itself in many ways in the atomic and molecular properties. For example, the dramatic increase in the $(ns^2np^1)^2P$–$(ns^1np^2)^4P$ energy separation of Tl in comparison to In (Figure 48) is due to the relativistic stabilization of the $6s^2$ shell in Tl. Most of the observed trends in Figures 45–47 are attributed to this. The bonding in TlH and PbH is considerably weakened in comparison to that in their lighter analogues since stronger bonds are formed through ns^2np^1–ns^1np^2 hybridization.

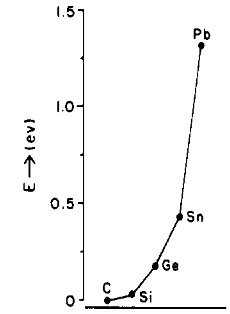

Figure 49. $^3P_0$–$^3P_2$ spin–orbit splittings for C to Pb (reprinted from ref 13; copyright 1989 American Chemical Society).

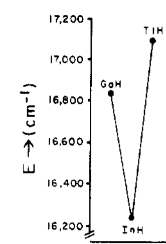

Figure 50. $^3\Pi_{0^+}$–$^1\Sigma_{0^+}^+$ energy separations of GaH to TlH.

TABLE 30. Periodic Table of Spin–Orbit Splittings for Heavy Hydrides

GeH $^2\Pi_{1/2}$–$^2\Pi_{3/2}$ 869 cm^{-1}	AsH $^3\Sigma_{0^+}^-$–$^3\Sigma_1^-$ 59 cm^{-1}	SeH $^2\Pi_{3/2}$–$^2\Pi_{1/2}$ 1934 cm^{-1}
SnH $^2\Pi_{1/2}$–$^2\Pi_{3/2}$ 2180 cm^{-1}	SbH $^3\Sigma_{0^+}^-$–$^3\Sigma_1^-$ 655 cm^{-1}	TeH $^2\Pi_{3-2}$–$^2\Pi_{1/2}$ 3900 cm^{-1}
PbH $^2\Pi_{1/2}$–$^2\Pi_{3/2}$ 6946 cm^{-1}	BiH $^3\Sigma_{0^+}^-$–$^3\Sigma_1^-$ 5000 cm^{-1}	

There is another important relativistic effect, namely, spin–orbit coupling relevant to energy separations and bonding of very heavy molecules. Figure 49 shows the $^3P_0$–$^3P_2$ energy separations of elements C through Pb. As seen from this figure, the spin–orbit splitting goes up dramatically as one moves down the periodic table from Sn to Pb. The changes in the spectroscopic constants in Table 29 are in part due to the spin–orbit splitting.

Table 30 shows the spin–orbit splittings for the ground states of the GeH–PbH to SeH–TeH species. As seen from this table the spin–orbit splittings increase dramatically in moving from SnH to PbH and SbH to BiH. The spin–orbit effects are so large in BiH and PbH that they cause many avoided crossings in the potential energy curves of these species. These features were discussed in section III.M.

Next we compare the energy separations of a select low-lying excited electronic state and the ground state for the hydrides considered in this review. Figure 50 shows the $^3\Pi_{0^+}$–$^1\Sigma_{0^+}^+$ energy separations of GaH–TlH. As seen from this figure there is a pronounced increase in this energy splitting in moving from InH to TlH, whereas it decreases in moving from GaH to InH. In general, energy separations of the corresponding states should decrease with increase in principal quantum number in the absence of spin–orbit and other relativistic effects. This trend is obeyed by GaH and InH pairs. The anomaly in TlH is mainly a consequence of

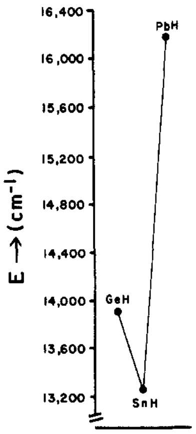

Figure 51. $^4\Sigma^-_{1/2}$–$^2\Pi_{1/2}$ energy separations of GeH to PbH.

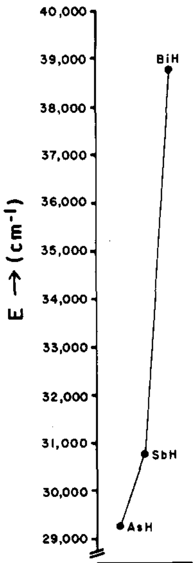

Figure 52. $^3\Pi_{0^+}$–$^3\Sigma^-_{0^+}$ energy separations of AsH to BiH. Note that for BiH, the designation 0^+(IV) is more appropriate than $^3\Pi_{0^+}$ since spin–orbit contamination is quite large for BiH.

relativistic effects discussed earlier.

Figure 51 shows the $^4\Sigma^-_{1/2}$–$^2\Pi_{1/2}$ energy separations of the GeH–PbH triad. Again this separation decreases in moving from GeH to SnH but increases dramatically in moving from SnH to PbH. The spin–orbit effects are also considerably larger for PbH. Figure 52 shows the $^3\Pi_{0^+}$–$^3\Sigma^-_{0^+}$ separations for the AsH–BiH triad. For BiH, this state is so contaminated by the spin–orbit coupling that the designation $^3\Pi_{0^+}$ is inappropriate. In the original manuscript[180] this state was designated as 0^+(IV) (fourth root of the 0^+ RCI calculations). This energy separation once again dramatically increases in moving from SbH to BiH, while it is not substantially different for SbH in comparison to AsH. The dramatic increase in BiH is due to both mass–velocity stabilization effects and the large spin–orbit effects. In any event, relativistic effects make a dramatic impact in the sixth-row compounds.

The comparison of the properties of HBr and HI is also of interest. The $^3\Pi_{0^+}$–$X^1\Sigma^+$ vertical energy separations of the two species are 73 042 and 49 605 cm^{-1}. The $^3\Pi_{0^+}$ states of both species are repulsive and thus vertical separations are compared. The much smaller energy separation for HI is consistent with the experimentally observed electronic spectra of these two species.

TABLE 31. Periodic Table of the Known Spectroscopic Constants of Heavy Fluorides[a]

GaF $^1\Sigma^+$, 1.774 Å 622 cm^{-1}, 5.98 eV μ_e = 2.45 D	GeF $^2\Pi_{1/2}$, 1.745 Å 666 cm^{-1}, 5.0 eV	AsF $^3\Sigma^-_{0^+}$, 1.736 Å 686 cm^{-1}, 4.2 eV
InF $^1\Sigma^+$, 1.985 Å 535 cm^{-1}, 5.25 eV μ_e = 3.40 D	SnF $^2\Pi_{1/2}$, 1.944 Å 578 cm^{-1}, 4.90 eV	SbF $^3\Sigma^-_{0^+}$, 1.92 Å 706 cm^{-1}, 4.4 eV
TlF $^1\Sigma^+$, 2.04 Å 592 cm^{-1}, 4.57 eV μ_e = 4.20 D	PbF $^2\Pi_{1/2}$, 2.08 Å 540 cm^{-1}, 3.75 eV	BiF $^3\Sigma^-_{0^+}$, 2.09 Å 502 cm^{-1}, 2.63 eV

[a] The value in Å is R_e; the values in cm^{-1} and eV are ω_e and D_e, respectively. μ_e is the dipole moment in Debye, with the convention of positive value meaning positive charge is on the metal atom.

TABLE 32. Spin–Orbit Coupling Constants for the GeF–PbF and AsF–BiF Triads

GeF $^2\Pi_{1/2}$–$^2\Pi_{3/2}$ 934 cm^{-1}	AsF $^3\Sigma^-_{0^+}$–$^3\Sigma^-_1$ 139 cm^{-1}
SnF $^2\Pi_{1/2}$–$^2\Pi_{3/2}$ 2317 cm^{-1}	SbF $^3\Sigma^-_{0^+}$–$^3\Sigma^-_1$ 796 cm^{-1}
PbF $^2\Pi_{1/2}$–$^2\Pi_{3/2}$ 8264 cm^{-1}	BiF $^3\Sigma^-_{0^+}$–$^3\Sigma^-_1$ 9216 cm^{-1}

VII. Comparison of the Spectroscopic Properties of Heavy Halides

Table 31 comprises the ground-state spectroscopic constants of heavy fluorides in periodic tabular form. The spectroscopic properties of many low-lying electronic states of TlF, PbF, and BiF were calculated by Balasubramanian.[198,208,232] O'Hare et al.[307] carried out theoretical calculations on the ground state of AsF. The dissociation energy ($D_0°$) in Table 31 for AsF is from this reference. These authors also calculated the electronic dipole moment of AsF as 1.75 D and the electron affinity as 1.1 eV. The level of electron correlation treatment available then was not adequate enough to calculate the dipole moments and electron affinities, in general, accurately.

As seen from Table 31, the D_e's uniformly drop in moving from GaF to TlF. The experimental electronic dipole moments of GaF–TlF are available (see Table 31). The comparison of the dipole moments of these three species clearly reveals the increased electropositivity of the thallium atom in this group.

The comparison of the spin–orbit coupling constants is also of considerable interest. Table 32 shows the spin–orbit splittings of the GeF–PbF and AsF–BiF triads. The $^2\Pi_{1/2}$–$^2\Pi_{3/2}$ spin–orbit splitting dramatically increases from 2317 to 8264 cm^{-1} in moving from SnF to PbF while the corresponding $^3\Sigma^-_{0^+}$–$^3\Sigma^-_1$ splitting increases from 796 to 9216 cm^{-1} in moving from SbF to BiF. Thus, the spin–orbit effects are substantially larger for the sixth-row fluorides in comparison to the fifth-row fluorides.

The energy separations of low-lying excited electronic states with respect to the ground state are also of considerable interest. Figure 53 compares the $^3\Pi_{0^+}$–$^1\Sigma^+_{0^+}$(X) energy separations of the GaF–TlF triad. All three energy separations are from experimental spectroscopic

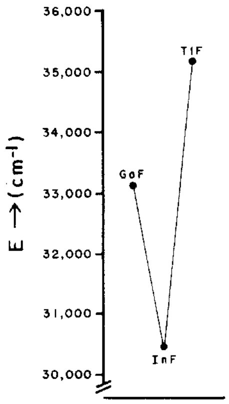

Figure 53. Comparison of the $^3\Pi_{0^+}$–$^1\Sigma^+_{0^+}$(X) energy separations for GaF to TlF.

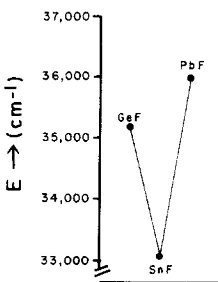

Figure 54. $^4\Sigma^-_{1/2}$–$^2\Pi_{1/2}$ energy separations of GeF to PbF.

data. As seen from Figure 53, this energy separation decreases in moving from GaF to InF but increases in moving from InF to TlF. The $^3\Pi_{0^+}$ state arises from a regular $^3\Pi$ and thus the 0^+ component should be lower than $^3\Pi_1$. The main difference between TlF and InF should be in the magnitude of spin–orbit contamination. For TlF, Balasubramanian[198] found that both the ground state ($^1\Sigma^+_{0^+}$) and the $^3\Pi_{0^+}$ state were actually mixed. That is, the $^3\Pi_{0^+}$ state was found to be a mixture of $^3\Pi_{0^+}$ and $^1\Sigma^+_{0^+}$. This mixing lowers the $^1\Sigma^+_{0^+}$ state but increases the energy of the $^3\Pi_{0^+}$ state. The larger $^3\Pi_{0^+}$–$^1\Sigma^+_{0^+}$ splitting for TlF should thus be due to spin–orbit contamination.

Figure 54 shows the $^4\Sigma^-_{1/2}$–$X^2\Pi_{1/2}$ energy splittings for GeF–PbF. Again, this splitting decreases in moving from GeF to SnF but increases in moving from SnF to PbF. Figure 55 shows the $^1\Sigma^+_{0^+}$–$X^3\Sigma^-_{0^+}$ energy separations of the AsF–BiF triad. Note the dramatic increase in this energy separation for BiF. It was very clear that the large change in BiF is a consequence of spin–orbit contamination. For BiF, the $X^3\Sigma^-_{0^+}$ ground state was found[232] to be 66% $^3\Sigma^-$ and 20% $^1\Sigma^+_{0^+}$. The state labeled A0$^+$(II) was found to be 58% $^1\Sigma^+_{0^+}$, 23% $^3\Sigma^-_{0^+}$, and 7% $^3\Pi_{0^+}$. This substantial mixing of different states lowers the energy of the $^3\Sigma^-_{0^+}$(X) ground state and raises the energy of the $^1\Sigma^+_{0^+}$ state substantially, leading to a much larger energy separation for BiF.

Although all the heavy chlorides have not been studied theoretically, the spectroscopic properties of PbCl and SnCl have been obtained.[238,249] A comparison of these two species seems to provide some interesting information. For both SnCl and PbCl the ground state is of $^2\Pi_{1/2}$ symmetry. The spin–orbit splitting for the $^2\Pi$ state is 2357 cm^{-1} for SnCl and 8272 cm^{-1} for PbCl (expt). The bond length of the ground state of PbCl[238] is 2.61 Å in comparison to a value of 2.48 Å for SnCl.[249] The $^2\Sigma^+_{1/2}$–$^2\Pi_{1/2}$ energy separations for SnCl and PbCl

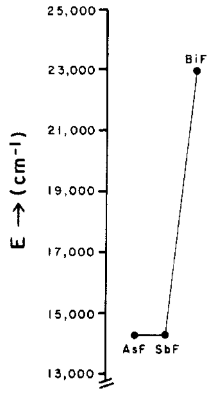

Figure 55. $^1\Sigma^+_{0^+}$–$^3\Sigma^-_{0^+}$ energy separations of AsF to BiF.

TABLE 33. Comparison of the Ground-State Properties of the Heavy Group IV Oxides and Sulfides[a,b]

GeO $^1\Sigma^+$, 1.625 Å 986 cm^{-1}, 6.78 eV μ = 3.27 D	GeS $^1\Sigma^+$, 2.01 Å 576 cm^{-1}, 5.67 eV μ = 2.00 D
SnO $^1\Sigma^+$, 1.83 Å 815 cm^{-1}, 5.49 eV μ = 4.32 D	SnS $^1\Sigma^+$, 2.21 Å 487 cm^{-1}, 4.77 eV μ = 3.17 D
PbO $^1\Sigma^+$, 1.922 Å 721 cm^{-1}, 3.83 eV μ = 4.64 D	PbS $^1\Sigma^+$, 2.29 Å 429 cm^{-1}, 3.49 eV μ = 3.59 D?, 4.02 D?

[a] The value in Å is R_e; the values in cm^{-1} and eV are ω_e and D_e, respectively. μ_e is the dipole moment in Debye, with the convention of positive value meaning positive charge is on the metal atom. [b] Two values are listed for the dipole moment of PbS. The 3.59 value is from ref 308, while the 4.02 value is from ref 302. The discussion is section VIII supports the 3.59 value.

are 19415 and 21865 cm^{-1}, respectively. For GeCl, this energy separation, although not known precisely since the observed bands are diffuse, should be about 22600 cm^{-1}.[32] Again, the trend observed for energy separations in fluorides is observed for chlorides.

VIII. Comparison of Heavy Chalconides

Since SCF/RCI calculations have been completed only on SnO, SnS, PbO, and PbS species, the comparison of chalconides here is restricted to oxides and sulfides. For comparison, I took the available experimental information[32] on GeO and GeS. Table 33 lists the spectroscopic constants on the ground states of the GeO–PbO and GeS–PbS triads in a periodic tabular form. As seen from this table the dissociation energies, D_e, decrease uniformly in going down the periodic table, although the decrease is larger in comparing PbO with SnO and PbS with SnS.

The experimental dipole moments of the heavy group IV oxides and sulfides are available for comparison. The dipole moments of these species in general increase as one goes down the periodic table. This is consistent with the theoretical trend for the hydrides (GeH–PbH). For both oxides and sulfides the polarity of the bond is M^+O^-. The experimental dipole moment of PbS appears to be somewhat uncertain (see Table 33). The value of 3.59 D was obtained from the Stark effect of the rotation spectrum by Hoeft et al.,[308] while the value of 4.02 D was obtained by Murty and Curl[302] around the same time. In any case the dipole moments of

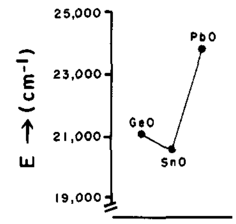

Figure 56. Comparison of the $^3\Sigma^-_{0^+}$–$^1\Sigma^+_{0^+}$ energy separations (T_e) for the GeO–PbO triad.

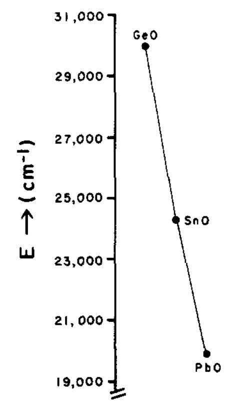

Figure 57. Comparison of the $^3\Pi_{0^+}$–$^1\Sigma^+_{0^+}$ energy separations (T_e) for the GeO–PbO triad.

sulfides are lower than those of oxides, as expected. In general, the sulfides have about 1.2–1.3 D lower electronic dipole moments than oxides. Since the dipole moment of PbO is 4.64 D, we predict that the dipole moment of PbS should be about 3.4–3.5 D. Thus, the value obtained by Hoeft et al.[308] through the Stark effect of the rotational spectra (3.59 D) appears to be more reliable. This is further supported by the fact that the difference in μ_e's of SnO and PbO should be approximately the same as that of the SnS and PbS pairs. Thus μ_e of PbS should be 0.32 D larger than the corresponding value of SnS or 3.49 D. All these arguments seem to support the μ_e obtained by Hoeft et al.[308]

Next we compare the energy separations of some low-lying electronic states of oxides and sulfides. The comparisons of the $^3\Pi_{0^+}$–$X^1\Sigma^+_{0^+}$ and $^3\Sigma^-_{0^+}$–$X^1\Sigma^+_{0^+}$ energy separations seem to provide interesting trends.

Figure 56 shows a comparison of the $^3\Sigma^-_{0^+}$–$^1\Sigma^+_{0^+}$ energy separations for the GeO–PbO triad. The $^3\Sigma^-_{0^+}$ state arises from the $\pi^3\pi^*$ configuration, where the π^* orbital is predominantly made of the heavy atom while the π orbital is predominantly made of the oxygen atom. Note the increase in the energy separation in moving from SnO to PbO. Figure 57 shows the $^3\Pi_{0^+}$–$^1\Sigma^+_{0^+}$ adiabatic energy separations (T_e) for the GeO–PbO triad. The T_e value for GeO is approximate.[32] The trend is somewhat different for the $^3\Pi_{0^+}$–$^1\Sigma^+_{0^+}$ energy separation. This separation monotonically decreases in moving from GeO to PbO. The $^3\Pi$ state arises from the $\sigma\pi^4\pi^*$ configuration, where the σ orbital is the bonding orbital made of the metal p_z orbital and oxygen p_z orbital. The main difference between the $^3\Sigma^-$ and $^3\Pi$ states is that $^3\Sigma^-$ arises from promotion of a nonbonding oxygen electron into a nonbonding metal orbital. Thus, the trend is dominated by relativistic effects. The $^3\Pi$ state, on the contrary, arises from the promotion of a bonding σ electron into a nonbonding metal orbital. Since the σ orbital itself is comprised of the heavy-atom orbital, the relative trend is not so much determined by relativistic effects. It is rather determined by electron correlation effects and the general trend of decrease in energy separations as one goes down the periodic table.

IX. Summary

In this review I critically examined the known theoretical and experimental spectroscopic properties of heavy hydrides (GaH–BiH$^+$), halides (TlF–BiF, PbCl, SnCl), and heavy group IV chalconides. The potential energy curves obtained through relativistic theoretical methods were presented for most of these species. The spectroscopic constants of the hydrides, halides, and chalconides were compared, and periodic trends were critically examined for each group. In all cases the sixth-row compounds exhibited deviations from the expected trends due to large relativistic and spin–orbit effects.

While the spectroscopic properties and potential energy curves of many of these species have now been obtained, our knowledge on the electronic and spectroscopic properties of many other compounds is still not fully complete. Whereas the experimental investigations of many of these compounds have provided a wealth of information on these species, a complete understanding of the available information did not come about until the latter part of this decade due to the lack of theoretical calculations earlier on these species. With the advent of supercomputers and the more powerful theoretical tools available today, theoretical calculations are on the increase. The interplay between the theoretical calculations and experiments has provided for a comprehensive understanding of many of these species. I suspect that there will be more theoretical calculations on other species in this class that have not been explored at all to date.

The dipole moments of these compounds are being investigated more theoretically than ever before. The periodic trends in the dipole moments and electronic transition moments of these compounds are very fascinating. More theoretical calculations of electronic dipole moments, transition states, and lifetimes of the excited electronic states are warranted in the future. It is hoped that such calculations would aid not only in our understanding of existing experimental information but also in the prediction of many new experiments.

X. Acknowledgments

I express special gratitude and thanks to Professor Kenneth S. Pitzer of the University of California, Berkeley, for providing constant encouragement to pursue theoretical calculations on very heavy compounds. I also thank my co-workers Drs. M. Z. Liao, J. Li, D. Chapman, S. H. Lin, N. Tanpipat, J. Bloor, Mr. G. B. Kim, and Ms. M. Han. I express special thanks to Professor Walter C. Ermler for sending the RECPs of many heavy elements prior to their publication. I am indebted to Ms. Anna Quan Leon and Ms. Debra Wolf for their excellent job in putting together the manuscript. Finally, I thank the National Science Foundation for support of the projects described in this review through Grant No. CHE8520556. I would like to thank the referees of this review for their invaluable suggestions.

XI. References

(1) Pitzer, K. S. *Acc. Chem. Res.* **1979**, *12*, 271.
(2) Pitzer, K. S. *Int. J. Quantum Chem.* **1984**, *25*, 131.
(3) Pyykkö, P.; Desclaux, J. P. *Acc. Chem. Res.* **1979**, *12*, 276.
(4) Krauss, M.; Stevens, W. J. *Annu. Rev. Phys. Chem.* **1984**, *35*, 357.
(5) Pyykkö, P. *Adv. Quantum Chem.* **1978**, *11*, 353.
(6) Pyykkö, P., Ed. *Proceedings of the Symposium on Relativistic Effects in Quantum Chemistry, Int. J. Quantum Chem.* **1984**, 25.
(7) Christiansen, P. A.; Ermler, W. C.; Pitzer, K. S. *Annu. Rev. Phys. Chem.* **1985**, *36*, 407.
(8) Balasubramanian, K.; Pitzer, K. S. *Adv. Chem. Phys.* **1987**, *67*, 287.
(9) Pyykkö, P. *Chem. Rev.* **1988**, *88*, 563.
(10) Schwarz, W. H. E. In *Theoretical Models of Chemical Bonding*; Maksić, Z. Ed., in press.
(11) Malli, G. *Stud. Phys. Theor. Chem.* **1982**, *21*, 199.
(12) Pyykkö, P. *Relativistic Theory of Atoms and Molecules*; Springer-Verlag: Berlin, New York, 1986.
(13) Balasubramanian, K. Feature Article, *J. Phys. Chem.*, in press.
(14) Balasubramanian, K. *J. Mol. Struct.* (*Theochem.*), special issue, in press.
(15) Lee, Y. S.; Ermler, W. C.; Pitzer, K. S. *J. Chem. Phys.* **1977**, *15*, 5861.
(16) Lee, Y. S.; Ermler, W. C.; Pitzer, K. S. *J. Chem. Phys.* **1980**, *73*, 360.
(17) Christiansen, P. A.; Lee, Y. S.; Pitzer, K. S. *J. Chem. Phys.* **1979**, *71*, 4445.
(18) Lee, Y. S.; Ermler, W. C.; Pitzer, K. S.; McLean, A. D. *J. Chem. Phys.* **1979**, *70*, 288.
(19) Kahn, L.; Baybutt, P.; Truhlar, D. G. *J. Chem. Phys.* **1976**, *65*, 3826.
(20) Ermler, W. C.; Lee, Y. S.; Christiansen, P. A.; Pitzer, K. S. *Chem. Phys. Lett.* **1981**, *71*, 70.
(21) Pacios, L. F.; Christiansen, P. A. *J. Chem. Phys.* **1985**, *82*, 2664.
(22) Hurley, M. M.; Pacios, L. F.; Christiansen, P. A.; Ross, R. B.; Ermler, W. C. *J. Chem. Phys.* **1986**, *84*, 6840.
(23) LaJohn, L. A.; Christiansen, P. A.; Ross, R. B.; Atashroo, T.; Ermler, W. C. *J. Chem. Phys.* **1987**, *87*, 2812.
(24) Cohen, J. J.; Wadt, W. R; Hay, P. J. *J. Chem. Phys.* **1979**, *71*, 2955.
(25) Hay, P. J.; Wadt, W. R. *J. Chem. Phys.* **1985**, *82*, 270.
(26) Wadt, W. R.; Hay, P. J. *J. Chem. Phys.* **1985**, *82*, 284.
(27) Hay, P. J.; Wadt, W. R. *J. Chem. Phys.* **1985**, *82*, 299.
(28) Christiansen, P. A.; Balasubramanian, K.; Pitzer, K. S. *J. Chem. Phys.* **1982**, *76*, 5087.
(29) Balasubramanian, K.; Pitzer, K. S. *J. Chem. Phys.* **1983**, *78*, 321.
(30) Pitzer, K. S.; Balasubramanian, K. *J. Phys. Chem.* **1982**, *86*, 3068.
(31) Stevens, W. J.; Basch, H.; Krauss, M. *J. Chem. Phys.* **1984**, *81*, 6026.
(32) Huber, K. P.; Herzberg, G. *Molecular Spectra and Molecular Structure. IV. Constants of Diatomic Molecules*; Van Nostrand Reinhold, New York, 1979.
(33) Garton, W. R. S. *Proc. Phys. Soc. London* **1951**, *A64*, 509.
(34) Neuhaus, H. *Nature* **1957**, *180*, 433.
(35) Neuhaus, H. *Ark. Fys.* **1959**, *14*, 551.
(36) Ginter, M. L.; Innes, K. K. *J. Mol. Spectrosc.* **1967**, *7*, 64.
(37) Ginter, M. L.; Battino, R. *J. Chem. Phys.* **1965**, *42*, 3222.
(38) Poynor, P. C.; Innes, K. K.; Ginter, M. L. *J. Mol. Spectrosc.* **1967**, *23*, 237.
(39) Kronekvist, M.; Langerquist, A.; Neuhaus, H. *J. Mol. Spectrosc.* **1971**, *39*, 516.
(40) Larsson, T.; Neuhaus, H. *Ark. Fys.* **1963**, *23*, 461.
(41) Larsson, T.; Neuhaus, H. *Ark. Fys.* **1966**, *31*, 299.
(42) Kim, G. B.; Balasubramanian, K. *J. Mol. Spectrosc.* **1989**, *134*, 412.
(43) Pettersson, L.; Langhoff, S. R. *J. Chem. Phys.* **1986**, *85*, 3130.
(44) Kleman, B.; Werhagen, E. *Ark. Fys.* **1953**, *6*, 359.
(45) Kleman, B.; Werhagen, E. *Ark. Fys.* **1953**, *6*, 399.
(46) Barrow, R. F.; Drummond, G.; Garton, W. R. S. *Proc. Phys. Soc. London* **1953**, *66A*, 191.
(47) Howell, H. G. *Proc. Phys. Soc. London* **1945**, *57*, 37.
(48) Klynning, L.; Lindgren, B. *Ark. Fys.* **1966**, *32*, 575.
(49) Osmudsen, J. F.; Abele, C. C.; Eden, J. G. *J. Appl. Phys.* **1985**, *57*, 2921.
(50) Osmudsen, J. F.; Abele, C. C.; Eden, J. G. *J. Chem. Phys.* **1985**, *83*, 2139.
(51) Perrin, J.; Aarts, J. F. M. *Chem. Phys.* **1983**, *80*, 351.
(52) Brown, J. M.; Evenson, K. M.; Sears, T. J. *J. Chem. Phys.* **1985**, *83*, 3275.
(53) Pettersson, L. G. M.; Langhoff, S. R. *Chem. Phys. Lett.* **1986**, *125*, 429.
(54) Werner, H. J.; Buckingham, A. D. *Chem. Phys. Lett.* **1986**, *125*, 433.
(55) Chapman, D. A.; Li, J.; Balasubramanian, K.; Lin, S. H. *J. Chem. Phys.* **1988**, *88*, 3826.
(56) Veseth, L. *J. Mol. Spectrosc.* **1973**, *48*, 283.
(57) Balasubramanian, K.; Li, J. *J. Mol. Spectrosc.* **1988**, *128*, 413.
(58) Dixon, R. N.; Lamberton, H. M. *J. Mol. Spectrosc.* **1968**, *25*, 12.
(59) Lindgren, B. *Phys. Scr.* **1975**, *12*, 164.
(60) Brown, J. M.; Fackerell, A. D. *Phys. Scr.* **1982**, *25*, 351.
(61) Balasubramanian, K.; Nannegari, V. *J. Mol. Spectrosc.*, in press.
(62) Radford, R. E. *J. Chem. Phys.* **1964**, *40*, 2732.
(63) Carrington, A.; Currie, G. N.; Lucas, N. J. D. *Proc. R. Soc., Ser. A* **1970**, *A315*, 355.
(64) Lindgren, B. *J. Mol. Spectrosc.* **1968**, *28*, 536.
(65) Donovan, B. J.; Little, D. J.; Konstantatos, J. *J. Chem. Soc., Faraday Trans. 2* **1972**, *68*, 1812.
(66) Smyth, C. K.; Brauman, J. I.; John, I. *J. Chem. Phys.* **1972**, *56*, 5993.
(67) Bollmark, P.; Lindgren, B.; Rydh, B.; Sassenberg, V. *Phys. Scr.* **1978**, *17*, 561.
(68) Bollmark, P.; Lindgren, B.; Sassenberg, V. *Phys. Scr.* **1980**, *21*, 811.
(69) Cliff, D. I.; Davies, P. B.; Handy, B. J.; Thrush, B. A. *Chem. Phys. Lett.* **1980**, *75*, 9.
(70) Brown, J. M.; Carrington, A.; Sears, T. *J. Mol. Phys.* **1979**, *37*, 1837.
(71) Brown, J. M.; Carrington, A.; Fackerell, A. D. *Chem. Phys. Lett.* **1980**, *75*, 13.
(72) Brown, J. M.; Fackerell, A. D. *Phys. Scr.* **1982**, *25*, 351.
(73) Gibson, S. T.; Freene, J. P.; Berkowitz, J. *J. Chem. Phys.* **1986**, *85*, 4815.
(74) Metzger, M. R.; Rhee, C. H. *Cryst. Liq. Cryst.* **1982**, *85*, 1471.
(75) Balasubramanian, K.; Han, M.; Liao, M. Z. *Chem. Phys. Lett.* **1987**, *139*, 551.
(76) Price, W. C. *Proc. R. Soc., Ser. A* **1938**, *167*, 216.
(77) Barrow, R. F.; Stamper, J. G. *Proc. R. Soc., Ser. A* **1961**, *263*, 259.
(78) Barrow, R. F.; Stamper, J. G. *Proc. R. Soc., Ser. A* **1961**, *263*, 277.
(79) Ginter, M. L.; Tilford, S. G. *J. Mol. Spectrosc.* **1970**, *34*, 206.
(80) Ginter, M. L.; Tilford, S. G. *J. Mol. Spectrosc.* **1971**, *37*, 159.
(81) Stamper, J. G.; Barrow, R. R. *J. Phys. Chem.* **1961**, *65*, 250.
(82) Mulliken, R. S. *Phys. Rev.* **1936**, *50*, 1017.
(83) Mulliken, R. S. *Phys. Rev.* **1937**, *51*, 310.
(84) van Dijk, F. A.; Dymanus, A. *Chem. Phys.* **1974**, *6*, 474.
(85) Bernage, P.; Niay, P. *J. Quant. Spectrosc. Radiat. Transfer* **1977**, *18*, 315.
(86) Niay, P.; Bernage, P.; Coquant, C.; Fayt, C. *Can. J. Phys.* **1977**, *55*, 1829.
(87) Dabbousi, O. B.; Meerts, W. L.; de Leeuw, F. H.; Dymanus, A. *Chem. Phys.* **1973**, *2*, 473.
(88) Babrov, H. J.; Shabot, A. L.; Rao, B. S. *J. Chem. Phys.* **1965**, *42*, 4124.
(89) Straub, P. A.; McLean, A. D. *Theor. Chim. Acta* **1974**, *32*, 227.
(90) Botschwina, P.; Meyer, W. *J. Chem. Phys.* **1977**, *67*, 2390.
(91) Werner, H. J.; Rosmus, P. *J. Chem. Phys.* **1980**, *73*, 2319.
(92) Ogilvie, J. F.; Rodwell, W. R.; Tipping, R. H. *J. Chem. Phys.* **1980**, *73*, 5221.
(93) Andzelm, J.; Klobukowski, M.; Radzio-Andzelm, E. *J. Comput. Chem.* **1984**, *5*, 146.
(94) Chapman, D. A.; Balasubramanian, K.; Lin, S. H. *Chem. Phys.* **1987**, *118*, 333.
(95) Alajajian, S. H.; Chutjian, A. *Phys. Rev.* **1988**, *A37*, 3680.
(96) Adams, N. G.; Smith, D.; Viggiano, A. A.; Paulson, J. F.; Henchman, M. J. *J. Chem. Phys.* **1986**, *84*, 6728.
(97) Le Coat, Y.; Azria, R.; Tronc, M. *J. Phys.* **1985**, *B18*, 809.
(98) Le Coat, Y.; Azria, R.; Tronc, M. *J. Phys.* **1982**, *B15*, 1569.
(99) Abouaf, R.; Teillet-Billy, D. *Chem. Phys. Lett.* **1980**, *73*, 106.
(100) Azria, R.; Le Coat, Y.; Simon, D.; Tronc, M. *J. Phys.* **1980**, *B13*, 1909.
(101) Abouaf, R.; Teillet-Billy, D. *J. Phys.* **1977**, *B10*, 2261.
(102) Rohr, K.; Linder, F. *J. Phys.* **1976**, *B9*, 2521.
(103) Ziesel, J. P.; Nenner, I.; Schulz, G. J. *J. Chem. Phys.* **1975**, *63*, 1943.
(104) Teillet-Billy, D.; Gauyacq, J. P. *J. Phys.* **1984**, *B17*, 3329.
(105) Hazi, A. U. *J. Phys.* **1983**, *B16*, 29.
(106) Krauss, M.; Stevens, W. J. *J. Chem. Phys.* **1981**, *74*, 570.
(107) Goldstein, E.; Segal, G. A.; Wetmore, R. W. *J. Chem. Phys.* **1978**, *68*, 271.
(108) Jordan, K. D.; Wendolski, J. *J. Chem. Phys.* **1977**, *21*, 145.
(109) Taylor, H. S.; Goldstein, E.; Segal, G. A. *J. Phys.* **1977**, *B10*, 2253.
(110) Crawford, O. H.; Koch, B. J. D. *J. Chem. Phys.* **1974**, *60*, 4512.
(111) Fiquet-Fayard, F. *J. Phys.* **1974**, *B7*, 810.
(112) Jordan, K. D.; Herzenberg, A.; Luken, W. *J. Chem. Phys.* **1976**, *64*, 2760.
(113) Fiquet-Fayard, F. *Vacuum* **1974**, *24*, 533.

(114) O'Malley, T. F.; Taylor, H. S. *Phys. Rev.* **1968**, *A176*, 207.
(115) Bondybey, W.; Pearson, P. K.; Schaefer, H. F. *J. Chem. Phys.* **1972**, *57*, 1123.
(116) Hartman, W. M.; Gilbert, T. L.; Kaiser, K. A.; Wahl, A. C. *Phys. Rev. B* **1970**, 1140.
(117) Weiss, A. W.; Krauss, M. *J. Chem. Phys.* **1970**, *52*, 4363.
(118) Michels, H. H.; Harris, R. E.; Browne, J. C. *J. Chem. Phys.* **1968**, *48*, 2821.
(119) Taylor, H. S.; Bobrowicz, F. W.; Hay, P. J.; Dunning, T. H. *J. Chem. Phys.* **1976**, *65*, 1182.
(120) Chapman, D. A.; Balasubramanian, K.; Lin, S. H. *J. Chem. Phys.* **1987**, *87*, 5325.
(121) Stevens, W. J.; Karo, A. M.; Hiskes, J. R. *J. Chem. Phys.* **1981**, *74*, 3989.
(122) Chapman, D. A.; Balasubramanian, K.; Lin, S. H. *Chem. Phys. Lett.* **1985**, *118*, 192.
(123) Bernage, P.; Niay, P. *J. Quant. Spectrosc. Radiat. Transfer* **1977**, *18*, 315.
(124) Burrus, C. A. *J. Chem. Phys.* **1974**, *60*, 2991.
(125) Hotop, H.; Lineberger, W. C. *J. Phys. Chem. Ref. Data* **1975**, *4*, 539.
(126) Liu, B.; Siegbahn, P. E. *J. Chem. Phys.* **1968**, *68*, 2457.
(127) Taylor, H. S.; Harris, F. E. *J. Chem. Phys.* **1963**, *39*, 1012.
(128) Spence, D.; Chupka, W. A.; Stevens, C. M. *J. Chem. Phys.* **1982**, *76*, 2759.
(129) Chapman, D. A.; Balasubramanian, K.; Lin, S. H. *Phys. Rev. A* **1988**, *38*, 6098.
(130) Grundström, *Z. Phys.* **1939**, *113*, 721.
(131) Kleman, D. Dissertation, Stockholm, 1953.
(132) Neuhaus, H. *Z. Phys.* **1958**, *150*, 4.
(133) Neuhaus, H. *Z. Phys.* **1958**, *152*, 402.
(134) Ginter, M. L. *J. Mol. Spectrosc.* **1963**, *11*, 301.
(135) Larsson, T.; Neuhaus, H. *Ark. Fys.* **1964**, *27*, 275.
(136) Freed, K. F. *J. Chem. Phys.* **1966**, *45*, 1714.
(137) Ginter, M. L. *J. Mol. Spectrosc.* **1966**, *20*, 240.
(138) Larsson, T.; Neuhaus, H.; Aslund, N. *Ark. Fys.* **1968**, *37*, 114.
(139) Veseth, L.; Lofthus, A. *J. Mol. Spectrosc.* **1974**, *49*, 414.
(140) Veseth, L. *J. Mol. Spectrosc.* **1976**, *59*, 51.
(141) Balasubramanian, K., manuscript in preparation.
(142) Watson, W. W.; Simon, R. *Phys. Rev.* **1939**, *55*, 358.
(143) Watson, W. W.; Simon, R. *Phys. Rev.* **1940**, *57*, 708.
(144) Hougen, J. T. *Can. J. Phys.* **1962**, *40*, 598.
(145) Klynning, L.; Lindgren, B.; Aslund, N. *Ark. Fys.* **1965**, *30*, 141.
(146) Klynning, L. *Ark. Fys.* **1966**, *31*, 281.
(147) Kopp, I.; Hougen, J. T. *Can. J. Phys.* **1967**, *45*, 2581.
(148) Kovacs, I.; Korwar, V. M. *J. Phys.* **1971**, *B4*, 759.
(149) Kovacs, I.; Vujisic, B. *J. Phys.* **1971**, *B4*, 1123.
(150) Kovacs, I.; Pacher, P. *J. Phys.* **1971**, *B4*, 1633.
(151) Veseth, L. *Physica* **1971**, *56*, 286.
(152) Balasubramanian, K.; Pitzer, K. S. *J. Mol. Spectrosc.* **1984**, *103*, 105.
(153) Bollmark, P.; Lindgren, B. *Chem. Phys. Lett.* **1967**, *1*, 480.
(154) Basco, N.; Yee, K. K. *Spectrosc. Lett.* **1968**, *1*, 13.
(155) Bollmark, P.; Lindgren, B. *Phys. Scr.* **1974**, *10*, 325.
(156) Lindgren, B.; Nilsson, C. H. *J. Mol. Spectrosc.* **1975**, *55*, 407.
(157) Khan, M. A.; Khan, Z. M. *Proc. R. Soc., Ser. A* **1966**, *88*, 211.
(158) Balasubramanian, K.; Tanpipat, N.; Bloor, J. *J. Mol. Spectrosc.* **1987**, *124*, 458.
(159) Little, D. J.; Donovan, R. J.; Butcher, R. J. *J. Photochem.* **1973**, *2*, 451.
(160) Freidhoff, C. B.; Snodgrass, J. T.; Coe, J. V.; McHugh, K. M.; Bowen, K. H. *J. Chem. Phys.* **1986**, *84*, 1051.
(161) Balasubramanian, K.; Han, M.; Liao, M. Z. *J. Chem. Phys.* **1987**, *86*, 4979.
(162) Ginter, M. L.; Tilford, S. G.; Bass, A. M. *J. Mol. Spectrosc.* **1975**, *57*, 271.
(163) Tilford, S. G.; Ginter, M. L.; Bass, A. M. *J. Mol. Spectrosc.* **1970**, *34*, 327.
(164) Clear, R. D.; Riley, S. J.; Wilson, K. R. *J. Chem. Phys.* **1975**, *63*, 1340.
(165) Romand, J. *Ann. Phys. (Paris)* **1949**, *4*, 527.
(166) Datta, S.; Kundu, D. N. *Proc. Natl. Acad. Sci. India* **1941**, *7*, 311.
(167) Lee, Y.; Ermler, W. C.; Pitzer, K. S. *J. Chem. Phys.* **1980**, *73*, 360.
(168) Christiansen, P. A.; Pitzer, K. S. *J. Chem. Phys.* **1980**, *73*, 5160.
(169) Grundström, B.; Valberg, P. *Z. Phys.* **1938**, *108*, 326.
(170) Bulewicz, E. M.; Sugden, T. M. *Trans. Faraday Soc.* **1958**, *54*, 830.
(171) Neuhaus, H.; Muld, V. *Z. Phys.* **1959**, *153*, 412.
(172) Larsson, T.; Neuhaus, H. *Ark. Fys.* **1963**, *23*, 461; **1966**, *31*, 299.
(173) Watson, W. W. *Phys. Rev.* **1938**, *54*, 1068.
(174) Gerö, L. *Z. Phys.* **1940**, *116*, 379.
(175) Balasubramanian, K.; Pitzer, K. S. *J. Phys. Chem.* **1984**, *88*, 1146.
(176) Hulthen, E.; Neuhaus, H. *Phys. Rev.* **1956**, *102*, 1415.
(177) Neuhaus, H. *Z. Naturforsch.* **1966**, *21a*, 2113.
(178) Heimer, A. *Z. Phys.* **1935**, *85*, 328.
(179) Heimer, A. *Z. Phys.* **1936**, *103*, 621.
(180) Balasubramanian, K. *J. Mol. Spectrosc.* **1986**, *115*, 258.
(181) Balasubramanian, K. *Chem. Phys. Lett.* **1985**, *114*, 201.
(182) Balasubramanian, K. *J. Phys. Chem.* **1986**, *90*, 1043.
(183) Trenin, A. *Phys. Rev.* **1930**, *36*, 147.
(184) Trenin, A.; Popov, B. *Z. Phys.* **1932**, *75*, 338.
(185) Berkowitz, J.; Chupka, W. A. *J. Chem. Phys.* **1966**, *45*, 1287.
(186) Cubicciotti, D. *J. Phys. Chem.* **1964**, *68*, 1528, 3834; **1965**, *69*, 1410.
(187) Keneshea, F. J.; Cubicciotti, D. *J. Phys. Chem.* **1967**, *71*, 1958.
(188) Brom, J. M., Jr.; Fransen, H. F. *J. Chem. Phys.* **1971**, *54*, 2874.
(189) Cubicciotti, D. *High Temp. Sci.* **1970**, *2*, 65.
(190) Murad, E.; Hildebrand, D. L.; Main, R. P. *J. Chem. Phys.* **1966**, *45*, 263.
(191) Berkowitz, J.; Walter, T. A. *J. Chem. Phys.* **1968**, *49*, 1184.
(192) Barrow, R. F.; Cheall, H. F. K.; Thomas, P. M.; Zeeman, P. B. *Proc. Phys. Soc. London* **1958**, *71*, 128.
(193) Boizova, Z. V.; Butkow, K. V. *Phys. Z. Sowjetunion* **1936**, *5*, 705.
(194) Howell, H. G. *Proc. R. Soc. London, Ser. A* **1937**, *160*, 242.
(195) Mandel, M.; Barrett, A. H. *Phys. Rev.* **1955**, *98*, 1159. Barrett, A. H.; Mandel, M. *Phys. Rev.* **1958**, *109*, 1572.
(196) Drechsler, W.; Graff, G. *Z. Phys.* **1961**, *163*, 165.
(197) Ritchie, R. K.; Lew, H. *Can. J. Phys.* **1965**, *43*, 1701.
(198) Balasubramanian, K. *J. Chem. Phys.* **1985**, *82*, 3741.
(199) Rao, J. V. R.; Rao, P. T. *Indian J. Phys.* **1955**, *29*, 20.
(200) Morgan, F. *Phys. Rev.* **1936**, *49*, 47.
(201) Rochester, G. D. *Proc. R. Soc. London, Ser. A* **1936**, *153*, 407; **1938**, *167*, 567.
(202) Barrow, R. F.; Butler, D.; Johns, J. W. C.; Powell, J. L. *Proc. Phys. Soc. London* **1959**, *73*, 317.
(203) Singh, S. P. *Indian J. Pure Appl. Phys.* **1967**, *5*, 292.
(204) Singh, O. N.; Singh, I. S.; Singh, O. N. *Can. J. Phys.* **1972**, *50*, 2206.
(205) Lumley, D. J. W.; Barrow, R. F. *J. Phys.* **1977**, *B10*, 1537.
(206) Zmbov, K.; Hastie, J. W.; Margrave, J. L. *Trans. Faraday Soc.* **1968**, *64*, 861.
(207) Rao, K. M.; Rao, P. T. *Can. J. Phys.* **1964**, *42*, 690.
(208) Balasubramanian, K. *J. Chem. Phys.* **1985**, *83*, 2311.
(209) Rosano, W. J.; Parson, J. M. *J. Chem. Phys.* **1985**, *82*, 4401.
(210) Mezinger, M. *Adv. Chem. Phys.* **1980**, *42*, 1.
(211) Levy, M. R. *Prog. React. Kinet.* **1979**, *10*, 1.
(212) Ishikawa, T.; Parson, J. M. *J. Chem. Phys.* **1983**, *79*, 4261.
(213) Parson, J. M.; Wang, J. H.; Fang, C. C.; Cheong, B. S. *Chem. Phys. Lett.* **1988**, *152*, 330.
(214) Sohwenz, B. W.; Geiger, L. C.; Parson, J. M. *J. Chem. Phys.* **1981**, *74*, 1736.
(215) Howell, W. G. *Proc. R. Soc. London, Ser. A* **1936**, *155*, 141.
(216) Morgan, F. *Phys. Rev.* **1936**, *49*, 41.
(217) Rochester, G. D. *Phys. Rev.* **1937**, *51*, 489.
(218) Joshi, K. C. *Proc. Phys. Soc. London* **1961**, *78*, 610.
(219) Rao, T. A.; Rao, P. T. *Indian J. Phys.* **1962**, *36*, 85.
(220) Rao, K. M.; Rao, P. T. *Indian J. Phys.* **1965**, *39*, 572.
(221) Rao, T. A.; Rao, P. T. *Can. J. Phys.* **1962**, *40*, 1077.
(222) Patel, M. M.; Narayanan, P. S. *Indian J. Pure Appl. Phys.* **1967**, *5*, 223.
(223) Mohanty, B. S.; Rai, D. K.; Upadhya, K. N.; Singh, N. L. *J. Phys. B* **1968**, *1*, 523.
(224) Chaudry, A. K.; Upadhya, K. N.; Rai, D. K.; Mohanty, B. S. *J. Phys. B* **1968**, *1*, 1223.
(225) Chaudry, A. K.; Upadhya, K. N.; Rai, D. K. *J. Phys. B* **1969**, *2*, 628.
(226) Avasthi, M. N. *Spectrosc. Lett.* **1970**, *3*, 157.
(227) Murthy, P. S.; Rao, D. V.; Reddy, Y. P.; Rao, P. T. *Spectrosc. Lett.* **1975**, *8*, 217.
(228) Chakko, K. J.; Patel, M. M. *Indian J. Pure Appl. Phys.* **1979**, *17*, 189.
(229) Kuijpers, P.; Dynamus, A. *Chem. Phys.* **1977**, *24*, 97.
(230) Jones, W. E.; McLean, T. D. *J. Mol. Spectrosc.* **1980**, *83*, 317; **1981**, *90*, 481.
(231) Gaydon, A. G. *Dissociation Energy of Diatomic Molecules*, 3rd ed.; Chapman and Hall: London, 1968.
(232) Balasubramanian, K. *Chem. Phys. Lett.* **1986**, *127*, 324.
(233) Wieland, K.; Newburgh, R. *Helv. Phys. Acta* **1952**, *25*, 87.
(234) Cordes, H.; Gehrke, F. *Z. Phys. Chem.* **1966**, *51*, 281.
(235) Rao, V. S.; Rao, P. T. *Z. Phys.* **1966**, *181*, 58.
(236) Hastie, J. W.; Bollm, H.; Morrison, J. D. *J. Chem. Phys.* **1967**, *47*, 1580.
(237) Singh, S. P. *Indian J. Pure Appl. Phys.* **1970**, *8*, 114.
(238) Balasubramanian, K. *J. Mol. Spectrosc.* **1988**, *127*, 97.
(239) Jevons, W. *Proc. R. Soc. London, Ser. A* **1926**, *110*, 365.
(240) Ferguson, W. F. C. *Phys. Rev.* **1928**, *32*, 607.
(241) Fowler, C. A. *Phys. Rev.* **1942**, *62*, 141.
(242) Sarma, P. R. K.; Venkateswarlu, P. *J. Mol. Spectrosc.* **1965**, *17*, 252.
(243) Hastie, J. W.; Hauge, R. H.; Margrave, J. L. *J. Mol. Spectrosc.* **1969**, *29*, 152.

(244) Oldershaw, G. A.; Robinson, K. *J. Mol. Spectrosc.* **1969**, *32*, 469.
(245) Richter, W. *Z. Phys. Chem.* **1970**, *71*, 303.
(246) Chatalic, A.; Iacocca, D.; Pannetier, G. *J. Chim. Phys. Phys.-Chim. Biol.* **1972**, *69*, 82.
(247) Pannetier, A.; Deschamps, P. *J. Chim. Phys. Phys.-Chim. Biol.* **1968**, *65*, 1164.
(248) Mulliken, R. S. *Phys. Rev.* **1925**, *28*, 481.
(249) Balasubramanian, K. *J. Mol. Spectrosc.* **1988**, *132*, 280.
(250) Lin, M. C. *Adv. Chem. Phys.* **1980**, *42*, 113.
(251) Toby, S. *Chem. Rev.* **1984**, *84*, 277.
(252) Rauhut, M. M. *Acc. Chem. Res.* **1969**, *2*, 80.
(253) McCaPara, F. Q. *Rev., Chem. Soc.* **1966**, *20*, 485.
(254) Mahanti, P. G. *Z. Phys.* **1931**, *68*, 114.
(255) Loomis, W.; Watson, T. F. *Phys. Rev.* **1934**, *45*, 805.
(256) Jevons, F. W. *Proc. Phys. Soc. London* **1938**, *50*, 910.
(257) Eisler, B.; Barrow, R. F. *Proc. Phys. Soc. London, Ser. A* **1949**, *62*, 740.
(258) Barrow, R. F.; Rowlinson, J. *Proc. R. Soc. London, Ser. A* **1954**, *224*, 374.
(259) Lagerqvist, A.; Nilsson, N. E. L.; Wigartz, K. *Ark. Fys.* **1959**, *15*, 521.
(260) Deutsch, E. M.; Barrow, R. F. *Nature* **1964**, *201*, 815.
(261) Joshi, M. M.; Yamdagni, R. *Indian J. Phys.* **1967**, *33*, 275.
(262) Capelle, G. A.; Linton, C. *J. Chem. Phys.* **1976**, *65*, 5361.
(263) Colin, R.; Drowart, J.; Verhagen, G. *Trans. Faraday Soc.* **1965**, *61*, 1364.
(264) Nair, K. P. R.; Singh, R. B.; Rai, D. K. *J. Chem. Phys.* **1965**, *43*, 3570.
(265) Torring, T. *Z. Naturforsch.* **1967**, *22a*, 1234.
(266) Smith, J. J.; Meyer, B. *J. Mol. Spectrosc.* **1968**, *27*, 304.
(267) Hoeft, J.; Lovas, F. J.; Tiemann, E.; Tischer, R.; Torring, T. *Z. Naturforsch.* **1969**, *24a*, 1222.
(268) Ogen, J. S.; Ricks, M. J. *J. Chem. Phys.* **1970**, *53*, 896.
(269) Dube, R. S.; Rai, D. K. *J. Phys. B* **1971**, *4*, 579.
(270) Honerjäger, R.; Tischer, R. *Z. Naturforsch.* **1973**, *28a*, 1372.
(271) Balasubramanian, K.; Pitzer, K. S. *Chem. Phys. Lett.* **1983**, *100*, 273.
(272) Dyke, J. M.; Morris, A.; Ridha, A. M.; Snijders, J. G. *Chem. Phys.* **1982**, *67*, 245.
(273) Balasubramanian, K. *J. Phys. Chem.* **1984**, *88*, 5759.
(274) Bloomenthal, S. *Phys. Rev.* **1930**, *35*, 34.
(275) Howell, H. *Proc. R. Soc. London, Ser. A* **1936**, *153*, 683.
(276) Vago, E. G.; Barrow, R. F. *Proc. Phys. Soc. London* **1947**, *59*, 449.
(277) Barrow, R. F.; Deutsch, E. M.; Travis, D. N. *Nature* **1984**, *191*, 374.
(278) Torring, T. *Z. Naturforsch.* **1964**, *19a*, 1426.
(279) Drowart, J.; Colin, R.; Exsteem, G. *Trans. Faraday Soc.* **1965**, *61*, 1376.
(280) Nair, K. P. R.; Singh, R. B.; Rai, D. K. *J. Chem. Phys.* **1965**, *43*, 3570.
(281) Oldenborg, R. C.; Dickson, C. R.; Zare, R. N. *J. Mol. Spectrosc.* **1975**, *58*, 283.
(282) Kurylo, M. J.; Brdun, W.; Abramowitz, S.; Krauss, M. *J. Res. Natl. Bur. Stand., Sect. A* **1976**, *80*, 167.
(283) Linton, C.; Broida, H. P. *J. Mol. Spectrosc.* **1976**, *62*, 396.
(284) Brom, J. M.; Beatie, W. H. *J. Mol. Spectrosc.* **1980**, *81*, 445.
(285) Balasubramanian, K.; Pitzer, K. S. *J. Phys. Chem.* **1983**, *87*, 4857.
(286) Basch, H.; Stevens, W.; Krauss, M. *Chem. Phys. Lett.* **1981**, *74*, 2416.
(287) Rochester, G. D. *Proc. R. Soc. London, Ser. A* **1935**, *150*, 668.
(288) Shawhan, E. W. *Phys. Rev.* **1935**, *48*, 421.
(289) Douglas, A. E.; Howe, L. L.; Morton, R. J. *J. Mol. Spectrosc.* **1961**, *7*, 161.
(290) Yamdagni, R.; Joshi, M. M. *Indian J. Phys.* **1966**, *40*, 495.
(291) Smith, J. J.; Meyer, B. *J. Mol. Spectrosc.* **1968**, *27*, 304.
(292) Greenwood, D. J.; Linton, C.; Barrow, R. F. *J. Mol. Spectrosc.* **1981**, *89*, 134.
(293) Teichmann, R. A., III; Nixon, E. R. *J. Mol. Spectrosc.* **1977**, *65*, 258.
(294) Greenwood, D. J.; Barrow, R. F.; Linton, C. *J. Mol. Spectrosc.* **1981**, *86*, 480.
(295) Balasubramanian, K. *Chem. Phys. Lett.* **1987**, *139*, 262.
(296) Rochester, G. D.; Howell, H. G. *Proc. R. Soc. London, Ser. A* **1935**, *148*, 157.
(297) Barrow, R. F.; Fry, P. W.; LeBargy, R. C. *Proc. Phys. Soc. London* **1963**, *81*, 697.
(298) Marino, C. P.; Guerin, J. D.; Nixon, E. R. *J. Mol. Spectrosc.* **1974**, *51*, 160.
(299) Teichman, R. A., III; Nixon, E. R. *J. Mol. Spectrosc.* **1975**, *54*, 78.
(300) Burkin, B.; Carleer, M.; Colin, R.; Dreze, C.; Ndikumana, T. *J. Phys. B* **1980**, *13*, 3783.
(301) Knöckel, M.; Kröckertskothen, T.; Tiemann, E. *Chem. Phys.* **1985**, *93*, 349.
(302) Murty, A. N.; Curl, R. F., Jr. *J. Mol. Spectrosc.* **1969**, *30*, 102.
(303) Colin, R.; Drowart, J. *J. Chem. Phys.* **1962**, *37*, 1120.
(304) Balasubramanian, K. *J. Chem. Phys.* **1986**, *85*, 1443.
(305) Kim, G. B.; Balasubramanian, K., manuscript in preparation.
(306) Moore, C. E. *Table of Atomic Energy Levels*, U.S. National Bureau of Standards: Washington, DC, 1971; Vols. I–III.
(307) O'Hare, P. A. G.; Batana, A.; Wahl, A. C. *J. Chem. Phys.* **1973**, *59*, 6495.
(308) Hoeft, J.; Lovas, F. J.; Tiemann, E.; Torring, T. *Z. Naturforsch.* **1970**, *25a*, 539.
(309) Dube, R. S.; Upadhya, K. N.; Rai, D. K. *J. Quant. Spectrosc. Radiat. Transfer* **1970**, *10*, 1191.
(310) Dube, R. S. *Curr. Sci.* **1971**, *40*, 32.
(311) Urban, R.-D.; Magg, U.; Jones, H. *Chem. Phys. Lett.* **1989**, *154*, 135.
(312) Berkowitz, J. *J. Chem. Phys.* **1988**, *89*, 7065.
(313) Berkowitz, J.; Cho, H. *J. Chem. Phys.* **1989**, *90*, 1.
(314) Balasubramanian, K. *J. Chem. Phys.* **1989**, *91*, 2443.
(315) Bahnmaier, A. H.; Urban, R.-D.; Jones, H. *Chem. Phys. Lett.* **1989**, *155*, 269.
(316) Schwerdtfeger, P.; Silberbach, H.; Miehlich, B. *J. Chem. Phys.* **1989**, *90*, 762.
(317) Balasubramanian, K. *J. Chem. Phys.* **1988**, *89*, 5731.
(318) Hoeft, J.; Nair, K. P. R. *Chem. Phys. Lett.* **1989**, *155*, 273.
(319) Wolf, U.; Tiemann, E. *Chem. Phys. Lett.* **1987**, *139*, 191.
(320) Perumalswamy, K.; Rai, S. B.; Upadhya, K. N. *Physica C* **1986**, *141*, 315.
(321) Perumalswamy, K.; Rai, S. B.; Rai, D. K.; Upadhya, K. N. *Physica C* **1985**, *132*, 122.
(322) Borkowska-Burnecka, J.; Zyrnicki, W. *Physica C* **1983**, *115*, 415.
(323) Nampoori, V. P. N.; Kamalasanan, M. N.; Patel, M. M. *Indian J. Phys. B* **1977**, *51*, 401.
(324) Glenewinkel-Meyer, Th.; Kowalski, A.; Müller, B.; Ottinger, Ch.; Beckenridge, W. H. *J. Chem. Phys.* **1988**, *89*, 7112.
(325) Dyke, J. M.; Kirby, C.; Morris, A.; Gravenor, B. W. J.; Klein, R.; Rosmus, P. *Chem. Phys.* **1984**, *88*, 289.
(326) Wang, L.-S.; Niu, B.; Shirley, D. A.; Balasubramanian, K. *J. Chem. Phys.*, submitted.
(327) Vempati, S. N.; Jones, W. E. *J. Mol. Spectrosc.* **1988**, *127*, 232.
(328) Vempati, S. N.; Jones, W. E. *J. Mol. Spectrosc.* **1987**, *122*, 190.
(329) Vempati, S. N.; Jones, W. E. *J. Mol. Spectrosc.* **1986**, *120*, 441.
(330) Maki, A. G.; Lovas, C. J. *J. Mol. Spectrosc.* **1987**, *125*, 188.
(331) Mêlen, F.; Dubois, I. *J. Mol. Spectrosc.* **1987**, *124*, 476.
(332) Lakshminarayana, G.; Shetty, J. *J. Mol. Spectrosc.* **1987**, *122*, 417.
(333) Bopegedera, A. M. R. P.; Brazier, C. R.; Bernath, P. F. *Chem. Phys. Lett.*, in press.
(334) Ramos, A. F.; Pyper, N. C.; Malli, G. L. *Phys. Rev. A* **1988**, *38*, 2729.